

**Genetic Optimization of Biotin-Binding Proteins:  
Artificial Metalloenzymes and Beyond**

**Inauguraldissertation**

zur

Erlangung der Würde eines Doktors der Philosophie

vorgelegt der

Philosophisch-Naturwissenschaftlichen Fakultät

der Universität Basel

von

Alessia Sardo

aus Caltanissetta, Italien

Basel, 2010

Genehmigt von der Philosophisch-Naturwissenschaftlichen Fakultät auf Antrag von

Prof. Dr. T. R. Ward

Prof. Dr. W.-D. Woggon

Basel, den 22 Juni 2010

Dekan  
Dean Prof. Dr. E. Parlow

*Ai miei genitori, Eugenio e Rosa.*

*To my parents, Eugenio and Rosa.*

*Per aspera ad astra.*

*Lucius Annaeus Seneca, 3 BC – AD 65*



# Acknowledgments

I would like to thank all people who have contributed to my doctoral studies.

Foremost, I want to express my special gratitude to my supervisor Prof. Thomas R. Ward, for giving me the opportunity to work in such a stimulating research and multidisciplinary environment. I am further grateful for his tremendous support in all aspects involved in doing a PhD, both personal and professionally.

I also want to thank Prof. Wolf-Dietrich Woggon, for accepting to read and examine my work.

Dr. Marc Creus deserves a special thanks, for his brilliant insight and precious suggestions during my PhD. Many thanks for his scientific support, great friendship and extraordinary humanity.

Also, my deepest gratitude to Prof. Tilman Schirmer and Dr. Claudia Massa, from the Biozentrum, for the collaboration in the protein crystallization.

The generous supports from Marie Curie fellowship and Fonds National Suisse are greatly appreciated.

Furthermore, I wish to thank all the past and present members of the Ward group. In particular, Elisa, an extraordinary friend, for her precious presence in my life, private and professional. Yvonne, whose editing suggestions and precise sense of English contributed to the final version of this thesis. Sabina, for her friendship and contagious laughter. Thibaud, for his brilliant ideas and amazing support. Jeremy, for his good jokes and “clownish” attitude towards life – it was a breeze of fresh air after long hours in the lab. Cheikh, for his indisputable wisdom in life and in science. Fabien, the “wise” chemist, for his support and advice. Narasimha, for contagious passion and rigor on research. Tommaso, my fellow “Terron” citizen, for his friendship and opened language. Maurus,

for his big effort to understand my French. Tillmann, for his precious collaboration and constant availability. Valentin, for making his resourceful knowledge available to anyone. Ruben, for his good humor and hilarity. René, a “brilliant” friend, for his incredible support. Therese, Julien, Anca, Julieta, Anita, Christophe, Edy, Yves, Johannes, Karoline, Lu, Jincheng, Marc, Livia, Sarah, Koji for being part of the group.

Many thanks to Gregory, Gaetano and Paolo, from the Wennemers group, for the enjoyable “breakfast” time and pleasurable conversations.

A special thanks goes to Beatrice Erismann for taking care of all the administrative work and for making my student life at Unibas easier.

My deepest gratitude goes to my very dear friends: Sonia, Patricia, Egidio, Alessandro, Sana, Nicola, Paola, for supporting me during this time. You are the best!

A precious thanks is addressed to my big family, “one of a kind”. We are very close and I love them dearly. They believed in me, and gave me their unconditional support. Thanks for having made me who I am. Now you are also Doctors!

*Un prezioso ringraziamento é rivolto alla mia numerosa famiglia, “unica nel suo genere”. Siamo molti uniti e li amo profondamente. Hanno tutti creduto in me, dandomi il loro supporto incondizionato. Grazie per avermi resa quella che sono. Adesso anche voi siete Dottori!*

Finally, a special thanks is addressed to Saul who gave me the greatest joy of my life: my son, Mattia.

*Infine, un ringraziamento speciale é rivolto a Saul che mi dato la gioia più grande della mia vita: mio figlio, Mattia.*

---

# Table of Contents

<b>List of Abbreviations</b>	<b>vi</b>
<b>Chapter 1 Introduction</b>	<b>1</b>
<b>1.1 Biotin-Binding Proteins</b>	<b>1</b>
1.1.1 Biotin	1
1.1.2 Chicken Avidin	3
1.1.3 Bacterial Streptavidin	4
1.1.4 Structure of Avidin and Streptavidin	6
1.1.5 Strept(avidin)-Biotin Interaction	7
1.1.6 Heterologous Expression Systems for Streptavidin and Avidin	11
1.1.7 Biotin-(Strept)Avidin Technology	12
<b>1.2 Artificial Metalloenzymes</b>	<b>16</b>
1.2.1 Chirality	16
1.2.2 Enantioselective Catalysis	18
1.2.3 Homogeneous vs. Enzymatic Catalysis	21
1.2.4 Artificial Metalloenzymes	22
1.2.4.1 Anchoring of Catalyst into the Protein	23
<b>References</b>	<b>27</b>
<b>Chapter 2 Optimization of Streptavidin Production</b>	<b>30</b>
<b>2.1 Introduction</b>	<b>30</b>
2.1.1 Directed Evolution and Rational Protein Re-Design	30
2.1.2 Enantioselectivity of Enzymes Controlled by Directed Evolution	33
2.1.3 Chemogenetic Optimization of Artificial Metalloenzymes	34
2.1.4 First Round Evolution of Artificial Transfer Hydrogenases	35
2.1.4.1 Chemical Optimization of ATH	37

2.1.4.2	Saturation Mutagenesis at Position S112	38
2.1.4.3	Results of Chemogenetic Optimization	39
2.1.5	X-Ray Crystal Structure of an Artificial Transfer Hydrogenase	40
2.1.6	Expression and Purification of T7-Sav in Large-Scale	43
<b>2.2</b>	<b>Aim of the Work</b>	<b>45</b>
<b>2.3</b>	<b>Results and Discussion</b>	<b>45</b>
2.3.1	Saturation Mutagenesis at Positions K121 and L124	45
2.3.2	Streptavidin Isoforms Expression in Small-Scale Cell Culture	48
2.3.3	Immobilization as HTS Approach	50
2.3.4	Thermo-denaturation as Straightforward Purification Strategy	52
2.3.4.1	Thermo-Stability of Pure Streptavidin Variants	52
2.3.4.2	Hybrid Catalysts in Crude Cell Extract	54
2.3.4.3	Streptavidin Refolding	60
2.3.5	High-Throughput Expression in 96-Well Plate	63
<b>2.4</b>	<b>Materials and Methods</b>	<b>64</b>
2.4.1	Chemicals	64
2.4.2	Technical Equipment	66
2.4.3	Mutagenesis	66
2.4.4	Expression Strain	71
2.4.5	Streptavidin Production	72
2.4.5.1	Protein Expression in 20 L of <i>E. coli</i> Cell Culture	72
2.4.5.2	Protein Expression in 50 mL of <i>E. coli</i> Cell Culture	72
2.4.5.3	Protein Expression in 96-Well Plate Format	73
2.4.6	Streptavidin Purification	74
2.4.6.1	Purification on an Imino-Biotin Column	74
2.4.6.2	Streptavidin Extraction for Immobilization	74
2.4.6.3	Streptavidin Purification by Thermo-Denaturation	75
2.4.7	Streptavidin Refolding	76
<b>2.5</b>	<b>Conclusions</b>	<b>78</b>

<b>References</b>	<b>81</b>
<b>Chapter 3 DNA Recognition <i>in vitro</i></b>	<b>83</b>
<b>3.1 Introduction</b>	<b>83</b>
3.1.1 Organometallic Compounds in Cancer Chemotherapy	83
3.1.2 Metal Complex Binding to Cellular Thiols	84
3.1.3 Affinity modulation via a presenter protein	85
<b>3.2 Aim of the Work</b>	<b>90</b>
<b>3.3 Results and Discussion</b>	<b>91</b>
3.3.1 Introduction of a Biotinylated Ru (II) Complex into a Protein	91
3.3.2 Binding of Drug – Protein Assembly to Quadruplex DNA	93
3.3.3 Complex – DNA Interaction in the Absence of Streptavidin	98
3.3.4 Streptavidin – DNA Binding	100
3.3.5 Competition Studies with Interfering Glutathione	102
3.3.6 Target Selectivity against Single Stranded DNA	103
3.3.7 Competition Studies with Single Stranded DNA	105
3.3.8 Genetic Control of the Second Coordination Sphere	107
3.3.9 Chemo – Genetic Optimization with Increased dsDNA Affinity	108
3.3.10 Summary of $K_d$ Estimated by EMSA and Determined by ITC	110
<b>3.4 Materials and Methods</b>	<b>112</b>
3.4.1 Chemicals	112
3.4.2 Technical Equipment	114
3.4.3 DNA	114
3.4.4 Electrophoretic Mobility Shift Assays in Agarose Gel	115
3.4.5 Electrophoretic Mobility Shift Assays in Acrylamide Gel	117
3.4.6 Protein Expression and Purification	118
3.4.7 Site – Directed Mutagenesis	119
3.4.8 Isothermal Titration Calorimetry (ITC)	119
3.4.9 Crystallization	120
<b>3.5 Conclusions</b>	<b>121</b>

<b>Reference</b>	<b>124</b>
<b>Chapter 4 Novel Avidin from <i>B. pseudomallei</i></b>	<b>126</b>
<b>4.1 Introduction</b>	<b>126</b>
4.1.1 Avidins Useful in Biotechnology	126
4.1.2 Avidins from Different Organisms	127
<b>4.2 Aim of the Work</b>	<b>128</b>
<b>4.3 Results and Discussion</b>	<b>129</b>
4.3.1 Overexpression and Purification of Novel Avidins	129
4.3.2 Sequence Alignments and 3D-Modelling	130
4.3.3 Biotin-Binding Activity	133
4.3.4 Protein Stability	136
4.3.4.1 Resistance to Proteinase Digestion	136
4.3.4.2 Thermal Stability	138
4.3.4.3 Resistance to Reducing Agents	139
4.3.5 Protein Secretion into the Periplasm of <i>E. coli</i>	141
4.3.5.1 Secretory Signal Peptide	141
4.3.5.2 Periplasmic Expression in <i>E. coli</i>	141
4.3.6 Burkavidin Homogeneity	143
4.3.7 Burkavidin as an Artificial Metalloenzyme	144
<b>4.4 Materials and Methods</b>	<b>147</b>
4.4.1 Chemicals	147
4.4.2 Technical Equipment	149
4.4.3 Vector Generation	149
4.4.4 Expression and Purification	150
4.4.5 Preparation of Periplasmic Proteins from Bacterial Culture	152
4.4.6 Site – Directed Mutagenesis	152
4.4.7 Structural Modeling	153
4.4.8 Thermostability	153
4.4.9 Sensitivity to Proteinase Treatment	154

4.4.10 Isothermal Titration Calorimetry (ITC)	154
4.4.11 Titration by HABA	155
4.4.12 Isoelectric Focusing (IEF)	155
4.4.13 Gel Filtration	155
<b>4.5 Conclusions</b>	<b>156</b>
<b>References</b>	<b>158</b>
<b>Chapter 5 General Conclusion</b>	<b>160</b>
<b>References</b>	<b>163</b>
<b>APPENDIX A</b>	<b>I</b>
<b>APPENDIX B</b>	<b>III</b>
<b>APPENDIX C</b>	<b>VI</b>
<b>APPENDIX D</b>	<b>XIX</b>
<b>APPENDIX E</b>	<b>XXI</b>
<b>APPENDIX F</b>	<b>XXIII</b>
<b>APPENDIX G</b>	<b>XXV</b>
<b>APPENDIX H</b>	<b>XXVI</b>
<b>Curriculum Vitae</b>	<b>XXVII</b>

---

## List of Abbreviations

C	included in
Ac	acetate
Ala	alanine
APS	Ammonium Persulfate
Arg	arginine
Asn	asparagine
Asp	aspartic acid
AspAT	Aspartate Aminotransferase
ATH	Artificial Transfer Hydrogenase
Avi	avidin
AVR	Avidin-Related gene
B4F	Biotin-4-fFluorescein
BBB	Blood Brain Barrier
BBP-A	Biotin-Binding Protein A
BF <sub>4</sub>	tetrafluoroborate
BINAP	2,2'-bis(diphenylphosphanyl)-1,1'-binaphtyl
Biot	biotin
Burk	burkavidin
Cat	catalyst
C <sub>f</sub>	final concentration
CIDs	Chemical Inducers of Dimerization
COD	1,5-Cyclooctadien
CPPs	Cell-Penetrating Peptides
Cys	cysteine
DET	Diethyl Tartrate
DIPAMP	1,2-bis(o-anisylphenylphosphinyl)ethane
DMF	dimethylformamide



DNA	Deoxyribonucleic Acid
dNTP	deoxyribonucleotide triphosphate
DOPA	3,4-dihydroxyphenylalanine
TsDPEN	<i>N</i> -tosyl-(1 <i>S</i> ,2 <i>S</i> )-diphenylethyldiamin
dsDNA	double stranded Deoxyribonucleic Acid
DTT	dithiothreitol
<i>E. coli</i>	<i>Escherichia coli</i>
<i>e.g.</i>	<i>exempli gratia</i> , for example
ee	enantiomeric excess
EMSA	Electrophoretic Mobility Shift Assays
epPCR	error-prone Polymerase Chain Reaction
Et	ethyl
FDA	Food and Drug Administration
FPLC	Fast Protein Liquid Chromatography
FRAP	FKBP Rapamycin Associated Protein
Glu	glutamic acid
Gly	glycine
GSH	glutathione
HABA	2-[(4-hydroxyphenyl)azo]benzoic acid
HEPES	(4-(2-hydroxyethyl)-1-piperazineethanesulfonic acid
His	histidine
HTS	high throughput screening
<i>i.e.</i>	<i>id est</i> , that is
IEF	isoelectric focusing
<i>i</i> Pr	<i>iso</i> -propyl
IPTG	Isopropyl $\beta$ -D-1-thiogalactopyranoside
ITC	Isothermal Titration Calorimetry
$K_a$	association constant
$K_d$	dissociation constant
L	ligand
L3,4	loop 3,4
L7,8	loop 7,8
LB	Luria-Bertani broth
Leu	leucine

Me	methyl
MES	2-( <i>N</i> -morpholino)ethanesulfonic acid
Met	methionine
MHC	Major Histocompatibility Complex
MOPS	3-( <i>N</i> -morpholino)propanesulfonic acid
NMR	Nuclear Magnetic Resonance
OD	Optical Density
PBS	Phosphate Buffered Saline
PCR	Polymerase Chain Reaction
PDB	Protein Data Bank
Phe	phenylalanine
<i>pI</i>	isoelectric point
PMSF	phenylmethanesulfonylfluoride
r.t.	room temperature
Rhod	Rhodavidin
RMSD	Root Mean Square Deviation
RNA	Ribonucleic Acid
Sav	Streptavidin
Sc	scrambled
SDS	Sodium Dodecyl Sulfate
SDS-PAGE	Sodium Dodecyl Sulfate – Polyacrylamide Gel Electrophoresis
Ser	serine
ssDNA	single stranded Deoxyribonucleic Acid
TBE	Tris Borate EDTA
TCR	T cell receptor
TEMED	Tetramethylethylenediamine
TfRMAb	Transferrin Receptor Monoclonal Antibody
Thr	threonine
TP	Tryptone Phosphate
Trp	tryptophan
TS	Transition State
Ts	Tosyl
Tyr	tyrosine
UV-VIS	Ultraviolet-Visible

Val	valine
VIPa	Vasoactive Intestinal Peptide analogue
vs.	<i>versus</i>
WT	Wild-Type

---

# Chapter 1

## Introduction

*All truths are easy to understand once they are discovered; the point is to discover them*

---

Galileo Galilei

### 1.1 Biotin-Binding Proteins

#### 1.1.1 Biotin

Originally called vitamin H <sup>[1]</sup>, biotin is an essential water-soluble vitamin with a molecular weight of 244 g mol<sup>-1</sup>. It is a bicyclic molecule composed of a ureido (tetrahydroimidizalone) ring fused to a tetrahydrothiophene ring, which supports a valeric acid side chain.

Biotin is an optically active molecule with three chiral centres, as shown in figure 1.1 <sup>[2]</sup>.

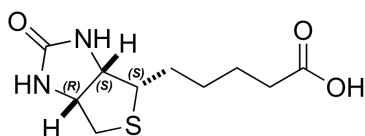


Fig 1.1 (+)-biotin, known as vitamin H, with three chiral centres

The tissues with the highest amounts of biotin are the liver, kidney and pancreas.

Daily biotin requirements are relatively small and biotin is present in many foods. However, high levels of avidin, a glycoprotein which forms a very stable non-covalent complex with biotin ( $K_d=10^{-15}$  M), were identified in chicken egg-whites<sup>[3]</sup>. For this reason, the excessive consumption of raw egg-white prevents the body from absorbing vitamin H and leads to a rare nutritional problem, known as “egg-white injury”<sup>[4]</sup>.

Biotin binds covalently to the  $\epsilon$ -amino group of a lysine residue in carboxylases, forming a biocytin complex. This covalent linkage is broken by biotinidase, an enzyme responsible for biotin recycling from the carboxylase. Thus, removed from the biocytin complex, biotin is again available for other enzymes<sup>[5]</sup>.

The four carboxylases<sup>[6]</sup> which bind biotin as coenzyme and which are involved in metabolic reactions are: *acetyl-CoA carboxylase*, which produces malonyl-CoA through two catalytic activities (biotin carboxylase and carboxyltransferase) for the biosynthesis of fatty acids; *pyruvate carboxylase*, involved in the formation of oxaloacetate from pyruvate as precursor for gluconeogenesis; *propionyl-CoA carboxylase*, which provides methylmalonyl-CoA which is involved in the metabolism of amino acids and fatty acids, and *3-methylcrotonyl-CoA carboxylase*, which catalyses the carboxylation of 3-methylcrotonyl-CoA which is implicated in the degradation of leucine.

Beyond the biochemical role in carboxylation reactions, biotin regulates gene expression at the transcriptional or post-transcriptional level, interfering with fetal development and cell biology<sup>[7]</sup>.

### ***1.1.2 Chicken Avidin***

Chicken avidin is a homotetrameric protein consisting of four antiparallel  $\beta$ -barrels with a molecular weight of approximately 63 kDa <sup>[8]</sup>. Estrogenic hormones stimulate avidin synthesis in the chick oviduct <sup>[9]</sup>. The protein is secreted in its natural host and the signal peptide is cleaved following secretion <sup>[10]</sup>.

Each monomer consists of eight antiparallel  $\beta$ -strands, bears 128 amino acids and binds non-covalently to a single biotin molecule with very high affinity ( $K_d = 1.3 \cdot 10^{-15}$  M at pH 5). The protein is positively charged ( $pI = 10.5$ ) with eight arginine and nine lysine residues in each monomer. The glycosylation content, composed of four to five mannose and three *N*-acetylglucosamine residues, accounts for about 10% of the molecular mass <sup>[11]</sup>.

Avidin is water soluble and stable over wide pH and temperature ranges and in the presence of chaotropic reagents <sup>[11a, 12]</sup>. Stability is increased when biotin is bound. The high thermostability seems to be correlated with the presence of intramonomeric disulphide bridges, formed between C4 – C83 cystein residues <sup>[13]</sup>.

The presence of biotin reduces the flexibility of the loop L3,4 which is involved in van der Waals interactions with biotin, and makes avidin less susceptible to proteolytic cleavage <sup>[13b]</sup>.

The high  $pI$  of avidin and the presence of carbohydrate residues constitute a drawback in certain biotechnological applications, such as in drug delivery and imaging. For example, the positive charges on avidin and its glycosylation content can induce non-specific binding to DNA and cell

surfaces. These properties also lead to rapid clearance of avidin from the blood, with protein accumulation in the kidneys <sup>[11b, 14]</sup>.

Despite the centennial discovery of avidin, an exhaustive description of its biological functions still remains a challenge. The wide avidin distribution in the female reproductive tract and in the egg-white of many species is a suggestion of its important role in ovum survival and embryonic growth <sup>[15]</sup>.

However, avidin functions are not simply confined to reproductive sphere, since some non-oviductal chicken tissues, infected by bacteria or fungi, induce avidin production as defense mechanism against infection. Avidin is hence an antibiotic protein that inhibits microbial growth through biotin depletion <sup>[16]</sup>.

Under stress conditions, avidin is produced even in chicken myoblasts and chondrocytes to prevent cell proliferation through extracellular biotin-binding and fatty acid biosynthesis inhibition <sup>[17]</sup>.

### ***1.1.3 Bacterial Streptavidin***

Streptavidin is an alternative biotin-binding protein with four antiparallel  $\beta$ -barrels, isolated from the bacterium *Streptomyces avidinii*.

Also streptavidin, isolated during an antibiotic investigation, inhibits bacterial proliferation by acting as biotin scavenger.

The biotin-binding site is located at one end of each  $\beta$ -barrel and each monomer contributes to the binding on the neighboring subunit <sup>[18]</sup>. Thus, the streptavidin homotetramer acts as a dimer of dimer, with slightly lower affinity for biotin ( $K_d = 4 \cdot 10^{-14}$  M) compared to avidin <sup>[13a]</sup>.

Although avidin is structurally and functionally comparable to streptavidin, there are differences in isoelectric point, glycosylation, primary structure and pharmacokinetics. Streptavidin is a non-glycosylated protein with a mildly acidic isoelectric point ( $pI = 6-7$ )<sup>[14, 19]</sup>. For this reason, streptavidin is preferred over avidin in biotechnological applications due to less non-specific binding to cell surfaces and DNA<sup>[20]</sup>.

Despite being devoid of cysteines and, consequently, disulphide bridges, streptavidin exhibits a thermal and structural stability similar to that of avidin, especially in the presence of biotin. The monomeric interactions become even tighter upon biotin binding. For this reason, holo-streptavidin maintains its tetrameric structure even in the presence of SDS, urea or heat treatment<sup>[20]</sup>.

After expression in *Streptomyces avidinii*, streptavidin is a polypeptide of 159 residues termed “mature streptavidin”, which is characterized by poor solubility and high propensity for aggregation<sup>[20]</sup>. During secretion, a peptide sequence consisting of 24 amino acids is proteolytically cleaved. Upon longer culture incubation, further proteolytic cleavages occur in both the *N* and *C* termini regions. The resulting most stable form of protein, consisting of residues 13-139, is called “core streptavidin” and is characterized by high solubility, low tendency to aggregate and enhanced binding affinity for biotin<sup>[20-21]</sup>.

Regarding pharmacokinetics, streptavidin has an appreciably longer plasma half-life in blood compared to avidin, with a final accumulation in the kidneys<sup>[22]</sup>.



### 1.1.4 Structure of Avidin and Streptavidin

Sequence alignment of avidin and streptavidin reveals that most of the conserved residues are directly involved in biotin binding <sup>[8a, 23]</sup>. The homology in the alignment of the two sequences is characterized by 30% of identity and 41% of similarity <sup>[8a]</sup> (**Fig. 1.2**).

Particularly interesting is the homology around tryptophans 21-79-120 of streptavidin and the corresponding tryptophan residues 10-70-110 of avidin, implicated in the biotin-binding <sup>[24]</sup>.

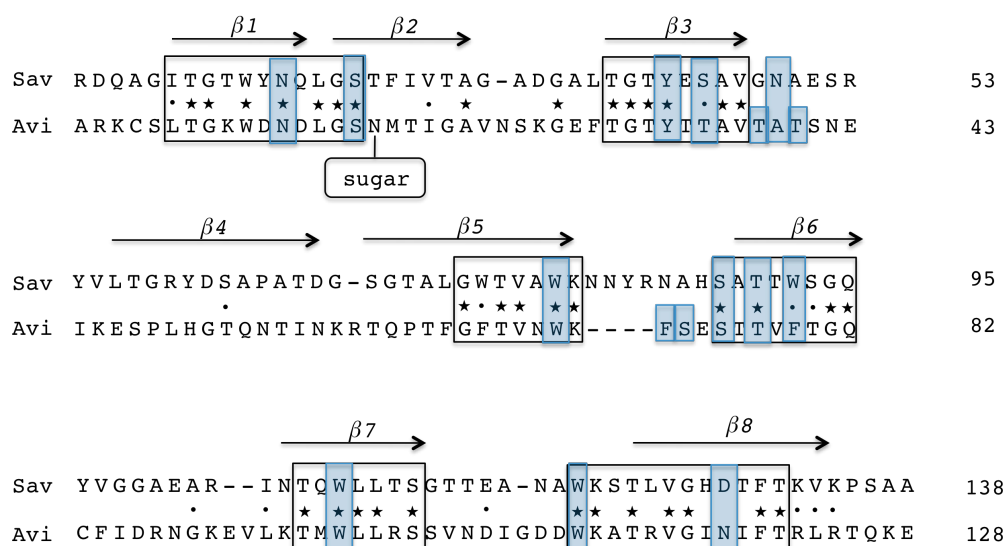


**Fig. 1.2** Sequence alignment of primary structures of avidin (residues 1-128) and streptavidin (residues 12-138). Positions of the eight  $\beta$ -strands are indicated by black arrows. The six highly homologous sequences are highlighted by rectangular boxes. Residues directly involved in biotin-binding are shaded in blue. Conserved and similar residues are marked by stars and dots, respectively (modified from a figure by Livnah *et al.*) <sup>[8a]</sup>

Streptavidin and avidin have an almost identical secondary structure, characterized by eight antiparallel  $\beta$ -strands, which fold to give an antiparallel  $\beta$ -barrel tertiary structure (**Fig 1.3**).

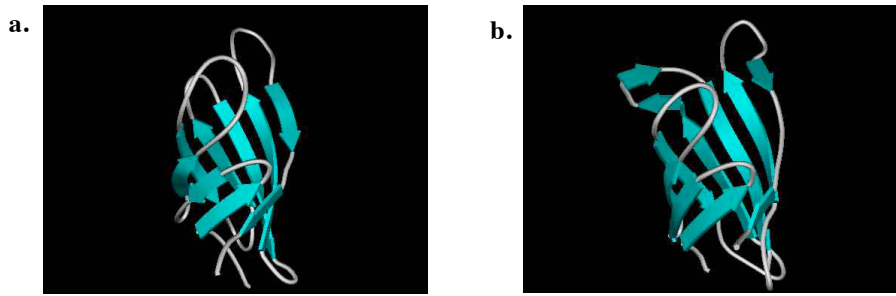


**Fig. 1.3 Antiparallel  $\beta$ -barrel tertiary structures of a) avidin and b) streptavidin**

However, their structures differ mainly in the size and conformation of the six extended hairpin loops that connect the strands. In avidin the L3,4 loop is three residues longer than the corresponding loop in streptavidin <sup>[23b, 25]</sup>. Upon binding biotin, the loop closes, thus wrapping the ligand almost completely both in avidin and in streptavidin.

Quaternary assemblies, containing four closely related biotin-binding sites, characterize both proteins. The biotin-binding site is located at one end of each  $\beta$ -barrel and is formed by the inner amino acids of the barrel and a Trp residue from the neighbouring subunit. The tryptophan from the adjacent monomer, corresponding to Trp-120 in streptavidin and Trp-110 in avidin, is involved in inter-monomeric contacts and stabilizes the tetrameric protein in the bound state <sup>[26]</sup>.

### ***1.1.5 Strept(avidin)-Biotin Interaction***

A deep biotin-binding pocket, which is partially occupied by five water molecules in the absence of biotin, is located at the centre of each subunit in both tetrameric proteins. Upon biotin binding, water is displaced <sup>[8a]</sup> and

biotin is tightly anchored via various residues in the pocket with the valeryl side-chain carboxylate exposed to the solvent.

Hydrophilic residues are involved in hydrogen bonds with biotin, while aromatic amino acids create a hydrophobic compartment to accommodate the hydrophobic biotin scaffold <sup>[27]</sup>.

The avidin residues Trp-70, Phe-72, Phe-79, Trp-97, and Trp-110 from the neighboring monomer, are involved in hydrophobic interactions with biotin. The corresponding hydrophobic residues in streptavidin are provided by Trp-79, Trp-92, Trp-108, and Trp-120 from the adjacent monomer <sup>[28]</sup>.

Trp-110 of avidin and the analogous Trp-120 of streptavidin act as a hydrophobic lid for the binding pocket <sup>[29]</sup>.

The ureido oxygen of the biotin bicycle forms hydrogen bonds with the streptavidin polar residues Asn-23, Ser-27 and Tyr-43 similarly to Asn-12, Ser-16 and Tyr-33 in avidin <sup>[30]</sup>. The ureido nitrogens, involved in hydrogen bonds with Thr-35 and Asn-118 in avidin, interact with Ser-45 and Asp-128 in streptavidin. The valeric carboxylate of biotin forms only two hydrogen bonds with streptavidin (Asn-49 and Ser-88) as against five in avidin (Thr-38, Ala-39, Thr-40, Ser-73 and Ser-75). Furthermore, as discussed the loop L3-4 in streptavidin is three residues shorter compared to the analogous loop in avidin (**Fig. 1.4**). For these reasons, streptavidin has a slightly lower affinity for biotin with respect to avidin <sup>[31]</sup>.

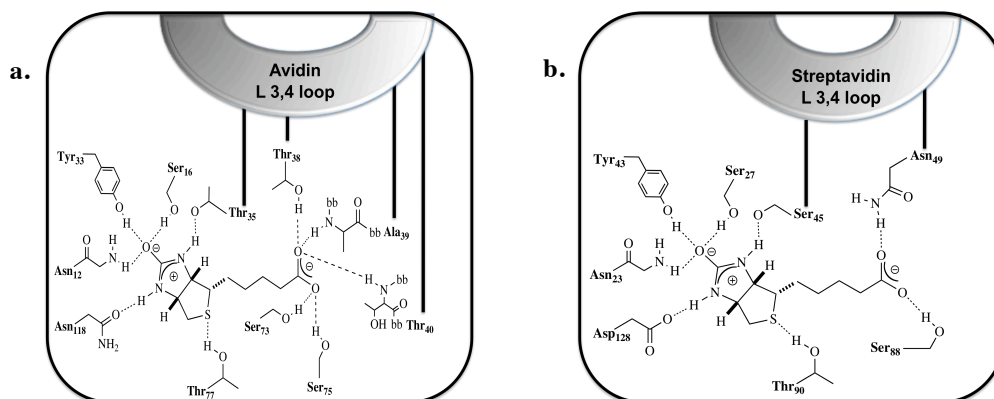


**Fig. 1.4 Hydrogen-bonding interactions between biotin and L3,4 loop region of a) avidin and b) streptavidin.** One residue on the streptavidin L3,4 loop is involved in hydrogen-bonding interaction with the biotin carboxylate, whereas three hydrogen-bonds mediate interaction between avidin L3,4 loop and one of the carboxylate oxygens of biotin

**Table 1.1 Summary of biotin-strept(avidin) interactions**

<b>INTERACTION</b>	<b>AVIDIN</b>	<b>STREPTAVIDIN</b>
H-bond	Asn-12	Asn-23
H-bond	Ser-16	Ser-27
H-bond	Tyr-33	Tyr-43
H-bond <sup>a</sup>	Thr-35	Ser-45
H-bond <sup>a</sup>	Asn-118	Asp-128
H-bond <sup>b</sup>	Thr-77	Thr-90
H-bond <sup>c</sup>	Ala-39	Asn-49
H-bond <sup>c</sup>	Ser-75	Ser-88
H-bond <sup>c</sup>	Thr-38	—
H-bond <sup>c</sup>	Thr-40	—
H-bond <sup>c</sup>	Ser-73	—
Hydrophobic	Trp-70	Trp-79
Hydrophobic	Phe-79	Trp-92
Hydrophobic	Trp-97	Trp-108
Hydrophobic <sup>d</sup>	Trp-110	Trp-120
Hydrophobic	Phe-72	—

<sup>a</sup> Hydrogen-bonding interaction between a nitrogen atom of the biotin ureido moiety and L3,4 loop of both proteins.

<sup>b</sup> Hydrogen-bond involving the sulphur atom of the biotin tetrahydrothiophene moiety.

<sup>c</sup> Hydrogen-bond between the biotin valeryl chain and L3,4 loop of both proteins.

<sup>d</sup> Amino acid residues from the adjacent monomer.

### ***1.1.6 Heterologous Expression Systems for Streptavidin and Avidin***

Chicken avidin and its bacterial analogue streptavidin constitute important tools in many biotechnological applications, which take advantage of the extremely high affinity for biotin. For this reason, large-scale production is required to keep up with demand <sup>[32]</sup>.

However, avidin and streptavidin production in their native host suffers from several restrictions.

Streptavidin expression in *Streptomyces avidinii* takes a relatively long time to culture (up to 10 days). Furthermore, the final product is a mixture of heterogeneous molecules, which require a further proteolytic cleavage <sup>[10b,21]</sup>.

Avidin constitutes only 0.05% of egg-white total protein <sup>[10b]</sup> and large batch-to-batch variations have been observed <sup>[33]</sup>.

Therefore, a lot of effort has been invested to identify successful heterologous systems for avidin and streptavidin expression.

High-yield production of avidin in a soluble form has been achieved in eukaryotic structures, such as baculovirus-infected insect cells <sup>[34]</sup>, *Pichia pastoris* <sup>[35]</sup>, transgenic maize <sup>[36]</sup>, tobacco and apple plant <sup>[37]</sup>. However, high-costs of insect cultures and time-consuming plant construction acted as a deterrent to the application of these expression systems. Therefore, recent studies focused on bacterial production of active avidin as a deglycosylated protein, lacking of post-translational addition of carbohydrate residues. This novel avidin, more exploitable in biotechnological applications, was expressed in the periplasmic space of *E. coli*, by replacing the native signal peptide with a secretion signal peptide from *Bordetella avium* OmpA <sup>[10b]</sup>.

On the contrary, recombinant streptavidin was principally produced in different prokaryotic systems such as *Bacillus subtilis*<sup>[38]</sup> and *Escherichia coli*<sup>[26]</sup>.

The cloned gene of streptavidin was efficiently expressed in the cytoplasm of *E. coli* by using T7 RNA polymerase/T7 promoter expression system. The protein was clustered in inclusion body and, afterwards, refolded after solubilization via dialysis against guanidinium chloride (6 M, pH 1.5)<sup>[26]</sup>.

Although inclusion bodies can offer certain advantages, such as protein protection from proteolysis and partial purification by centrifugation, a soluble and active protein is often preferred. Consequently, recent studies have focused on finding engineered systems to increase streptavidin solubility in the expression strain.

T7-tagged streptavidin, with *N*-terminal residues replaced by a T7-tagged peptide, was efficiently expressed in the cytoplasm of *E. coli* as functional protein<sup>[30,39]</sup>.

Moreover, a periplasmic production of streptavidin in a soluble form was performed in *E. coli* by using a signal peptide from *bacterial* OmpA<sup>[40]</sup>.

### ***1.1.7 Biotin-(Strept)Avidin Technology***

Owing to its unique and extraordinary characteristics, the biotin-(strept)avidin system has been exploited as important tool in a plethora of medical and biotechnological applications<sup>[41]</sup>.

High stability of biotin-(strept)avidin complex ensured tight connection between biotinylated binders, which are selectively bound to specific targets, and (strept)avidin probes. The combined use of different binders and assorted probes increases the versatility of the system (**Fig. 1.5**)<sup>[42]</sup>.

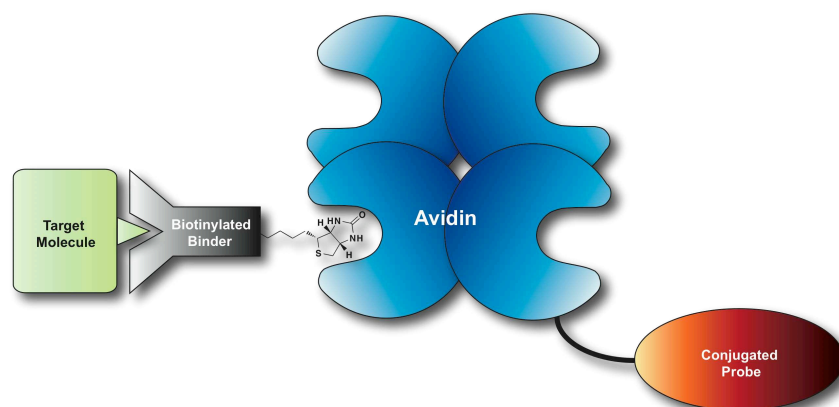


**Fig. 1.5 The essential components of avidin-biotin technology.** Upon binding that involves a biologically active target molecule and a biotinylated binder, avidin probe recognizes specifically this biotinylated complex (modified from Ref. 43) <sup>[42]</sup>

This established solidity has encouraged their use in many biological fields, including affinity chromatography <sup>[43]</sup>, immunoassays <sup>[44]</sup>, affinity cytochemistry and nanotechnology <sup>[45]</sup>.

However, some disadvantages in (strept)avidin-biotin technology may hinder their application. The irreversible binding between (strept)avidin and biotin and the tetrameric avidin tendency to form oligomers can be a drawback <sup>[33, 46]</sup>.

Then, the basic nature of avidin and the presence of carbohydrate moieties may limit the applicability of the system due to rapid clearance of avidin from the blood stream, and to unspecific and unwanted interactions with sugar-binding proteins (*e.g.* lectins) as well as DNA <sup>[47]</sup>.

For these reasons streptavidin, a non-glycosylated and uncharged analogue of avidin, has been selected as alternative in many applications. Nevertheless, streptavidin, more expensive than avidin, also presents its downsides, such as the presence of an Arg-Tyr-Asp sequence <sup>[48]</sup>, responsible for unspecific



interactions with cell surface receptors <sup>[49]</sup>, and high immunogenicity, which limits the application in drug targeting <sup>[50]</sup>.

Therefore, over the years a wide variety of chemically and genetically engineered avidin and streptavidin isoforms have been produced in order to improve their application in biotechnology <sup>[14]</sup> <sup>[51]</sup>.

An exciting exploitation of (strept)avidin-biotin technology is the affinity-based targeting of imaging agents and drugs. Avidin has been used as a tool to transfer a cerebral vasodilator, known as VIPa (Vasoactive Intestinal Peptide analogue), through the blood-brain barrier. A covalent conjugate of avidin and TfRMAb (Transferrin Receptor Monoclonal Antibody) acts as brain drug transport vector, which localizes the complex to the blood-brain barrier (BBB). Upon binding of biotinylated VIPa to avidin, the whole complex is internalized through receptor-mediated endocytosis. Brain-localized disulphide reductases rapidly release VIPa from the complex, activating the drug (**Fig. 1.6**) <sup>[52]</sup>.

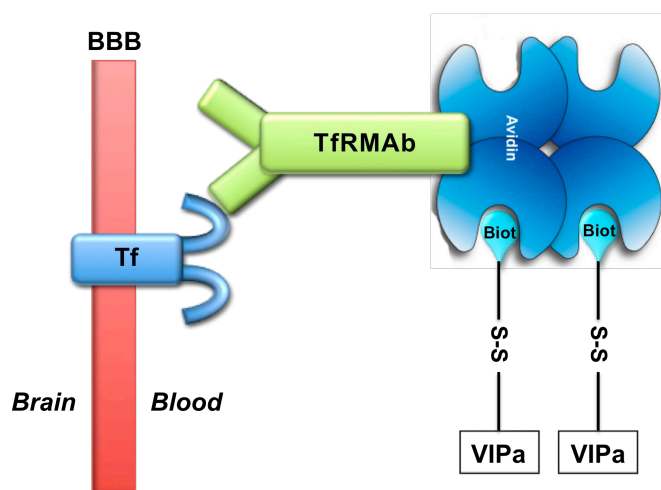


**Fig. 1.6 Avidin and covalently bound TfRMAb as a brain drug transport vector.** Upon interaction between transferrin and its specific antibody, the TfRMAb-avidin complex is localized to the blood-brain barrier. Subsequently, avidin binds to the biotinylated peptide drug and the whole assembly is internalized into the brain (modified from a figure by Bickel *et al.*) <sup>[52-53]</sup>

A further application *in vivo* of avidin and streptavidin as drug carriers is cancer pre-targeting therapy <sup>[54]</sup>. Upon administration, a biotinylated antibody binds to a specific antigen expressed in tumor cells, forming a stable complex. Subsequently, the antigen-antibody complex is recognized by (strept)avidin, which binds to the biotin moiety. A biotinylated radionuclide binds to the (strept)avidin-antibody-antigen assembly with consequent cancer detection and diagnosis, treatment monitoring and some direct therapeutic applications (**Fig. 1.7**) <sup>[54c]</sup>.

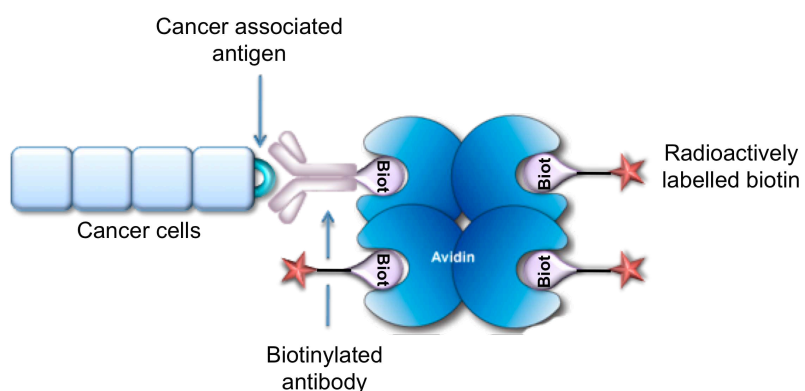


**Fig. 1.7 Immuno-imaging and radiotherapy.** The (strept)avidin-biotin technology is exploited for drug delivery in cancer cells (modified from a figure by Schettlers) <sup>[54a]</sup>

## 1.2 Artificial Metalloenzymes

### 1.2.1 Chirality

“ I call any geometrical figure, or group of points, chiral, and say it has chirality, if its image in a plane mirror, ideally realized, cannot be brought to coincide with itself.” <sup>[55]</sup>. This celebrated statement was attributed to mathematician and physicist Lord Kelvin, who coined the term chirality in 1873. Non-superimposability of the mirror image is a necessary and sufficient condition for chirality.

Nature is chiral. A fascinating example is provided by (+)- and (-)-limonene; these two enantiomers interact differently with the olfactory glands and are responsible for the characteristic orange and lemon smells, respectively <sup>[56]</sup>.

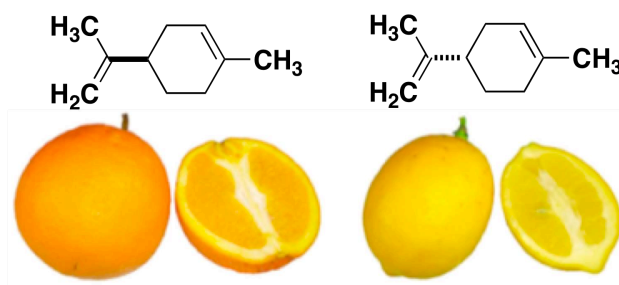


**Fig. 1.8 (R) and (S) enantiomers of limonene.** The naturally occurring (R) and (S) enantiomers of limonene smell of orange and lemon, respectively, since differently recognized by the chiral nasal receptors <sup>[56]</sup> (figure modified from [wheatoncollege website](#))

Many biological molecules, including amino acids, sugars, nucleic acids, vitamins, hormones and alkaloids, exist as one single enantiomer.

Enantiomers interact differently with chiral systems and, for example, two enantiopure components of an asymmetric substrate will interact differently

with a chiral enzyme. This biological phenomenon is called chiral recognition.

Chiral discrimination is of great importance especially in the medical field, since one enantiomer is often pharmaceutically active whereas the other can be inactive or even toxic.

The historical example of thalidomide emphasizes the importance of chirality in the pharmaceutical field. In the early 1960s, thousands of pregnant women took this antiemetic drug as racemic mixture to alleviate morning sickness. Unfortunately, thousands of children were born with severe malformations as a consequence. Only one enantiomer of thalidomide displayed antiemetic activity; the other enantiomer was teratogenic and harmed the developing fetus, causing deformities <sup>[57]</sup>.

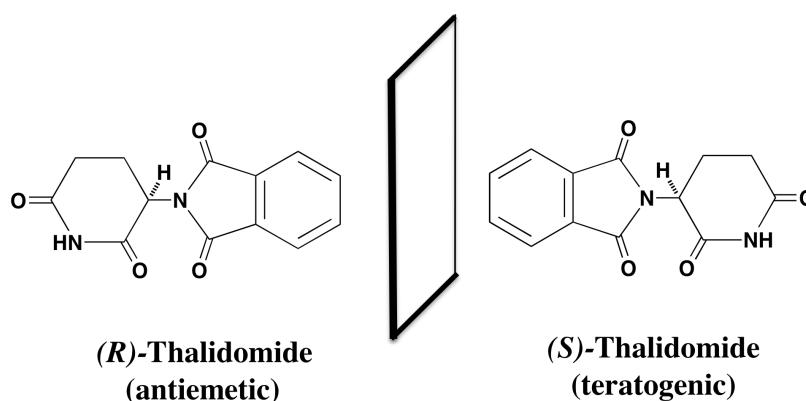


**Fig. 1.9** An example of problems caused by drug administration as racemate. Only the (*S*)-enantiomer of thalidomide caused birth deformities (distomer), while the (*R*)-enantiomer displayed therapeutic activity (eutomer) <sup>[57]</sup>

In the aftermath of the thalidomide tragedy, the USA Food and Drug Administration (FDA) introduced guidelines for the development of new stereoisomeric drugs. The statement required full pharmacological and

toxicological characterization of each enantiomer and encouraged the commercialization of enantiomerically pure drugs <sup>[58]</sup>.

### 1.2.2 Enantioselective Catalysis

First coined by Jöns Jakob Berzelius in 1835, the term catalysis refers to the acceleration of a chemical reaction induced by a substance, known as a catalyst, that participates in the reaction without undergoing any permanent chemical change.

Catalysts provide an alternative mechanism for the reaction, by stabilizing the transition state formed between the reactants and providing a more favorable spatial orientation for product formation <sup>[59]</sup>.

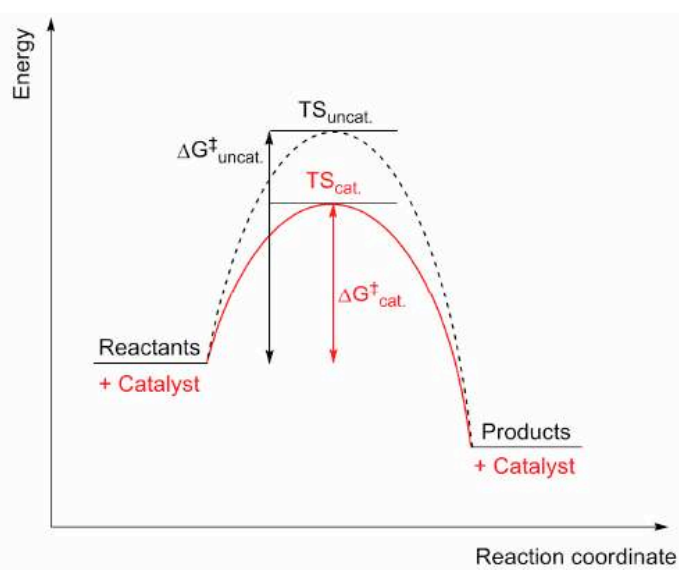


**Fig. 1.10 Stabilization of the transition state (TS) in the presence of a catalyst**

Catalysts change the kinetics of a chemical process, while the overall thermodynamics are maintained: only a thermodynamically favorable reaction can be speeded up by a catalyst.

From a physical viewpoint, catalysts can be divided into two categories <sup>[60]</sup>:

- Homogeneous catalysts: exist in the same phase as reactants and products, these highly efficient catalysts act in mild reaction conditions.
- Heterogeneous catalysts: exist in a different phase than reactants and products. They guarantee easy separation from products.

From a chemical perspective, homogeneous catalysts can be further classified into three different types:

- Organocatalysts: small organic molecules which can act as catalysts.
- Organometallic catalysts: metal complexes with metal-carbon bonds or with ligands such as phosphines, hydrides and amines <sup>[61]</sup>.
- Biocatalysts: biological macromolecules such as enzymes and ribozymes.

Organometallic complexes with chiral ligands around the metal catalyze enantioselective reactions <sup>[62]</sup>.

The trio Knowles-Noyori-Sharpless pioneered the field of asymmetric catalysis and, for this reason, they were awarded the 2001 Nobel Prize in chemistry.

Barry K. Sharpless developed chiral catalysts for asymmetric oxidations such as, for example, chiral epoxidation. An allylic alcohol was catalytically oxidized to the chiral epoxide (*R*)-glycidol using titanium tetra(isopropoxide) and optically active diethyl tartrate ((+)-DET) catalysts <sup>[63]</sup>.

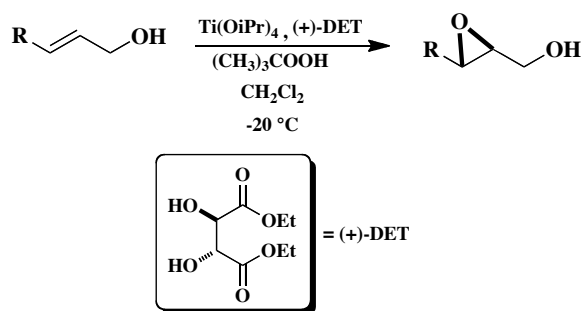


**Fig. 1.11** Asymmetric oxidation of allylic alcohols to chiral epoxides <sup>[63b]</sup>

William Knowles produced the first high enantioselective transition metal catalyst for asymmetric hydrogenation of dehydro amino acids <sup>[64]</sup>. Rhodium complexes containing chiral phosphine ligands were able to catalyze the enantioselective addition of H<sub>2</sub> to a prochiral olefinic substrate, generating a chiral product <sup>[65]</sup>. This process was exploited to produce the anti-Parkinson drug, L-dopa, using the chelating diphosphine ligand (*R,R*)-DIPAMP <sup>[66]</sup>.

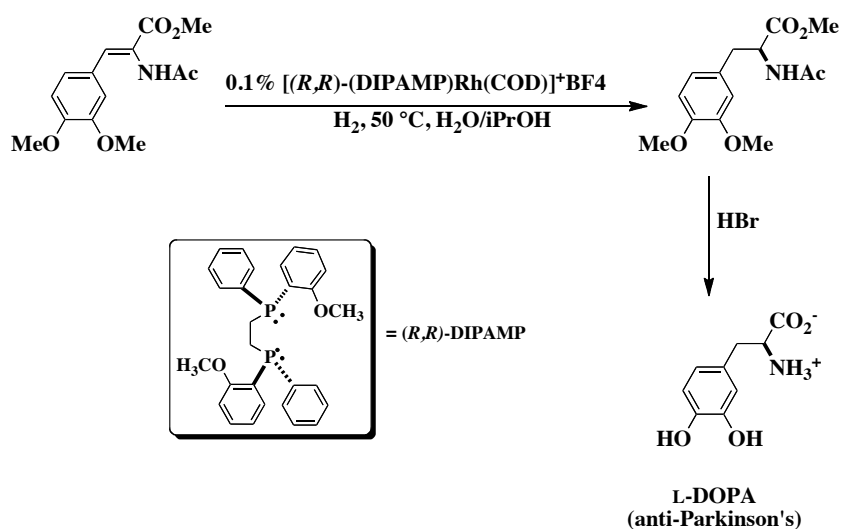


**Fig. 1.12** Enantioselective synthesis of anti-Parkinson L-DOPA <sup>[66b]</sup>

Ryoji Noyori devised highly enantioselective asymmetric hydrogenation reactions <sup>[67]</sup>. This catalytic reaction, performed with (*S*)-BINAP-

ruthenium (II) complex, was exploited for the enantioselective production of the anti-inflammatory drug naproxen <sup>[68]</sup>.

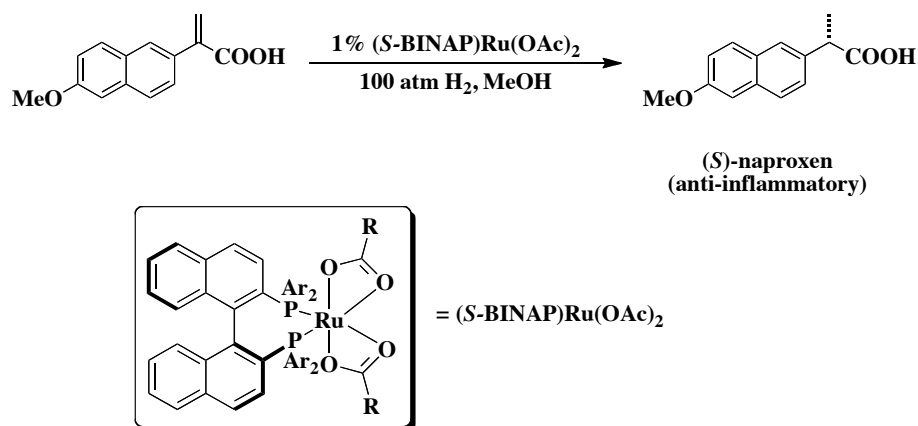


**Fig. 1.13** Enantioselective production of the anti-inflammatory Naproxen <sup>[68b]</sup>

In the past decades, new asymmetric catalysts have been developed through the successful combination of metal centre and ligands, which modulate the steric and electronic properties of the catalyst.

### 1.2.3 Homogeneous vs. Enzymatic Catalysis

In a biomimetic spirit, ligand design was often based on principles from enzymatic reactions, but there are significant differences between homogeneous and enzymatic catalysis <sup>[69]</sup>. Enzymes influence the enantioselectivity of a reaction through the conformation of active site. Their catalytic site can be accessible through a restricted channel, which also controls the selectivity of the reaction.

The first-coordination sphere of the metal in organometallic catalysts influences the enantioselectivity of a reaction as well as providing electronic



and steric control. Solvent, salts and counter ions, constituting the second-coordination sphere also have a steric and electronic influence.

The high specificity of an enzyme often limits the scope of applications, even if the recent directed evolution approach has evolved promiscuous enzymatic activity <sup>[70]</sup>.

Homogeneous catalysts display a large substrate scope and both enantiomers of a chiral product can be produced.

Organometallic catalysts are more suitable for non-polar substances (*e.g.*, H<sub>2</sub>, CO and olefins), whereas biocatalysts are effective with polar substrates (*e.g.*, carbohydrates and biopolymers). Concerning solvent compatibility, enzymes react in aqueous media, while homogeneous catalysts react predominantly in organic solvent.

These features, outlined in the table 1.1, highlight the relative complementarity between homogeneous and enzymatic catalysis <sup>[71]</sup>.

**Table 1.2 Representative features of enzymatic and homogeneous catalysis <sup>[71]</sup>**

	Enzymatic Catalysis	Homogeneous Catalysis
Turnover Number	Large	Small
Optimization	Genetic	Chemical
Substrate Scope	Small	Large
Enantiomers	Single Enantiomer	Access to Both Enantiomers
Reaction Medium	Mostly Aqueous	Mostly Organic

#### ***1.2.4 Artificial Metalloenzymes***

Life depends upon metals. These elements play an important role in the activity of biological macromolecules, acting as electron transfer agents <sup>[72]</sup>.

Metals usually perform their functions in the active sites of enzymes, acting as cofactors. Nitrogen, oxygen or sulfur atoms from polypeptide chains or protein prosthetic groups are involved in metal ion coordination.

Proteins containing a metal ion cofactor (metalloenzymes) function as carrier proteins, signal transduction proteins and enzymes. Metal ions can be attached to the protein active site as part of a prosthetic group, *e.g.* Fe (II) in hemoglobin, or built into the structure of the enzyme molecule, *e.g.* Zn (II) in alcohol dehydrogenase <sup>[73]</sup>.

In enzymes the metal (usually a transition metal) is embedded in a highly organized protein framework, which provides exceptional control through the second coordination sphere.

In the light of the relative complementarity between homogeneous and enzymatic catalysts, much effort has been aimed towards the design of enantioselective artificial metalloenzymes. These hybrid systems combine the principal features of these two catalytic kingdoms.

Artificial metalloenzymes result from the incorporation of an achiral active catalytic moiety into a chiral pocket of the host protein, which provides a well-defined second coordination sphere and controls enantioselectivity .

#### *1.2.4.1 Anchoring of Catalyst into the Protein*

Over the years different strategies, such as covalent and supramolecular approaches, have been applied to anchor the catalytic metal complex into the protein in order to obtain an artificial metalloenzyme <sup>[74]</sup>.

For covalent anchoring, the protein is covalently coupled to an organometallic moiety in order to achieve a hybrid catalyst. As pioneer of this

method, Kaiser demonstrated that “chemical mutations” of specific amino acid residues, close to the active site, lead to a “semisynthetic” enzyme, with different catalytic activity compared to the original protein <sup>[75]</sup>. His main work focused on the conversion of a hydrolytic enzyme (papain) into a semisynthetic oxido-reductase by a covalent linkage of various flavins to the Cys25 of papain <sup>[76]</sup>.

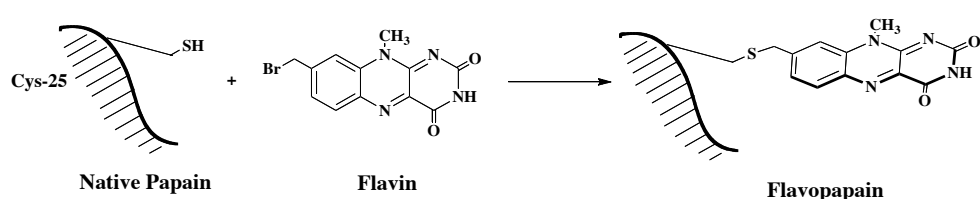


**Fig. 1.14** Covalent modification of Cys25 in the active site of papain by a flavin derivative <sup>[75]</sup>

The resulting flavopapain performed efficient oxidation of *N*-alkyl-1,4-dihydronicotinamides <sup>[76]</sup>.

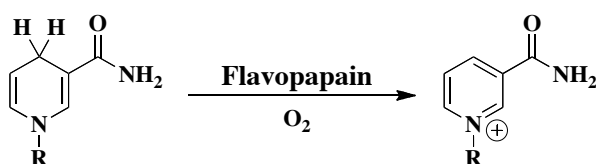


**Fig. 1.15** *N*-alkyl-1,4-dihydronicotinamides oxidation performed by flavopapain <sup>[76]</sup>

Since this work, many other proteins have been covalently modified by incorporating transition metal complexes to yield promising hybrid catalysts. Hilvert developed a methodology to convert the serine-protease subtilisin into an artificial peroxidase through chemical modification of the active site

Ser221 into seleno-cysteine. The resulting seleno-subtilisin catalyzes the stereoselective reduction of racemic hydroperoxides <sup>[77]</sup>.

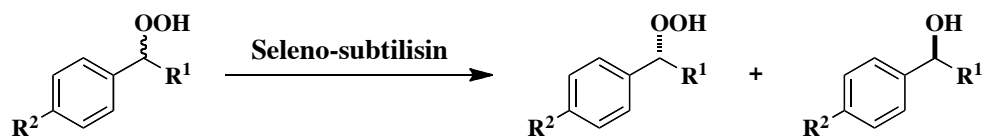


**Fig. 1.16** Asymmetric seleno-subtilisin catalyzed reduction of racemic hydroperoxides <sup>[77b]</sup>

Supramolecular anchoring is a non-covalent approach based on the high affinity between a protein (host) and a small molecule (guest).

Chemical modifications of the guest, such as, for example, introduction of a spacer or modification of the ligand scaffold, ensure the selective attachment of the catalyst into the protein. Protein mutagenesis can be used to optimize artificial metalloenzyme performance through genetic modification <sup>[71, 78]</sup>.

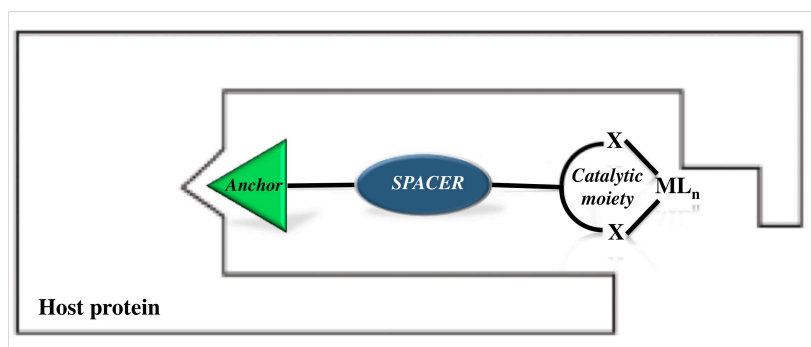


**Fig. 1.17** Supramolecular anchoring of an active catalyst within a host protein. Host protein displays high affinity for the anchor represented by green triangle. Chemo-genetic modifications can improve the performance of the artificial metalloenzyme, without influencing the host-guest binding affinity <sup>[71]</sup>

Serum albumins are plasma transport proteins with high affinity towards different hydrophobic guests. The hydrophobic and chiral pocket provides an asymmetric environment for the transition state. These proteins have been

exploited for the supramolecular incorporation of metal-containing cofactors, for the catalysis of enantioselective reactions.

An asymmetric hydrogenation catalyst introduced by Wilson and Whitesides, in 1978, constituted a turning point in the artificial metalloenzymes field. Avidin was converted into an enantioselective hybrid enzyme by embedding an achiral biotinylated rhodium-diphosphine moiety within the biotin-binding pocket <sup>[79]</sup>.

As Whitesides confirmed, protein chirality can significantly control the enantioselectivity of reactions, and the Rh(I)-diphosphine complex was not inactivated by protein interactions or aqueous solutions.

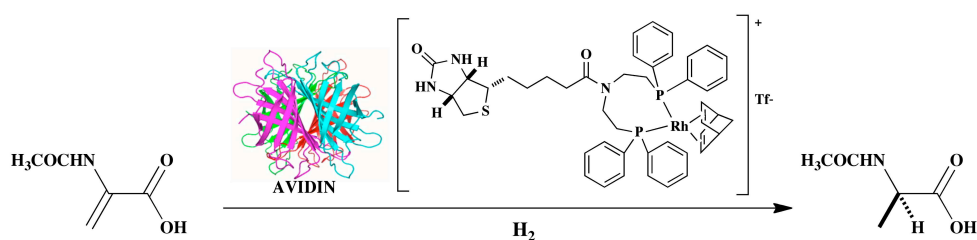


**Fig. 1.18 Asymmetric hydrogenation of *N*-acetamidoacrylate into *N*-acetamidoalanine, catalyzed by Whitesides's system.** The biotinylated rhodium-diphosphine complex embedded into the avidin scaffold is the first example of artificial metalloenzymes based on avidin-biotin technology <sup>[80]</sup>

At the interface between organometallic catalysis and enzymatic chemistry, artificial metalloenzymes represent a complementary approach to asymmetric transformations. Substrate scope and operating conditions are mainly influenced by the catalytic metal-ligand components, while enantioselection depends upon the biomolecular scaffold. Chemo-genetic optimization of this semisynthetic catalytic system can increase the performance of artificial metalloenzymes.

# REFERENCES

- [1] P. György, C. S. Rose, K. Hofmann, D. B. Melville, V. Vigneaud, *Science* **1940**.
- [2] W. R. Streit, P. Entcheva, *Appl. Microbiol. Biotechnol.* **2003**, *61*, 21.
- [3] N. Kresge, R. Simoni, R. Hill, *J. Biol. Chem.* **2004**, *279*, e5.
- [4] P. Gyorgy, C. S. Rose, R. E. Eakin, E. E. Snell, R. J. Williams, *Science* **1941**, *93*, 477.
- [5] R. McMahon, *Annu. Rev. Nutr.* **2002**, *22*, 221.
- [6] J. Knappe, *Annu. Rev. Biochem.* **1970**, *39*, 757.
- [7] R. Rodriguez-Melendez, J. Zempleni, *J. Nutr. Biochem.* **2003**, *14*, 680.
- [8] a)O. Livnah, E. Bayer, M. Wilchek, J. Sussman, *Proc. Natl. Acad. Sci. USA* **1993**, *90*, 5076; b)O. H. Laitinen, A. T. Marttila, K. J. Airene, T. Kulik, O. Livnah, E. A. Bayer, M. Wilchek, M. S. Kulomaa, *J. Biol. Chem.* **2001**, *276*, 8219.
- [9] a)L. Chan, A. R. Means, B. W. O'Malley, *Proc. Nat. Acad. Sci. U.S.A.* **1973**, *70*, 1870; b)B. O'Malley, *Biochemistry* **1967**, *6*, 2546.
- [10] a)H. Nielsen, J. Engelbrecht, S. Brunak, G. v. Heijne, *Protein Eng.* **1997**, *10*, 1; b)V. P. Hytönen, O. H. Laitinen, T. T. Airene, H. Kidron, N. J. Meltola, E. J. Porkka, J. Hörhä, T. Paldanius, J. A. E. Määttä, H. R. Nordlund, *Biochem. J.* **2004**, *384*, 385.
- [11] a)R. Bruch, H. B. White, *Biochemistry* **1982**, *21*, 5334; b)A. T. Marttila, K. J. Airene, O. H. Laitinen, T. Kulik, E. A. Bayer, M. Wilchek, M. S. Kulomaa, *FEBS Lett.* **1998**, *441*, 313.
- [12] A. T. Marttila, O. H. Laitinen, K. J. Airene, T. Kulik, E. A. Bayer, M. Wilchek, M. S. Kulomaa, *FEBS Lett.* **2000**, *467*, 31.
- [13] a)H. R. Nordlund, O. H. Laitinen, S. T. H. Uotila, T. Nyholm, V. P. Hytonen, J. P. Slotte, M. S. Kulomaa, *J. Biol. Chem.* **2003**, *278*, 2479; b)D. Ellison, J. Hinton, S. J. Hubbard, R. J. Beynon, *Prot. Sci.* **1995**, *4*, 1337.
- [14] S. F. Rosebrough, D. F. Hartley, *J. Nucl. Med.* **1996**, *37*, 1380.
- [15] R. Hertz, W. H. Sebrell, *Science* **1942**, *96*, 257.
- [16] H. A. Elo, S. Räisänen, P. J. Tuohimaa, *Cell. Mol. Life Sci.* **2005**, *36*, 312.
- [17] B. Zerega, L. Camardella, S. Cermelli, R. Sala, R. Cancedda, F. Descalzi Cancedda, *J. Cell Sci.* **2001**, *114*, 1473.
- [18] W. A. Hendrickson, A. Pahler, J. L. Smith, Y. Satow, E. A. Merritt, R. P. Phizackerley, *Proc. Nati. Acad. Sci. USA* **1989**, *86*, 2190.
- [19] a)G. P. Kurzban, E. A. Bayer, M. Wilchek, P. M. Horowitz, *J. Biol. Chem.* **1991**, *266*, 14470; b)C. J. van Oss, R. F. Giese, P. M. Bronson, A. Docoslis, P. Edwards, W. T. Ruyechan, *Colloids Surf., B.* **2003**, *30*, 25.
- [20] T. Sano, M. W. Pandori, X. Chen, C. L. Smith, C. R. Cantor, *J. Biol. Chem.* **1995**, *270*, 28204.

- [21] E. A. Bayer, H. Ben-Hur, Y. Hiller, M. Wilchek, *Biochem. J.* **1989**, 259, 369.
- [22] D. S. Wilbur, P. S. Stayton, R. To, K. R. Buhler, L. A. Klumb, D. K. Hamlin, J. E. Stray, R. L. Vessella, *Bioconjugate Chem.* **1998**, 9, 100.
- [23] a)H. R. Nordlund, V. P. Hytonen, O. H. Laitinen, M. S. Kulomaa, *J. Biol. Chem.* **2005**, 280, 13250; b)P. C. Weber, D. H. Ohlendorf, J. J. Wendoloski, F. R. Salemme, *Science* **1989**, 243, 85.
- [24] C. E. Argarana, I. D. Kuntz, S. Birken, R. Axel, C. R. Cantor, *Nucl. Acids Res.* **1986**, 14, 1871.
- [25] a)Y. Eisenberg-Domovich, Y. Pazy, O. Nir, B. Raboy, E. A. Bayer, M. Wilchek, O. Livnah, *Proc. Nat. Acad. Sci. U.S.A.* **2004**, 101, 5916; b)Y. Eisenberg-Domovich, V. P. Hytonen, M. Wilchek, E. A. Bayer, M. S. Kulomaa, O. Livnah, *Acta Crystallogr., Sect. D: Biol. Crystallogr.* **2005**, 61, 528; c)T. Sano, C. R. Cantor, *Proc. Natl. Acad. Sci. USA* **1995**, 92, 3180.
- [26] T. Sano, C. R. Cantor, *Proc. Natl. Acad. Sci.* **1990**, 87, 142.
- [27] L. Pugliese, M. Malcovati, A. Coda, M. Bolognesi, *J. Mol. Biol.* **1994**, 235, 42.
- [28] A. Chilkoti, P. S. Stayton, *J. Am. Chem. Soc.* **1995**, 117, 10622.
- [29] O. H. Laitinen, V. P. Hytönen, H. R. Nordlund, M. S. Kulomaa, *Cell. Mol. Life Sci.* **2006**, 63, 2992.
- [30] L. Le Trong, N. Humbert, T. R. Ward, R. E. Stenkamp, *J. Mol. Biol.* **2006**, 356, 738.
- [31] S. Freitag, I. Le Trong, L. Klumb, P. S. Stayton, R. E. Stenkamp, *Protein Sci.* **1997**, 6, 1157.
- [32] H. R. Nordlund, V. P. Hytönen, J. Hörhä, J. A. E. Määttä, D. J. White, K. Halling, E. J. Porkka, J. P. Slotte, O. H. Laitinen, M. S. Kulomaa, *Biochem. J.* **2005**, 392, 485.
- [33] E. A. Bayer, S. Ehrlich-Rogozinski, M. Wilchek, *Electrophoresis* **1996**, 17, 1319.
- [34] K. J. Airene, C. Oker-Blom, V. S. Marjomäki, E. A. Bayer, M. Wilchek, M. S. Kulomaa, *Protein Expression Purif.* **1997**, 9, 100.
- [35] A. Zocchi, A. Marya Jobé, J. M. Neuhaus, T. R. Ward, *Protein Expression Purif.* **2003**, 32, 167.
- [36] E. E. Hood, D. R. Witcher, S. Maddock, T. Meyer, C. Baszczyński, M. Bailey, P. Flynn, J. Register, L. Marshall, D. Bond, *Mol. Breeding* **1997**, 3, 291.
- [37] R. M. Twyman, E. Stoger, S. Schillberg, P. Christou, R. Fischer, *Trends Biotechnol.* **2003**, 21, 570.
- [38] V. Nagarajan, R. Ramaley, H. Albertson, M. Chen, *Appl. Environ. Microbiol.* **1993**, 59, 3894.
- [39] A. Gallizia, C. d. Lalla, E. Nardone, P. Santambrogio, A. Brandazza, A. Sidoli, P. Arosio, *Protein Expression Purif.* **1998**, 14, 192.
- [40] S. Voss, A. Skerra, *Protein Eng.* **1997**, 10, 975.
- [41] C. T. K. Diamandis E. P., *Clin. Chem* **1991**, 37/5, 625.
- [42] M. Wilchek, E. A. Bayer, *Methods Enzymol.: Avidin-Biotin Technology*, Academic Press, San Diego **1990**, 184, 5.
- [43] E. Morag, E. A. Bayer, M. Wilchek, *Anal. Biochem.* **1996**, 243, 257.
- [44] M. J. Khosravi, R. C. Morton, *Clin.Chem* **1991**, 37/1, 58.

- [45] K. K. Caswell, J. N. Wilson, U. H. F. Bunz, C. J. Murphy, *J. Am. Chem. Soc.* **2003**, *125*, 13914.
- [46] J. K. Rätty, K. J. Airene, A. T. Marttila, V. Marjomäki, V. P. Hytönen, P. Lehtolainen, O. H. Laitinen, A. J. Mähönen, M. S. Kulomaa, S. Ylä-Herttua, *Mol. Therapy* **2004**, *9*, 282.
- [47] V. P. Hytönen, O. H. Laitinen, A. Grapputo, A. Kettunen, J. Savolainen, N. Kalkkinen, A. T. Marttila, H. R. Nordlund, T. K. M. Nyholm, G. Paganelli, *Biochem. J.* **2003**, *372*, 219.
- [48] E. A. B. a. M. W. Ronen Alon, *Biochem. Biophys. Res. Commun.* **1990**, *170*, 1236.
- [49] R. Alon, E. A. Bayer, M. Wichek, *Biochem. Biophys. Res. Commun.* **1990**, *170*, 1236.
- [50] M. Chinol, P. Casalini, M. Maggiolo, S. Canevari, E. S. Omodeo, P. Caliceti, F. M. Veronese, M. Cremonesi, F. Chiolerio, E. Nardone, *Br. J. Cancer* **1998**, *78*, 189.
- [51] O. H. L. Ari T. Marttila, Kari J. Airene, Tikva Kulik, Edward A. Bayer, M. S. K. Meir Wilchek, *FEBS Lett.* **2000**, *467*, 31.
- [52] U. Bickel, T. Yoshikawa, W. M. Pardridge, *Adv. Drug Delivery Rev.* **2001**, *46*, 247.
- [53] W. Pardridge, *Int. Congress Series* **2005**, *1277*, 49.
- [54] a)H. Schettters, *Biomol. Eng.* **1999**, *16*, 73; b)H. Sakahara, T. Saga, *Adv. Drug Delivery Rev.* **1999**, *37*, 89; c)G. Paganelli, C. Grana, M. Chinol, M. Cremonesi, C. De Cicco, F. De Braud, C. Robertson, S. Zurrida, C. Casadio, S. Zoboli, *Eur. J. Nucl. Med. Mol. Imaging* **1999**, *26*, 348.
- [55] L. L. Whyte, *Nature* **1958**, *182*, 198.
- [56] E. Brenna, C. Fuganti, S. Serra, *Tetrahedron-Asymmetry* **2003**, *14*, 1.
- [57] M. Miller, K. Strömmland, *Teratology* **1999**, *60*, 306.
- [58] J. Tomaszewski, M. M. Rumore, *Drug. Dev. Ind. Pharm.* **1994**, *20*, 119.
- [59] a)J. Kraut, *Science* **1988**, *242*, 533; b)L. Young, C. B. Post, *Biochemistry* **1996**, *35*, 15129.
- [60] F. Fache, B. Dunjic, P. Gamez, M. Lemaire, *Top. Catal.* **1997**, *4*, 201.
- [61] H. U. Blaser, A. Indolese, A. Schnyder, *Curr. Sci.* **2000**, *78*, 1336.
- [62] E. N. Jacobsen, A. Pfaltz, H. Yamamoto, *Comprehensive Asymmetric Catalysis*, Springer, Berlin **1999**, I-III.
- [63] a)K. Katsuki, K. B. Sharpless, *J. Am. Chem. Soc.* **1980**, *102*, 5974; b)K. B. Sharpless, *Angew. Chem. Int. Ed.* **2002**, *41*, 2024.
- [64] W. S. Knowles, M. J. Sabacky, *Chem. Commun.* **1968**, 1445.
- [65] W. S. Knowles, *Angew. Chem. Int. Ed.* **2002**, *41*, 1998.
- [66] a)W. S. Knowles, M. J. Sabacky, B. D. Vineyard, *J. Chem. Soc. Chem. Commun.* **1972**, *10*; b)W. S. Knowles, *J. Chem. Educ.* **1986**, *63*, 222.
- [67] R. Noyori, *Angew. Chem. Int. Ed.* **2002**, *41*, 2008.
- [68] a)A. Miyashita, A. Yasuda, H. Takaya, K. Toriumi, T. Ito, T. Souchi, R. Noyori, *J. Am. Chem. Soc.* **1980**, *102*, 7932; b)T. Ohta, H. Takaya, M. Kitamura, K. Nagai, R. Noyori, *J. Org. Chem.* **1987**, *52*, 3176.
- [69] F. Rosati, G. Roelfes, *ChemCatChem* **2010**, DOI: 10.1002/cctc.201000011.
- [70] O. Khersonsky, C. Roodveldt, D. S. Tawfik, *Curr. Opin. Chem. Biol.* **2006**, *10*, 498.



- [71] C. M. Thomas, T. R. Ward, *Chem. Soc. Rev.* **2005**, *34*, 337.
- [72] a)J. LeGall, B. C. Prickril, I. Moura, A. V. Xavier, J. J. G. Moura, H. B. Hanh, *Biochemistry* **1988**, *27*, 1636; b)K. Karlin, *Science* **1993**, *261*, 701.
- [73] D. R. Williams, *Chem. Rev.* **1972**, *72*, 203.
- [74] T. Heinisch, T. R. Ward, *Curr. Opin. Chem. Biol.* **2010**.
- [75] E. T. Kaiser, D. S. Lawrence, *Science* **1984**, *226*, 505.
- [76] C. Radziejewski, D. P. Ballou, E. T. Kaiser, *J. Am. Chem. Soc.* **1985**, *107*, 3352.
- [77] a)Z.-P. Wu, D. Hilvert, *J. Am. Chem. Soc.* **1989**, *111*, 4513; b)Z.-P. Wu, D. Hilvert, *J. Am. Chem. Soc.* **1990**, *112*, 5647.
- [78] T. R. Ward, *Bio-inspired Catalysts*, Springer, Verlag Berlin Heidelberg **2009**.
- [79] T. Heinisch, T. R. Ward, *Curr. Opin. Chem. Biol.* **2009**, *14*, 1.
- [80] M. E. Wilson, G. M. Whitesides, *J. Am. Chem. Soc.* **1978**, *100*, 306.

---

# Chapter 2

## Optimization of Streptavidin Production

*The man of action has  
to believe, the inquirer  
has to doubt – the  
scientific investigator  
is both*

---

Charles Sanders Peirce

### 2.1 Introduction

#### *2.1.1 Directed Evolution and Rational Protein Re-Design*

Protein engineering is a young discipline developed as a means to obtain valuable proteins. By modifying a protein sequence, protein engineering provides modified macromolecules with increased activity or a more comprehensible structure-activity relationship.

Protein engineering methodology entails two general approaches: rational re-design and directed evolution.

Rational re-design is performed by site-directed mutagenesis, a straightforward and inexpensive technique that allows site-specific mutation into the gene encoding for the protein of interest <sup>[1]</sup>.

Since a single point mutation may significantly disrupt protein folding, rational re-design requires large knowledge about protein structure and

sequence-activity relationship. According to rational protein re-design, only “logical” amino acid residues, as for example residues close to the active site or within the binding pocket, are usually modified, in accordance with three dimensional crystal structures <sup>[2]</sup>.

The increasing number of protein structures, solved by NMR spectroscopy or X-ray diffraction, has improved access to public data promoting rational re-design strategy. Furthermore, molecular modeling provides a method to predict the effects of selected mutations on the selectivity, activity or stability of a protein <sup>[3]</sup>.

In contrast, directed evolution, also called molecular evolution or evolutive biotechnology, involves random mutagenesis of the gene of interest to generate mutant libraries <sup>[2]</sup>. This approach requires several rounds of “screening and selection” of mutants with improved features, including an appropriate high throughput screening system for identifying the evolved variants.

Different methods can introduce random mutations into genes. Error-prone polymerase chain reaction (epPCR), based on the error rates of DNA polymerases, represents a milestone in this field. This strategy induces amino acid substitutions in the encoded protein through errors in DNA amplification as a consequence of imperfect reaction conditions (*e.g.* by varying nucleotide ratios or by adding  $Mn^{2+}$  to increase the error-rate or  $Mg^{2+}$  to stabilize non-complementary base-pairs) <sup>[4]</sup>.

Another important methodology exploited in directed evolution to introduce point mutations into genes is known as saturation mutagenesis <sup>[5]</sup>. This approach entails the insertion of codons encoding all possible 20 amino acids

at an established position of the protein, generating a library of 20 protein variants <sup>[6]</sup>.

An alternative strategy to introduce random mutations within the gene generating new proteins with novel activities is DNA shuffling. This strategy, also called “sexual PCR” because it is akin to the generation of genetic diversity during meiosis, involves gene fragmentation by DNase I and subsequent reassembly by PCR <sup>[7]</sup>.

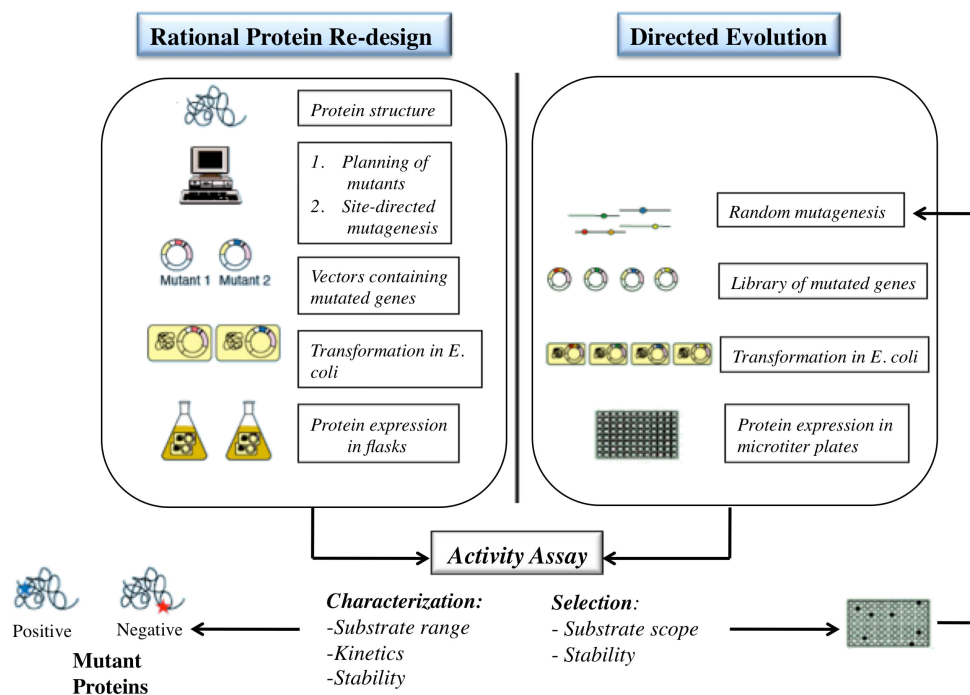


**Fig. 2.1 Rational Protein Re-Design and Directed Evolution.** Rational re-design strategy requires a protein structure to tailor new mutants. After expression in the host organism (*e. g. E. coli*), variants are purified and analyzed for suitable properties. Directed evolution is performed by random mutagenesis, which generates mutant gene libraries. Protein libraries are expressed in the host organism and screened. Selection is based on different parameters, such as substrate scope and protein stability <sup>[2]</sup>

A successful combination of rational re-design and directed evolution offers the exciting possibility to generate mutant gene libraries with desired structural and functional properties <sup>[2]</sup>.

### ***2.1.2 Enantioselectivity of Enzymes Controlled by Directed Evolution***

Asymmetric catalysis is of great importance in the chemical and biotechnological fields, since different agents often exert their specific effect only as enantiopure compounds. Besides organocatalysts, catalytic antibodies and organometallic complexes, enzymes can also perform catalytic transformations with high enantioselectivity <sup>[6]</sup>.

In 1994, Stemmer was the pioneer of *in vitro* DNA shuffling as a method to perform enzyme evolution <sup>[8]</sup>. Native  $\beta$ -galactosidase from *E. coli* is weakly specific for  $\beta$ -D-fucosyl substrates and displayed an enhanced  $\beta$ -fucosidase activity after seven rounds of DNA shuffling and colony screening on chromogenic fucose compounds <sup>[9]</sup>.

In 1998, Kagamiyama modified the substrate specificity of aspartate aminotransferase (AspAT) by directed evolution. Five rounds of DNA shuffling increased the activity of AspAT for the non-native substrates valine and 2-oxovaline <sup>[10]</sup>.

In 2000, Arnold inverted the enantioselectivity of hydantoinase by directed evolution. A combination of random mutagenesis, saturation mutagenesis, and screening led to conversion of the D-selective hydantoinase into an L-selective enzyme, with high-production of L-met <sup>[11]</sup>.

Directed evolution, as a means to control enzymatic activity, also increased the enantioselectivity (E) of a lipase from *P. aeruginosa* in favor of the (*S*)-configured acid (*S*-B) <sup>[6, 12]</sup>.

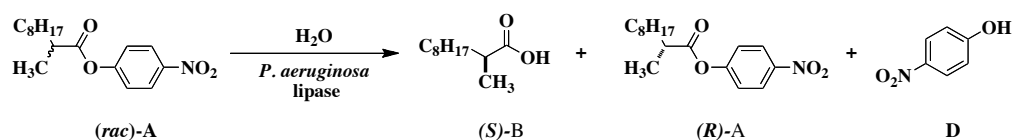


**Fig. 2.2** The hydrolytic kinetic resolution of a chiral ester catalyzed by a lipase from *P. aeruginosa*. The hydrolysis of the chiral ester (*rac*)-A resulted in the (*S*)-acid (*S*-B), the (*R*)-ester (*R*-A) and *p*-nitrophenol (**D**)<sup>[12]</sup>

Reetz subjected the gene encoding the lipase to random mutagenesis by epPCR and saturation mutagenesis. Through four generations of mutant lipases, the *ee* of the reaction increased from 2% to 81% at 25% conversion for the (*S*)-enantiomer, corroborating the validity of this strategy<sup>[12b]</sup>.

### 2.1.3 Chemogenetic Optimization of Artificial Metalloenzymes

Though biocatalysts can perform many enantioselective transformations, several limitations hamper their widespread application in organic chemistry. No enzyme catalyzes reactions such as hydroformylation, allylic substitution, or hydrovinylation<sup>[13]</sup>.

For this reason artificial metalloenzymes, characterized by a homogeneous catalyst embedded within a protein environment, constitute a promising alternative for the synthesis of enantiopure compounds<sup>[14]</sup>.

Inspired by the pioneering work of Whitesides and Wilson<sup>[15]</sup>, our research group improved the enantioselectivity of artificial metalloenzymes by chemogenetic “fine-tuning” of the hybrid catalyst<sup>[16]</sup>.

The hydrogenation of acetamidoacrylic acid, using diphosphine rhodium complexes within streptavidin as host protein, is the first published example of artificial hydrogenases based on biotin-(strept)avidin technology<sup>[17]</sup>. The chemogenetic approach has improved the yields of the reaction through a

combination of rational protein design of the second coordination sphere by site-directed mutagenesis and chemical modification of the homogeneous catalyst.

The substitution of a serine by a glycine residue at position 112 of streptavidin increased the *ee* of the reaction from 94% to 96% in favour of the (*R*)-product. On the contrary, enantioselectivity was reversed to the (*S*)-product by using avidin as host protein <sup>[18]</sup>.

A *meta*-substituted aromatic amino acid spacer ( $4^{meta}$ ) was introduced between biotin and the diphosphine moiety. This [Rh(**Biot-4<sup>meta</sup>**-1)COD]<sup>+</sup> ⊂ WT Sav catalyst afforded (*S*)-reduction products <sup>[14a]</sup>.

#### **2.1.4 First Round Evolution of Artificial Transfer Hydrogenases**

Inspired by Noyori-type asymmetric transfer hydrogenation of ketones <sup>[19]</sup> previous members of our research group invested a significant effort to optimize artificial transfer hydrogenases (ATH) based on the biotin-streptavidin technology.

Biotinylated catalyst precursors ( $[\eta^6\text{-(arene)Ru}(\mathbf{Biot-q-L})\text{Cl}]$ ) were implanted into streptavidin as host scaffold to perform asymmetric transfer hydrogenation reactions <sup>[16c, 20]</sup>.

In Noyori's system, the enantioselectivity of the reduction was indirectly controlled by the enantiopure ligand, which determined the absolute configuration at the Ru centre <sup>[21]</sup>. By contrast, in artificial metalloenzymes, the enantioselection was controlled by second coordination sphere interactions with the metal complex. In the absence of an enantiopure ligand,

the protein scaffold provides a chiral environment. Racemic-reduction product is formed in the absence of streptavidin.

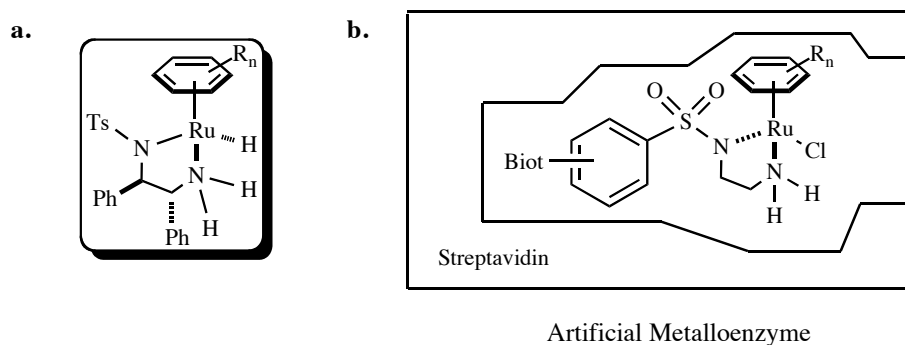


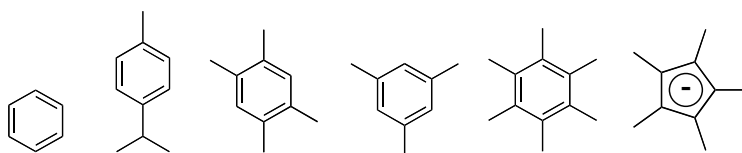
**Fig. 2.3 Schematic representation of a) Noyori's (*R,R*)-TsDPEN catalyst and b) artificial transfer hydrogenases based on biotin-streptavidin technology.** a) (*R,R*)-diamine ligand generates (*S*)-metal and (*R*)-reduction product in Noyori's system; b) ( $[\eta^6\text{-(arene)Ru}(\text{Biot-}q\text{-L})\text{Cl}]$ ) precatalyst (arene = *p*-cymene or benzene, *q* = *ortho*-, *meta*- or *para*-) performs the asymmetric reduction of acetophenone derivatives, in the presence of HCOONa as hydrogen source, B(OH)<sub>3</sub>, MOPS and DMF as buffer and organic co-solvents, when it is embedded into WT Sav scaffold, which determines the enantioselectivity of the reaction <sup>[20, 22]</sup>

A library of hybrid transfer hydrogenases was generated with the aim of optimizing the activity and selectivity of the artificial metalloenzymes, through minimal modifications of three important factors: chemical, genetic and substrate diversity <sup>[20]</sup>.

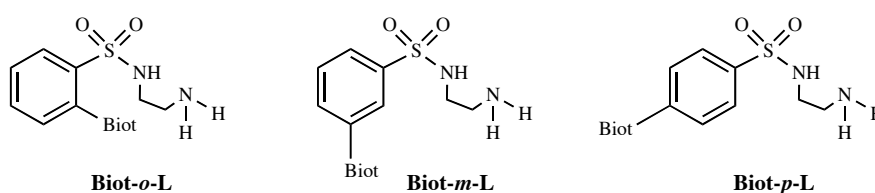
### CHEMICAL DIVERSITY

The chemical diversity was varied as follows:

#### Arene Cap



#### Biotin Anchor Position





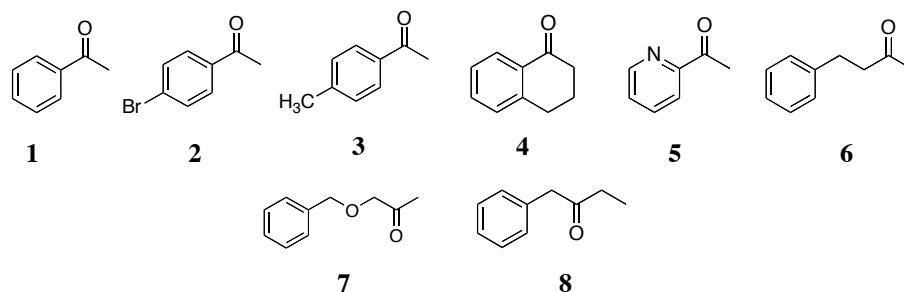
**Metal Centre:** Ru, Rh, Ir

### **GENETIC DIVERSITY**

19 Sav variants were produced by saturation mutagenesis at S112 position.

### **SUBSTRATE SCOPE**

The following substrates were used in transfer hydrogenation reactions catalyzed by artificial metalloenzymes:



#### *2.1.4.1 Chemical Optimization of ATH*

21 catalyst precursors were produced by varying the arene cap, the biotin anchor position and the metal centre. In a first screening, performed in the presence of two streptavidin isoforms (WT and P64G), only five metal complexes, bearing the **Biot-*p*-L** ligand, were found promising for the reduction of acetophenone derivatives **1-3**: ( $[\eta^6\text{-}(p\text{-cymene})\text{Ru}(\mathbf{Biot}\text{-}p\text{-L})\text{Cl}]$ ), ( $[\eta^6\text{-(benzene)}\text{Ru}(\mathbf{Biot}\text{-}p\text{-L})\text{Cl}]$ ), ( $[\eta^6\text{-(durene)}\text{Ru}(\mathbf{Biot}\text{-}p\text{-L})\text{Cl}]$ ), ( $[\eta^6\text{-(C}_5\text{Me}_5)\text{Ir}(\mathbf{Biot}\text{-}p\text{-L})\text{Cl}]$ ) and ( $[\eta^6\text{-(C}_5\text{Me}_5)\text{Rh}(\mathbf{Biot}\text{-}p\text{-L})\text{Cl}]$ )<sup>[16c]</sup>.

#### 2.1.4.2 Saturation Mutagenesis at Position S112

The subsequent optimization involved the second coordination sphere through saturation mutagenesis at position S112 of streptavidin. Docking studies, performed in collaboration with Dr. Sylwester Mazurek at the University of Ljubljana, identified residue S112 for genetic optimization due to close contacts between the side chain and the biotinylated metal.

The most stable docked structure of the artificial transfer hydrogenases [ $\eta^6$ -(*p*-cymene)Ru(**Biot-*p*-L**)H]  $\subset$  WT revealed an average distance Ru-C $_{\alpha}$  < 8 Å for two amino acid residues: S112 and S122. However, position S112 was selected for mutagenesis because its side chain points towards the piano-stool fragment in contrast with serine 122, which is oriented away from the complex (**Fig. 2.4**)<sup>[20]</sup>.

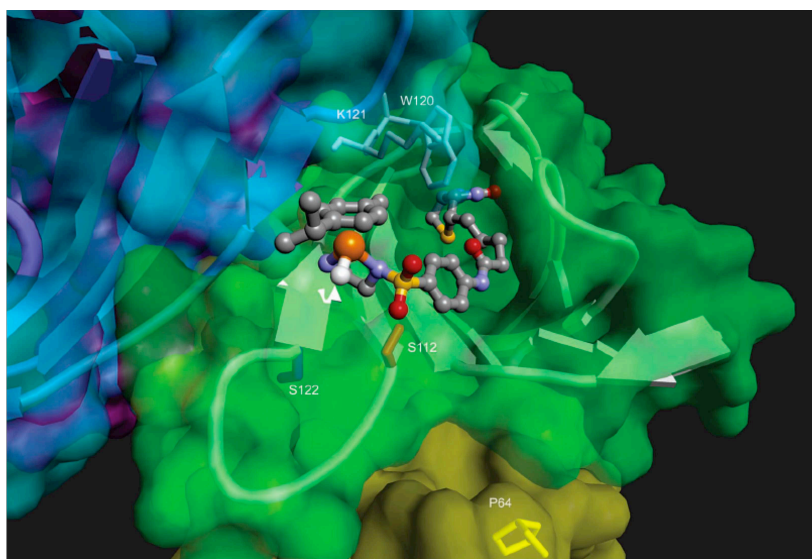


**Fig. 2.4 Docking studies between [ $\eta^6$ -(*p*-cymene)Ru(**Biot-*p*-L**)H] and WT Sav.** The biotinylated ruthenium complex is shown as ball-and-stick. WT streptavidin is represented by blue, green, yellow and violet subunits corresponding to A, B, C and D monomers, respectively. The secondary structure of monomers A and C is schematically drawn. The close lying S112 and S122 residues point towards the piano-stool moiety and away, respectively<sup>[20]</sup>

#### 2.1.4.3 Results of Chemogenetic Optimization

The 20 streptavidin variants derived from saturation mutagenesis at position S112 were evaluated in conjunction with the five most promising metal catalysts for the reduction of acetophenone derivatives **1-3**. The results of this screening were summarized in a fingerprint display, a color-coded format that permits rapid identification of enantioselectivity and conversion of the reaction, depending on substrate-protein-ligand combinations (**Fig. 2.5**).

Chemogenetic optimization evidenced that:

- The capping arene controls the enantioselectivity:  $\eta^6$ -(*p*-cymene)- and  $\eta^6$ -(durene)-complexes afforded (*R*)-reduction products, whereas  $\eta^6$ -(benzene)-complex produced (*S*)-enantiomers.
- Changing the residue of position S112 drastically influenced enantioselectivity and conversion: coordinating residues at position S112 (*e.g.* S112C, S112M, S112D, S112E or S112H) almost completely inhibited the transfer hydrogenation catalyzed by the artificial metalloenzyme, while cationic residues (*e.g.* S112K and S112R) and hydrophobic amino acids (*e.g.* S112Y, S112F, S112V, S112A) favoured (*S*)- and (*R*)-products, respectively, with relatively high conversion.

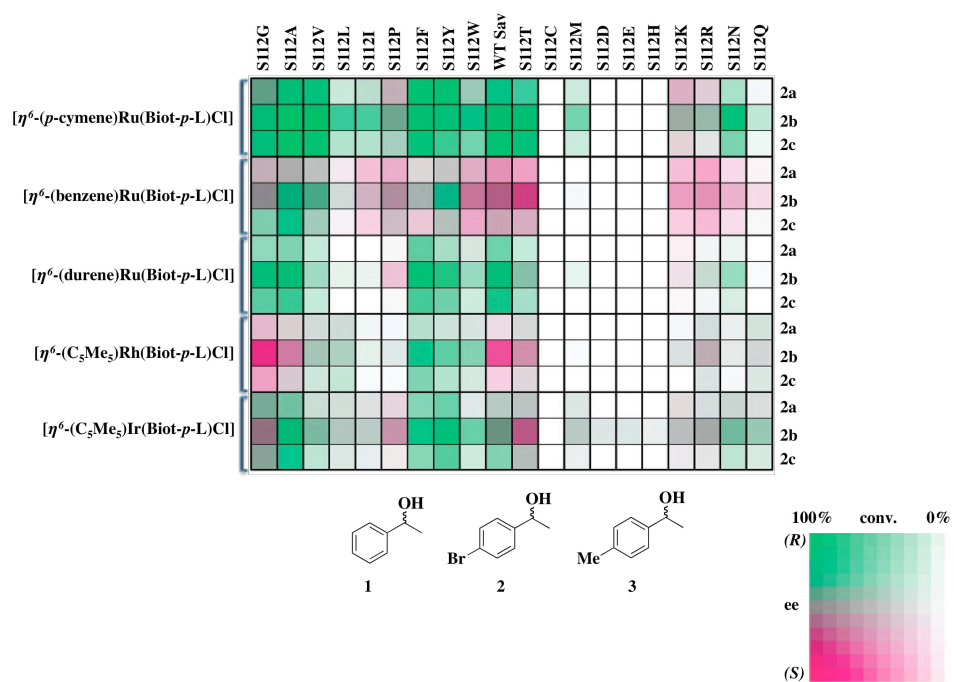


**Fig. 2.5 Fingerprint display of the results for the chemogenetic optimization of the artificial transfer hydrogenases.** Five biotinylated piano-stool ruthenium complexes were incorporated into 20 streptavidin isoforms S112X to perform the transfer hydrogenation of three prochiral ketones: acetophenone **1**, *p*-bromoacetophenone **2** and *p*-methylacetophenone **3** <sup>[20]</sup>

The  $[\eta^6-(p\text{-cymene})\text{Ru}(\text{Biot-}p\text{-L})\text{Cl}]$  was the most promising (*R*)-selective metal complex, while the  $[\eta^6-(\text{benzene})\text{Ru}(\text{Biot-}p\text{-L})\text{Cl}]$  catalyst resulted in (*S*)-products.

### 2.1.5 X-Ray Crystal Structure of an Artificial Transfer Hydrogenase

A structural and functional insight into the hybrid hydrogenase was an essential prerequisite to perform the second round evolution of artificial transfer hydrogenases. For this reason, the most promising hybrid protein catalysts involved in transfer hydrogenation were proposed for crystallization and structural analysis.

In 2007, the catalytically active  $[\eta^6\text{-(benzene)Ru}(\mathbf{Biot-p-L})\text{Cl}]$  was co-crystallized with the S112K streptavidin mutant <sup>[23]</sup>.

The crystal structure was solved by Dr. Isolde Le Trong and Prof. Ronald Stenkamp (University of Washington).

In this discussion of the refined model we focused mainly on the close contacts between the biotinylated Ru complex and amino acid residues in the protein scaffold.

A partial occupancy (only 20%) of the ruthenium complexes could be interpreted in several ways:

- i. Conformational flexibility inside the host protein.
- ii. Ruthenium decomplexation during co-crystallization in the presence of sodium citrate (0.1 M).
- iii. Steric clash between two neighboring biotinylated complexes, simultaneously present in two adjacent subunits of the S112K scaffold.

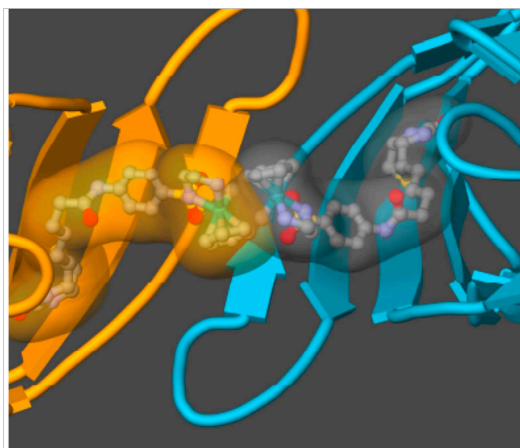


**Fig. 2.6 Close up view of two neighboring biotinylated Ru complexes within two adjacent subunits.** Simultaneous presence of  $[\eta^6\text{-(benzene)Ru}(\mathbf{Biot-p-L})\text{Cl}]$  complex in two adjacent monomers (A and B) of 112K Sav is hindered by close contacts between the two biotinylated complexes. The structural model focuses on the position of the metal moiety, located near a subunit-subunit interface (Ru...Ru distance: 4.44 Å)

This processed model, consistent with the docking results (described in subsection 2.1.4), confirmed the immediate vicinity between amino acid residue S112 and the ruthenium centre.

Other amino acid side chains were shown to lie in the proximity of the biotinylated complex. G48 (in the L3,4 loop) and H87 (in the L5,6 loop) of monomer A interact with the Ru catalyst. Position K121 was of particular interest, as this residue in subunit B (K121<sub>B</sub>) interacts with the  $\eta^6$ -(arene), while K121 of subunit A (K121<sub>A</sub>) may interact with the incoming substrate.

The substrate can also be influenced by interactions with other amino acid residues, identified along the expected trajectory of the substrate (*i.e.* N118, A119, W120 in the L7,8 loop). Additionally, the side chain of residue L124 lies close to the SO<sub>2</sub> moiety (linking the ruthenium piano-stool complex and the biotin anchor). It thus may influence the position of biotinylated ruthenium complex within the hydrophobic pocket.

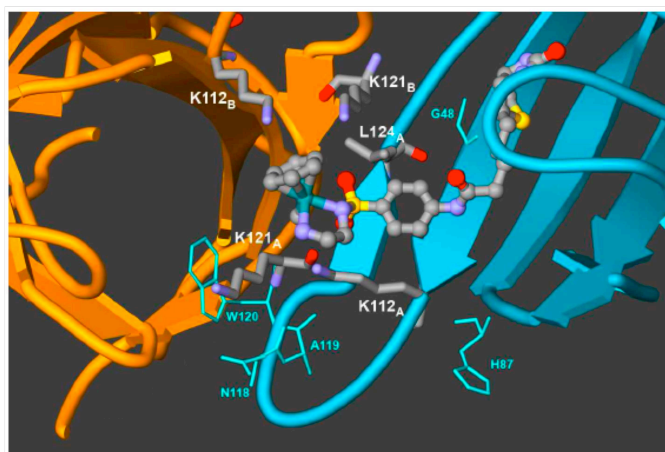


**Fig. 2.7 X-ray crystal structure of  $[\eta^6\text{-(benzene)Ru(Biot-}p\text{-L)Cl}] \subset \text{S112K}$ .** Close up view of the biotinylated ruthenium complex bound to the S112K monomer A (blue) and partially interacting with the other subunit B (orange). Residues K112<sub>A</sub>, K121<sub>A</sub> and L124<sub>A</sub> (monomer A) as well as K112<sub>B</sub> and K121<sub>B</sub> (monomer B), which lie close to the ruthenium metal, are highlighted as sticks. Residues G48, H87, N118, A119 and W120 are depicted as light blue lines

### ***2.1.6 Expression and Purification of T7-Sav in Large-Scale***

Chemogenetic optimization of artificial metalloenzymes requires large amounts of protein to carry out experiments, in the absence of a high-throughput screening (HTS) assay <sup>[14a, 16c, 17]</sup>.

Overexpression of streptavidin in the native host (*i.e. Streptomyces avidinii*) suffers from numerous restrictions including a relatively long time to culture and a final heterogeneous product. For these reasons, previous co-workers have invested much effort to optimize critical parameters of recombinant streptavidin expression in a soluble form.

The choice of *E. coli* as expression strain was motivated by many factors such as, for example, low cost, simple transformation protocol, easy fermentation and high protein yields. However, streptavidin overexpression in *E. coli* leads to several problems, for example, formation of inclusion bodies and biotin depletion, which ultimately inhibits the bacterial growth.

In order to overcome these problems, Dr. Nicolas Humbert in the Ward group carried out several experiments to increase protein solubility and cell growth.

The pET11b-Sav plasmid (provided by Prof. Santambrogio from University of Milan), where the protein gene was cloned between two phage promoters (T7 and T7term) in opposite orientations, was used as expression vector for recombinant T7-tagged streptavidin. This protein construct consists of 159 residues with the first 13 *N*-terminal amino acids replaced by a T7 epitope tag, an immunological marker that increases streptavidin solubility in the cytoplasm of *E. coli*.

The host BL21(DE3)pLysS *E. coli* strain, transformed by the recombinant vector pET11b-Sav, was selected as the system for high-level expression of streptavidin in a soluble form <sup>[24]</sup>.

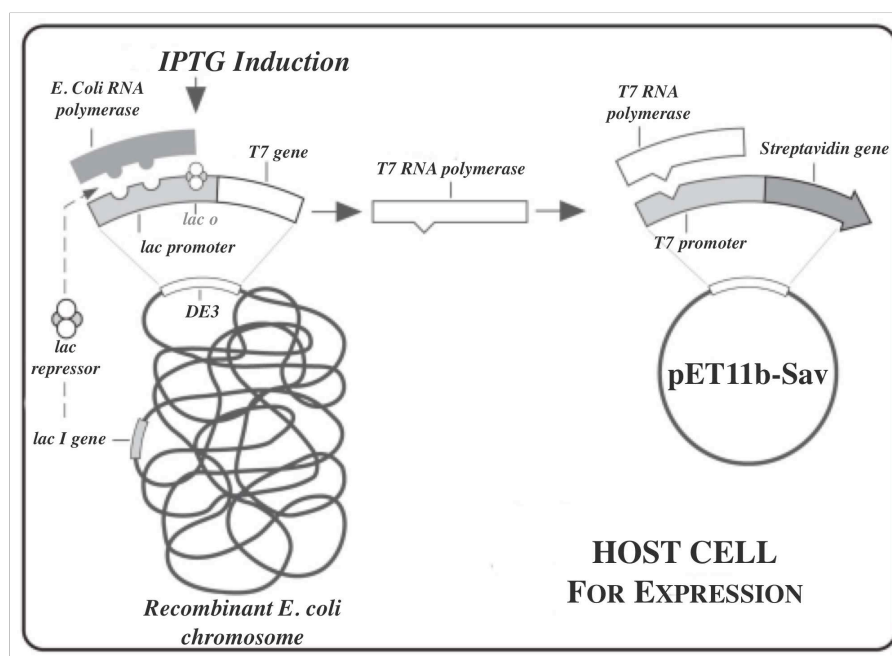


**Fig. 2.8 High-level expression of cloned streptavidin gene controlled by T7 RNA polymerase in BL21(DE3)pLysS *E. coli* strain.** In the absence of IPTG (a molecular mimic of *allo*-lactose), the *lac* repressor binds to the *lac* operon, preventing *E. coli* RNA polymerase binding and, consequently, T7 RNA polymerase and streptavidin gene transcription (figure modified from [sbl website](#))

Bacterial growth was, finally, optimized by raising the temperature from 30 °C to 37 °C.

Under these conditions, cultivation of the cells in a 10L fermentor yielded 230 mg/L of soluble streptavidin <sup>[25]</sup>.

The protein was purified by imino-biotin affinity chromatography. After lyophilisation, the biotin-binding sites were quantified by biotin-4-fluorescein titration <sup>[26]</sup>.

This complete process of streptavidin expression and purification requires a minimum of three weeks and is an extremely time-consuming process.



## **2.2 Aim of the Work**

In the context of artificial metalloenzymes, this work was aimed at improving hybrid catalysts through genetic evolution of the biotin-binding protein scaffold.

The broad aim of this chapter was to explore the influence of the second coordination sphere on enantioselective trends and catalytic performance of artificial transfer hydrogenases.

Having identified by X-ray crystallography two additional close lying residues, we speculated that saturation mutagenesis at those positions (K121 and L124) could improve the performance of the hybrid catalysts involved in the transfer hydrogenation through a “designed” evolution scheme.

To achieve this goal, we strived to implement a straightforward protein production and purification scheme, amenable to HTS.

For this purpose both streptavidin immobilization and thermal treatment of crude cell extracts were investigated.

## **2.3 Results and Discussion**

### ***2.3.1 Saturation Mutagenesis at Positions K121 and L124***

The X-ray crystal structure, described in subsection 2.1.5, provided a fascinating description of a hybrid catalyst involved in the transfer hydrogenation, highlighting the organization of the active site and the interactions between the ruthenium complex and protein scaffold.

Further rounds of optimization of the artificial metalloenzyme were performed by “designed evolution”. This term, coined by Dr. Marc Creus, alludes to a combination of rational choices related to metal ligands and protein residues with rounds of screening in order to fine-tune the best catalytic features that are unpredictable *a priori* <sup>[27]</sup>.

To implement “designed evolution” we selected the (*R*)- and (*S*)-selective variants (112A Sav and 112K Sav, respectively, identified in the first optimization round, see subsection 2.1.4), and additionally targeted two of the close-lying amino acid residues identified in the crystal structure.

The first chemogenetic optimization step yielded high (*R*)-selective and moderate (*S*)-selective combinations for the reduction of aromatic ketones. In contrast, very modest selectivities were obtained for the reduction of dialkyl ketones.

A designed evolution approach was performed to improve the enantioselectivity of enantioselective artificial transfer hydrogenases and to generate novel systems for the reduction of challenging dialkyl ketones.

Saturation mutagenesis at position S112 revealed a modest influence on dialkyl substrates. The enantiodiscrimination was weakly controlled by the interactions between dialkyl substrates and side chains at position 112.

Therefore, we performed a saturation mutagenesis at two unexplored positions of particular interest: K121, which possibly interacts both with the  $\eta^6$ -arene (K121<sub>B</sub>) and with the substrate (K121<sub>A</sub>) as well as L124, which may alter the position of the metal complex within the hydrophobic pocket.

Saturation mutagenesis at positions K121 and L124 was carried out in collaboration with Dr. Anita Ivanova and Dr. Marc Creus, by using the genetic

backgrounds of WT Sav (to generate single mutants) and S112A Sav or S112K Sav (to generate double mutants) for a total of 117 Sav isoforms.

For the second evolution round we chose the S112A mutant for its promising (*R*)-selectivity for the reduction of acetophenone derivatives as well as the S112K mutant for its promising (*S*)-selectivity.

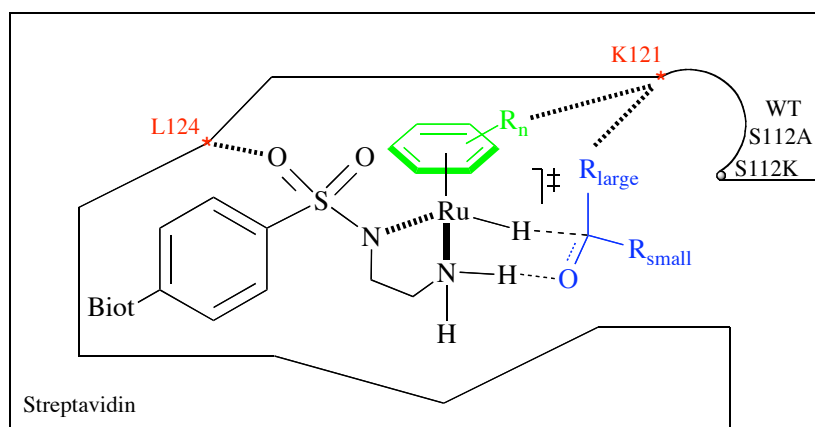


**Fig. 2.9** Second coordination sphere interactions between protein scaffold, biotinylated ruthenium catalyst and substrate

A total of 117 streptavidin isoforms were produced and screened in combination with either  $[\eta^6\text{-}(p\text{-cymene})\text{Ru}(\text{Biot-}p\text{-L})\text{Cl}]$  or  $[\eta^6\text{-}(\text{benzene})\text{Ru}(\text{Biot-}p\text{-L})\text{Cl}]$  complexes, for the reduction of *p*-bromoacetophenone **2** and 4-phenyl-2-butanone **6** (see subsection 2.1.4).

The successful insertion of mutations into the plasmids was verified by two methods: a restriction digest, to detect an inserted silent mutation (24/117 plasmids were analyzed), and DNA sequencing (Microsynth, Switzerland) (14/117 different plasmids were tested). Results confirmed a successful insertion in > 90% of mutations of the sequence analyzed.

### ***2.3.2 Streptavidin Isoforms Expression in Small-Scale Cell Culture***

The first round of ATH screening was performed with 3-4 mg (per catalytic experiment) of each of the 20 purified streptavidin mutants (S112X).

The second screening experiments called for a HTS approach to test the most promising catalysts in combination with the 117 protein variants. Indeed, the large-scale expression and purification was too lengthy to produce and purify these 117 mutants.

Thus, streptavidin production was scaled-down from 10 L of *E. coli* cell culture (previously performed in a 10 L fermentor) to 50 mL of culture (carried out in 250 mL baffled Erlenmeyer flasks).

However, high levels of protein expression were an important prerequisite to perform a HTS strategy.

Hence, in close collaboration with Dr. Anita Ivanova and Dr. Marc Creus, we optimized critical parameters of small-scale streptavidin expression.

Many variables, including medium, volume, speed, temperature and glucose supplement to cell culture, were reassessed and improved.

We devised a screening strategy for the selection of the most suitable medium for streptavidin expression, which led to the choice of Tryptone Phosphate (TP) Broth.

Different shaking-speeds and thermal conditions were screened to fine-tune high-yields streptavidin expression. At the end, cultures were incubated on an orbital shaker (415 rpm) and grown in baffled Erlenmeyer flasks for 6 hrs at 34.5 °C, in the absence of glucose supplement.

Harvested cells were frozen-thawed and resuspended in 1.5 mL of extraction buffer (pH 7.4) in the presence of DNase1. Pooled supernatants were titrated

for biotin-fluorescein binding activity in 96-well plates, from which the concentration of free streptavidin active sites was calculated.

The 117 Sav isoforms were directly screened for catalysis as crude cell extracts, alleviating the time-consuming process of protein purification and lyophilization.

Typically, 100 mL of culture (*e.g.* 2 x 50 mL) was sufficient for catalysis, although 24/117 new mutants did not express sufficient soluble protein for catalytic reactions and were not tested further.

Expression levels of single and double mutants per volume of culture are summarized in a fingerprint display.

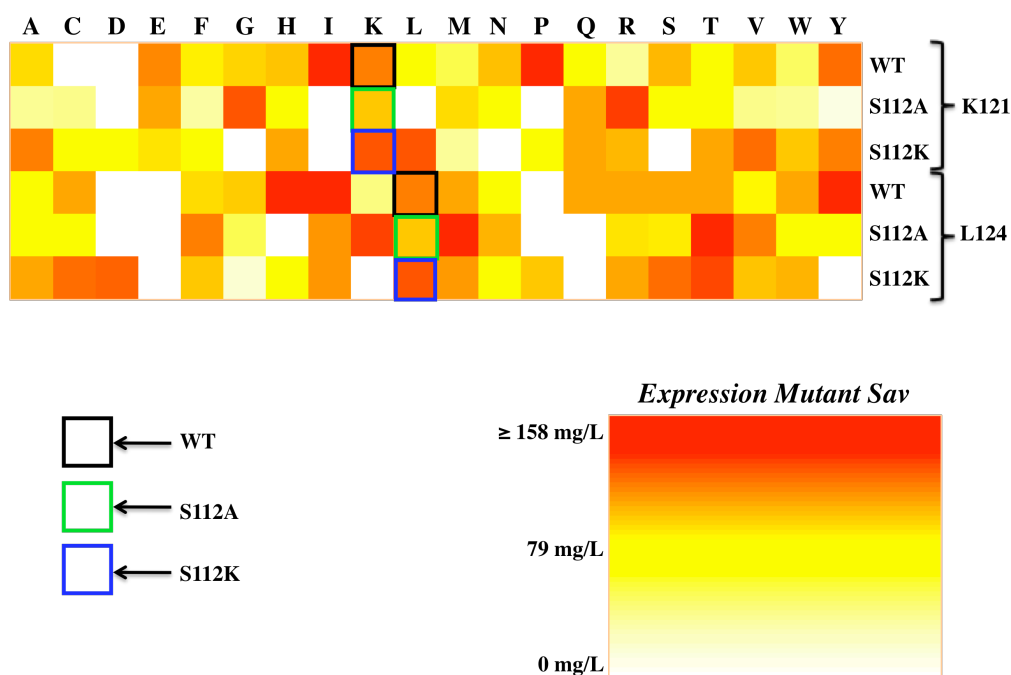


**Fig. 2.10 Expression levels of streptavidin isoforms per volume of culture.** Pooled extracts from a minimum of 100 mL cultures were titrated for biotin-fluorescein binding activity in 96-well plates. The active-site concentration was determined using a B4F titration<sup>[26]</sup>

### 2.3.3 Immobilization as HTS Approach

The presence of catalyst inhibitors in the cell extract has hampered the screening of crude cell supernatants for their catalytic performance in the presence of biotinylated catalysts.

Thus far, only pure streptavidin samples gave active metalloenzyme systems. However, the long streptavidin purification protocol represents a bottleneck for the evolution round and, *ipso facto*, a new production and purification protocol was sought to test the 117 new Sav mutants.

We addressed this challenge in collaboration with Dr. Anca Pordea and Mr. Thibaud Rossel (Ward group) by performing a Sav immobilization protocol with biotin-sepharose. In this straightforward approach streptavidin isoforms were directly immobilized from crude cell extract thanks to the exquisite affinity of the protein for biotin.

The tetrameric structure of streptavidin allowed to utilize one biotin-binding site for immobilization on biotin-sepharose, leaving the other three biotin-binding sites free to accommodate biotinylated catalyst.

The immobilized streptavidin was initially washed with guanidinium chloride (1 M) to remove other bacterial proteins and was mixed with the most promising precursor complexes ( $[\eta^6\text{-(benzene)Ru(Biot-}p\text{-L)Cl}]$  or  $[\eta^6\text{-(}p\text{-cymene)Ru(Biot-}p\text{-L)Cl}]$ ). In the presence of  $\text{HCOONa} \cdot \text{B(OH)}_3$  mixture as hydrogen source and substrates **2** and **6** (see subsection 2.1.4), catalysis was performed at 55 °C for 64 hrs.

Although the purification-immobilization strategy slightly compromised activity and selectivity of the transfer hydrogenation reaction, this protocol allowed a rapid screening to identify trends.

The enantioselective trends, observed with the immobilized ATH and summarized in a fingerprint display, revealed that:

- The capping arene influences enantioselectivity of the reaction. The substitution of  $\eta^6$ -(*p*-cymene) by  $\eta^6$ -(benzene) moiety results frequently in an inversion of the absolute configuration of the product.
- The artificial metalloenzymes incorporating S112A mutation give better enantioselectivities than WT and S112K derived isoforms.
- Saturation mutagenesis at position K121 brings more diversity than mutations in positions L124, probably due to the influence of the K121 side chain both on the piano-stool moiety and on the trajectory of incoming substrate.

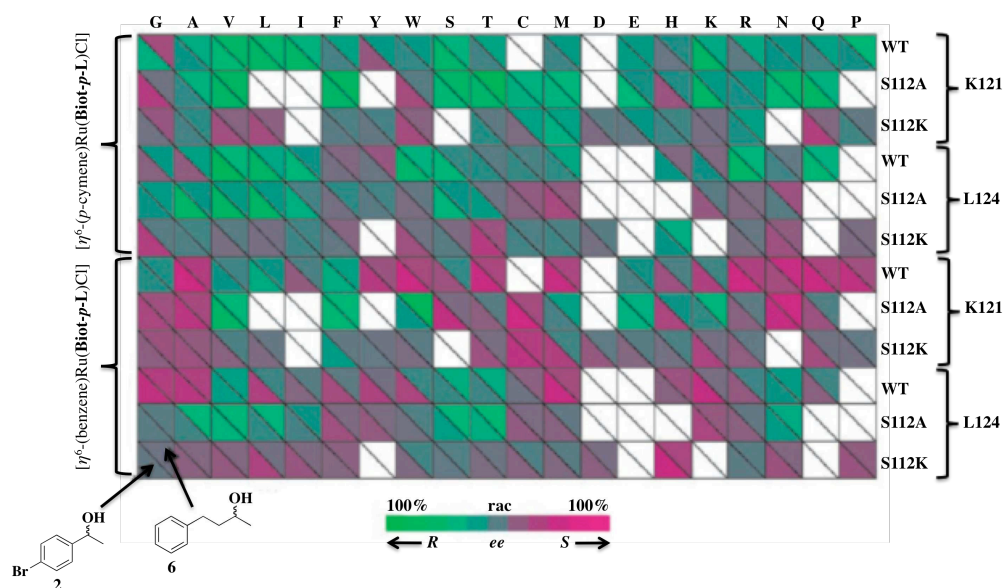


**Fig. 2.11 Fingerprint display of results for the chemogenetic optimization of immobilized ATH.** Catalyses were performed on crude cell extracts in the presence of biotin-sepharose-immobilized ATH. The most promising (*S*)- and (*R*)-selective precatalysts,  $[\eta^6$ -(benzene)Ru(**Biot-*p*-L**)Cl] and  $[\eta^6$ -(*p*-cymene)Ru(**Biot-*p*-L**)Cl] respectively, were incorporated in 117 streptavidin isoforms to perform the asymmetric reduction of two substrates (**2** and **6**)<sup>[23]</sup>

The most promising results in term of enantioselectivity and conversion were reproduced with purified streptavidin mutants. In most cases, an increase in *ee* and activity was observed with the purified protein.

### ***2.3.4 Thermo-denaturation as Straightforward Purification Strategy***

#### ***2.3.4.1 Thermo-Stability of Pure Streptavidin Variants***

Another strategy aimed at simplifying the lengthy streptavidin purification and, consequently, at maximizing high throughput catalytic screening was based on a thermo-denaturation protocol. This approach was inspired by Reetz's suggestion, where a thermo-stable enzyme (tHisF), easy to purify, was selected as scaffold for hybrid catalysts <sup>[28]</sup>.

We reasoned that the high thermal stability of streptavidin could be exploited to purify the protein by simple heat treatment <sup>[29]</sup>.

However, thermo-modification of the protein scaffold could negatively affect performance of artificial metalloenzymes in several transformations.

Thus, first we investigated thoroughly the relationship between heating and pure streptavidin folding and catalytic performance on pure streptavidin samples.

Three pure streptavidin isoforms were heated at increasing temperature for 5, 10 and 30 minutes. Long exposition-time and high temperature modified quaternary protein structure, as monitored by B4F titration <sup>[26]</sup> and SDS-PAGE assay.



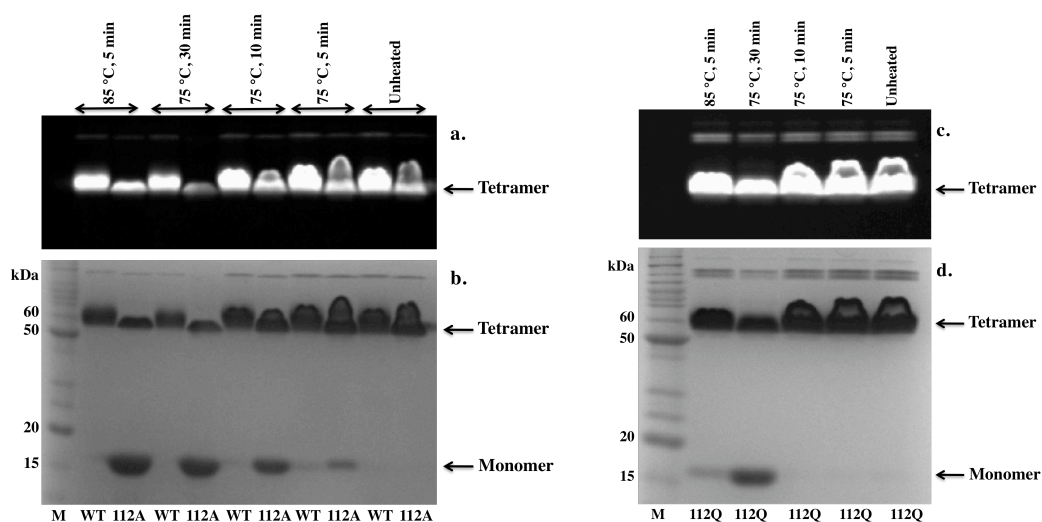


**Fig. 2.12 Thermo-stability of pure streptavidin variants monitored by non-denaturing SDS-PAGE.** After heat treatment, heated supernatants were loaded into the gels. From left to right temperature and exposition-time were reduced. a) and c) electrophoretic assays highlight biotin-fluorescein binding activity of proteins. The activity is compromised at 85 °C-5 min and at 75 °C-30 min, as evidenced by reduced fluorescence. b) and d) gels were stained in Coomassie Blue. The destaining reveals that tetrameric form of S112A and S112Q mutants is converted into monomer at 85 °C-5 min and at 75 °C-30 min

As template, we chose artificial allylic alkylases to perform catalytic reaction after heat treatment on pure streptavidin samples. “Fitness” of these hybrid catalysts was compromised by high temperature, as revealed by a reduced enantioselectivity (**Table 2.1**), which is consistent with loss of free active sites (**Table 2.1**) as well with a weak biotin-affinity (**Fig. 2.12**) observed after thermo-denaturation.

**Table 2.1 Results of [Pd(Ph<sub>2</sub>Allylic)Cl]<sub>2</sub> – catalyzed asymmetric allylic alkylation performed in the presence of heated pure protein.** Sav-WT was chosen as reference scaffold, whereas S112A and S112Q were selected, respectively, as the most promising (*R*)- and (*S*)-selective protein host, under standard conditions

<i>Entry</i>	<i>Protein</i>	<i>Condition</i>	<i>Active Site</i>	<i>ee</i> [%]	<i>Conv</i> [%]
1		Standard	3.6	65	87
2		75 °C, 5 min	3.6	65	86
3	<b>WT</b>	75 °C, 10 min	3.6	64	85
4		75 °C, 30 min	3.6	30	77
5		85 °C, 5 min	3.6	34	77
6		Standard	4	92	90
7		75 °C, 5 min	4	92	87
8	<b>S112A</b>	75 °C, 10 min	2	93	88
9		75 °C, 30 min	< 1.6	27	82
10		85 °C, 5 min	< 1.6	37	80
11		Standard	4	-35	99
12		75 °C, 5 min	4	-33	98
13	<b>S112Q</b>	75 °C, 10 min	4	-35	99
14		75 °C, 30 min	2.8	-19	89
15		85 °C, 5 min	4	-35	99

These trials provided useful information to perform a correct protocol of streptavidin purification based on thermo-denaturation on cellular extracts containing streptavidin.

Since high temperature destabilizes streptavidin mutants, we selected moderate conditions for thermal treatment of cell lysates in order to preserve protein folding and potentially high catalytic performance.

#### 2.3.4.2 Hybrid Catalysts in Crude Cell Extract

After these preliminary trials on heat-denaturation of pure streptavidin, we investigated streptavidin purification in cell extract via thermo-treatment

ranging from 65 °C to 95 °C. Different cellular components, such as unwanted mesophilic proteins, were removed by this step.

After expression, the cell lysate was exposed to high temperature for 10 minutes and the resulting cloudy suspension was centrifuged to separate the pellet from the supernatant.

Heated supernatants were loaded on polyacrylamide gels, which revealed high protein purity and strong biotin-fluorescein binding activity. The pellets were also analyzed and revealed increasing amounts of inactive monomer in a background of many protein species.

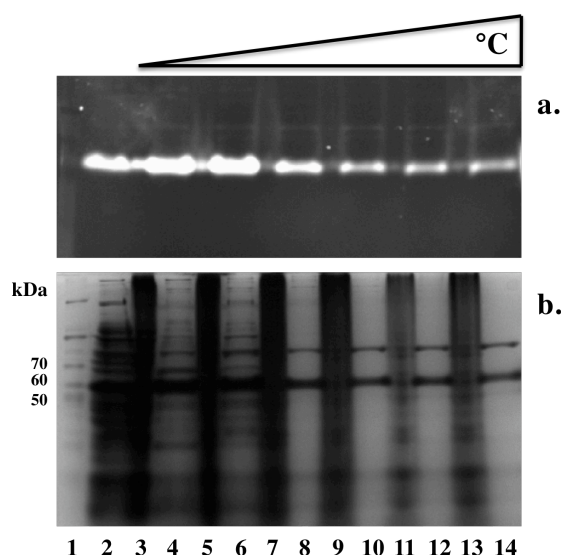


**Fig. 2.13 Thermo-denaturation as purification strategy estimated by non-denaturing SDS-PAGE.** The polyacrylamide gel was run after heating ranging from 65 °C to 95 °C for 10 minutes. Lane 1: protein marker (220 kDa). Lane 2: crude cell extract before heating. Lanes 3, 5, 7, 9, 11, 13: pellet after heat-treatment at different temperature (65 °C, 71 °C, 77 °C, 83 °C, 89 °C, 95 °C, respectively). Lanes 4, 6, 8, 10, 12, 14: supernatant post heating at different temperature (65 °C, 71 °C, 77 °C, 83 °C, 89 °C, 95 °C, respectively). Gel a. reveals B4F binding activity of streptavidin, which is compromised at very high temperature due to protein denaturation. Gel b. highlights increasing level of streptavidin purity in supernatant at rising temperature

Thus, the results of SDS-PAGE suggested that heat treatment of supernatants from cell lysates yielded reasonably pure streptavidin. We anticipated that this

straightforward purification protocol might be used to significantly simplify the screening effort.

Contrary to enzymes, which are naturally evolved as biocatalysts in living cells, organometallics and artificial metalloenzymes are not designed to catalyse reactions *in vivo* or in the presence of cell debris.

The presence of many cellular components, such as thiols, anionic nucleic acids or other metal-binders, can inhibit catalysis in crude cell extract.

However, stimulated by this challenging perspective and encouraged by recent work of Streu and Meggers, who described a “ruthenium-induced allylcarbamate cleavage in living cells”, we tested artificial metalloenzymes using crude cell extract <sup>[30]</sup>.

In 2009 Adriaenssens *et al.* published the first example of catalyzed C-C bond formation in *E. coli* cell lysate <sup>[31]</sup>. Consequently, we chose palladium-catalyzed asymmetric allylic alkylation as the reaction to be performed directly in heated crude cell extract, in collaboration with Mr. Cheikh Lo (Ward group)

[14c]

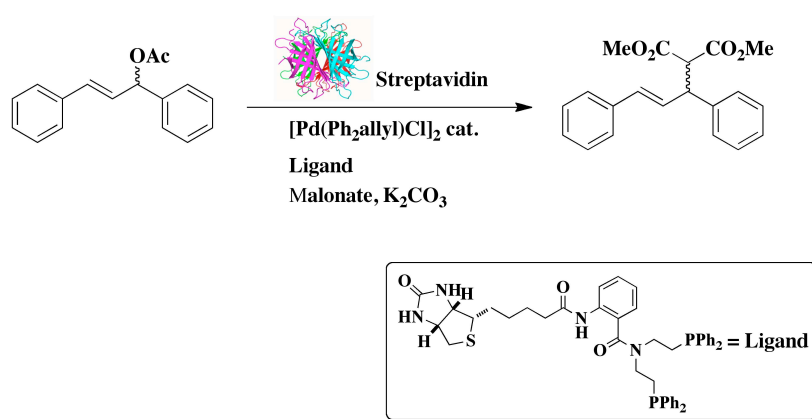


Fig. 2.14 Asymmetric allylic alkylation catalyzed by artificial metalloenzymes <sup>[14c]</sup>

The results of catalytic runs are summarized in Table 2.2. In light of the disappointing results obtained with heat-treated cell supernatants, we hypothesized that:

- i. The presence of DNA may inhibit catalysis
- ii. The presence of glutathione may also poison the precious metal <sup>[32]</sup>.

To alleviate these potential metal-binding macromolecules, the cell lysates were treated with DNaseI and dialysed against mQ-H<sub>2</sub>O, thus removing all low molecular weight species.

Despite these additional purification steps, the results remained disappointing, revealing a drastic reduction of catalytic activity (conversion) in crude cell extract.

These reactions were performed under classical conditions, although slightly more dilute. Dilution was necessary owing to a low streptavidin concentration in the crude cell extract.

**Table 2.2 Results of [Pd(Ph<sub>2</sub>Allylic)Cl]<sub>2</sub> – catalyzed asymmetric allylic alkylation performed in heated crude cell extract.** Catalysis performed in H<sub>2</sub>O in the absence of streptavidin leads to formation of racemic-allylic product with a modest conversion (entry 1). Pure streptavidin variants, acting as protein scaffold, afford enantioselective allylic alkylase in H<sub>2</sub>O (entries 2, 9, 12). Low conversion is constantly observed in the presence of crude cell extract expressing streptavidin. “Empty” extract is defined as *E. coli* cell extract not-expressing streptavidin, but from cells containing the plasmid without a gene insert, treated in the same way as for cells expressing Sav

<i>Entry</i>	<i>Protein (Sav)</i>	<i>Condition</i>	<i>ee[%]</i>	<i>Conv[%]</i>
1		Metal complex	2	39
2	<i>No</i>	Catalyst in crude "empty" extract	57	3.1
3		Catalyst in heated "empty" extract (75 °C, 10')	4	3.0
4		Catalyst in heated "empty" extract (75 °C, 10', dialysis)	3	25
5		Catalyst into pure streptavidin	79	59
6		Catalyst in crude extract	68	0.8
7		Catalyst in heated extract (75 °C, 10')	71	1.0
8	<i>WT</i>	Catalyst in heated extract (75 °C, 30')	62	2.9
9		Catalyst in heated extract (75 °C, 10', dialysis)	79	3.0
10		Spiking with pure protein (75 °C, 10')	57	1.4
11		Spiking with pure protein (75 °C, 10', dialysis)	78	5
12		Catalyst into pure streptavidin	91	98
13	<i>S112A</i>	Catalyst in heated extract (75 °C, 30')	9	15
14		Spiking with pure protein (75 °C, 10', dialysis)	89	9
15		Catalyst into pure streptavidin	-31	100
16	<i>S112Q</i>	Catalyst in heated extract (75 °C, 30')	40	1.0
17		Spiking with pure protein (75 °C, 10', dialysis)	34	22

On the basis of this screening, several features were identified:

- High conversion was observed when the catalytic reaction was performed in H<sub>2</sub>O in the presence of homogeneous catalyst (entry 1) as well as artificial allylic alkylase (entries 5, 12, 15), even under diluted conditions.
- The presence of crude cell extract inhibited catalysis in all cases, as confirmed by a very low conversion (entries 2, 3, 6, 7, 8, 9, 10, 11, 13, 14, 16, 17).

- Reduced catalytic activity was also observed with spiked protein on crude cell extract (entries 10, 11, 14, 17). This result confirmed a clear correlation between low conversion and components present in the cell lysate.
- No (*S*)-alkylation product, which is normally favoured by S112Q mutant (entry 15), was observed in the presence of *E. coli* cell lysate, expressing S112Q isoform (entries 16, 17) <sup>[14c]</sup>.

Compared to catalytic experiments using pure protein under otherwise identical conditions (concentration, temperature, pH, etc.), the results with thermo-treated cell lysates were disappointing (compare Table 2.1 and Table 2.2).

Catalytic inhibition could be related to the presence of unknown high-molecular-weight molecules (*e.g.* liposome or nucleic acids), which absorb at 250 nm, as revealed by the UV-VIS. A possible interaction between these macromolecules and the artificial metalloenzymes could hinder the reaction.

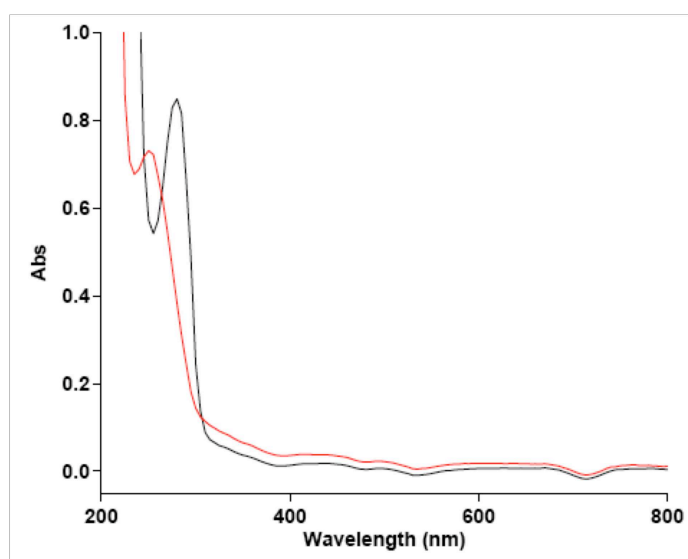


**Fig. 2.15 Adsorption spectrum (800-200 nm) of pure streptavidin and crude cell extract.** The black spectrum is typical of a pure protein, absorbing at 280 nm (final concentration 5  $\mu\text{M}$ ). The red spectrum, resulting from cell extract analysis, displays a maximum at 250 nm, which suggests the presence of unknown non-protein components. In cell lysate, the protein peak (0.11  $\mu\text{M}$ ), whose presence is confirmed by SDS-PAGE, is masked by the large peak at 250 nm

Extraction with organic solvents (*n*-butanol and ethyl acetate) was the last attempt aimed at removing eventual lipids from crude cell extract, which did not improve, however, catalytic activity. For all these reasons, we decided to shelve this challenging project.

#### 2.3.4.3 Streptavidin Refolding

As previous trials revealed, streptavidin is stable under thermal denaturation. Comparing thermal stability of three streptavidin isoforms (WT, S112A, S112Q), we identified a thermal vulnerability of S112A and S112Q mutants, whose tetrameric form is converted into monomer at 75 °C, and a highly stable tetrameric structure of WT, whose transition temperature (from tetramer to monomer) is superior to 90 °C.

A closely packed  $\beta$ -barrel may also warrant high stability of streptavidin over wide pH and in the presence of chaotropic reagents.

Over decades many researchers have carefully investigated relationship between denaturant agents and streptavidin integrity.

In 1990 Sano and Cantor argued that high concentrations of urea (6 M) induced conversion of tetrameric streptavidin into two dimers<sup>[33]</sup>. In 1991 this finding was refuted by Kurzban, who claimed the stability of the tetrameric form even in the presence of 6 M urea<sup>[34]</sup>.

Inspired by these findings, we tested streptavidin denaturation conditions, leading to full denaturation of the protein. This required protein dissolution in guanidinium chloride (6 M, pH 1.5) and heating at 95 °C for 5 minutes.

Previously in the group, denaturation was performed by a dialysis treatment in guanidinium chloride (6 M, pH 1.5) at room temperature, which was believed to



lead to streptavidin unfolding and biotin release <sup>[25]</sup>. Probably, extreme pH and chaotropic agent weakened biotin-binding affinity, but they did not affect tetrameric structure of streptavidin as revealed by SDS-PAGE assays.

A denaturation process implies inevitably a protein refolding protocol. Properly folded proteins can be produced from denatured proteins or naturally insoluble aggregates.

Genetic modifications of streptavidin revealed that point mutations could drastically affect protein solubility. For this reason, heterologous expression of streptavidin mutants leads sometimes to the formation of insoluble forms, called inclusion bodies <sup>[35]</sup>.

In collaboration with Ms. Karoline Kersten we performed expression of streptavidin mutant N23A/S27D/S45A, selected for its reduced biotin-affinity ( $K_d = 1.2 \cdot 10^{-3} \text{ M}$ ), which led to the formation of inclusion bodies, as revealed by SDS-PAGE assay.

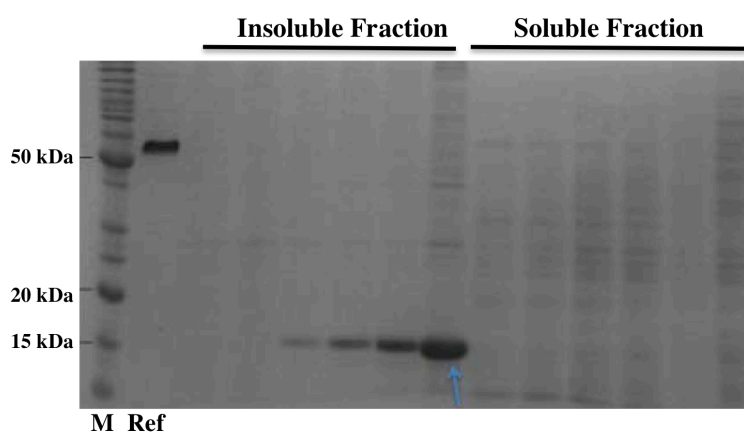


**Fig. 2.16 Heterologous expression of N23A/S27D/S45A mutant as inclusion body in the cytoplasm of *E. coli*, monitored by non-denaturing SDS-PAGE.** Lane 1, protein marker (220 kDa). Lane 2, protein reference, represented by Sav-His tagged, which is a soluble and tetrameric variant of streptavidin. Insoluble fractions, taken during culture, display increasing concentrations of streptavidin mutant as monomer, after IPTG induction. Soluble fractions are completely devoid of this protein

Refolding of this insoluble mutant was performed at 4 °C by adding the unfolded protein into the vortexing PBS, not in Tris/HCl (20 mM, pH 7.4) as proposed by previous co-workers [25]. Electrophoretic assays revealed the presence of a refolded tetrameric protein (N23A/S27D/S45A) in the supernatant fraction, after Coomassie staining (**Fig. 2.17b**) and a low biotin-affinity even in the active form, as confirmed by absence of B4F fluorescence (**Fig. 2.17a**).

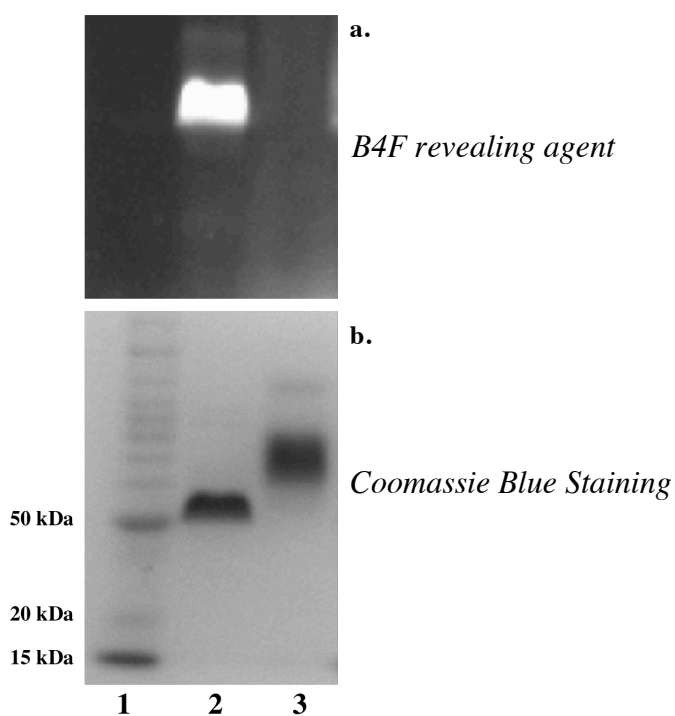


**Fig. 2.17 Successful refolding of N23A/S27D/S45A mutant, monitored by electrophoretic assay.** Lane 1, protein marker (220 kDa). Lane 2, Sav-His tagged as reference. Lane 3, refolded mutant N23A/S27D/S45A, displaying weak biotin affinity as revealed by B4F agent (gel a.) and a tetrameric structure (gel b.)

### ***2.3.5 High-Throughput Expression in 96-Well Plate***

Over the years, we implemented evolutionary approach on streptavidin framework to provide hybrid protein catalysts “made to order”.

However, finding improved variants in the immensity of protein space is a major challenge. Even a small change in sequence can be deleterious for protein expression and solubility, as revealed in fingerprint display of the level expression for 117 streptavidin isoforms in fig. 2.10.

To simplify streptavidin selection of the most promising mutants, protein expression was performed in 96-well plate with optimized characterization of protein. This high throughput system allowed a rapid screening of a streptavidin library to select the most promising mutants for high-level expression and biotin-binding, monitored by straightforward SDS-PAGE assays.

Exploration of distant “functional space” in streptavidin network led, for example, to useful variants, which are very different from wild-type protein. We introduced a phenotypic diversity by means of large mutations on the flexible loop L3,4 that is close to the binding site. This diversity was easily accessed by the new high-throughput approach, which identified two highly diversified variants (48T-49K-50N-51P mutant and 48T-49D-50P-51G mutant) with high expression and biotin binding activity.

Amino acid residues G48-N49-A50-E51 were randomly replaced by T-K-N-P in the homonymous mutant and T-D-P-G in the other one. Their high levels of expression revealed that the loop structure is not so critical for streptavidin folding. For this reason, this functional space can be explored to afford improved scaffold for hybrid protein catalysts.

In contrast, this new approach focused also on unsuccessful expression of different streptavidin isoforms, such as mutants at position H87. This amino acid residue is critical for streptavidin folding, as revealed by SDS-PAGE of H87 mutants performed after 96-well plate expression.

The power of pre-selection was linked with an optimized combinatorial screening of hybrid catalysts library.

In recent years, Dr. Nicolas Humbert (from Ward group) strove to express streptavidin in 96-well plate, but inadequate shaking and insufficient aeration hindered a successful result.

A 96-*deep* well plate with tips inside during culture was found to significantly increase the production levels thus allowing a faster screening approach to assess production levels of streptavidin mutants.

## **2.4 Materials and Methods**

### ***2.4.1 Chemicals***

Solvents used were all of analytical grade. All solutions were prepared using deionised water.

**Table 2.3 List of chemical and supplier**

<b>Chemical</b>	<b>Supplier</b>
Acrylamide	
Glucose	
SDS	
Chloramphenicol	
Ampicillin	AppliChem
PMSF	
IPTG	
Glycerol	
Tris	
Bactoyeast extract	Merck
Bactotryptone	BD
NaCl	
DMSO	
DTT	
KH <sub>2</sub> PO <sub>4</sub>	Fluka
Coomassie Brilliant Blue	
Triton X-100	
Lysozyme (from egg white)	
TEMED	
Acetic acid	VWR
Urea	
APS	
Na <sub>2</sub> HPO <sub>4</sub>	Sigma
B4F	
DNaseI	
Guanidinium/HCl	Acros Organics
BenchMark™ Protein Ladder	Invitrogen
Bromophenol Blue	Riedel-de Haën
dNTP	Promega
DpnI	
DNA ladder	Biolabs
Pfu Turbo	Stratagene

### ***2.4.2 Technical Equipment***

- Protein expression in 20 L of *E. coli* cell culture was performed in a fermentor NLF22 (Bioengineering®).
- Protein expression in 50 mL of *E. coli* cell culture was performed in 250 mL baffled Erlenmeyer flasks within an incubator shaker (New Brunswick Scientific Co Inc, USA).
- Protein expression in 96-well plate was performed in an incubator shaker (Ecotron®, Switzerland).
- PCR was performed in an eppendorf mastercycler gradient
- DNA concentration was determined by nanodrop 1000 spectrophotometer (Thermo Fisher Scientific).
- SDS-PAGE was analyzed with Molecular Image Gel Doc XR (Bio-Rad®, Switzerland).
- Protein was lyophilized in a lyophilizer FreeZone 2.5 L (benchtop of Labconco, USA).
- The active sites of proteins were determined with the Fluorescence Reader Safire (Tecan®)
- FPLC was performed by using äkta prime machine

### ***2.4.3 Mutagenesis***

Site-directed mutagenesis was carried out using the Quick-Change mutagenesis kit (Stratagene, Switzerland) on the pET11b-Sav plasmid. The forward (positive) and the reverse (negative) primers were partially overlapped with each other and fully complementary at the mutation site.

In many cases, a silent *ScaI* restriction site was introduced to distinguish mutated clones from the template DNA.

Saturation mutagenesis at positions K121 and L124 was carried out by using the genetic background of WT Sav (to generate single mutants) and S112A Sav or S112K Sav (to generate double mutants) for a total of 117 Sav isoforms.

**Table 2.4 List of mutagenic primers used for saturation mutagenesis on positions K121 and L124**

<b>Mutation</b>	<b>Primers (5'-3')</b>	<b>Silent Mutation</b>
K121A	<i>Upper</i> GCCTGGGCGTCCACGCTGGTCGGCCACGACACC	None
	<i>Lower</i> CGTGGACGCCAGGCGTTGGCCTCGGTGGTGCC	
K121E	<i>Upper</i> GCCTGGGAGTCCACGCTGGTCGGCCACGACACC	None
	<i>Lower</i> CGTGGACTCCCAGGCCTTGGCCTCGGTGGTGCC	
K121Y	<i>Upper</i> GCCTGGTATTCCACGCTGGTCGGCCACGACACC	None
	<i>Lower</i> CGTGAATACCAGGCGTTGGCCTCGGTGGTGCC	
K121G	<i>Upper</i> CGCCTGGGGGAGTACTCTGGTCGGCCACGACACC	None
	<i>Lower</i> GCCGACCAGAGTACTCCCCAGGCGTTGGCCTCGG	
K121T	<i>Upper</i> CGCCTGGACGAGTACTCTGGTCGGCCACGACACC	ScaI
	<i>Lower</i> GCCGACCAGAGTACTCGTCCAGGCGTTGGCCTCGG	
K121V	<i>Upper</i> CGCCTGGGTGAGTACTCTGGTCGGCCACGACACC	ScaI
	<i>Lower</i> GCCGACCAGAGTACTCAGCCAGGCGTTGGCCTCGG	
K121W	<i>Upper</i> CGCCTGGTGGAGTACTCTGGTCGGCCACGACACC	ScaI
	<i>Lower</i> GCCGACCAGAGTACTCCACCAGGCGTTGGCCTCGG	

K121M	<i>Upper</i> CGCCTGGATGAGTACTCTGGTCGGCCACGACACC <i>Lower</i> GCCGACCAGAGTACTCATCCAGGCGTTGGCCTCGG	ScaI
K121Q	<i>Upper</i> CGCCTGGCAGAGTACTCTGGTCGGCCACGACACC <i>Lower</i> GCCGACCAGAGTACTCTGCCAGGCGTTGGCCTCGG	ScaI
K121R	<i>Upper</i> CGCCTGGAGGAGTACTCTGGTCGGCCACGACACC <i>Lower</i> GCCGACCAGAGTACTCCTCCAGGCGTTGGCCTCGG	ScaI
K121C	<i>Upper</i> CGCCTGGTGCAGTACTCTGGTCGGCCACGACACC <i>Lower</i> GCCGACCAGAGTACTGCACCAGGCGTTGGCCTCG	ScaI
K121H	<i>Upper</i> CGCCTGGCACAGTACTCTGGTCGGCCACGACACC <i>Lower</i> GCCGACCAGAGTACTGTGCCAGGCGTTGGCCTCG	ScaI
K121I	<i>Upper</i> CGCCTGGATCAGTACTCTGGTCGGCCACGACACC <i>Lower</i> CCAGAGTACTGATCCAGGCGTTGGCCTCGGTGG	ScaI
K121P	<i>Upper</i> CGCCTGGCCGAGTACTCTGGTCGGCCACGACACC <i>Lower</i> GCCGACCAGAGTACTCGGCCAGGCGTTGGCCTCG	ScaI
K121D	<i>Upper</i> CGCCTGGGACAGTACTCTGGTCGGCCACGACACC <i>Lower</i> GCCGACCAGAGTACTGTCCCAGGCGTTGGCCTCG	ScaI
K121N	<i>Upper</i> CGCCTGGAACAGTACTCTGGTCGGCCACGACACC <i>Lower</i> GCCGACCAGAGTACTGTTCCAGGCGTTGGCCTCG	ScaI
K121L	<i>Upper</i> CGCCTGGTTGAGTACTCTGGTCGGCCACGACACC <i>Lower</i> GCCGACCAGAGTACTCAACCAGGCGTTGGCCTCG	ScaI
K121S	<i>Upper</i> CGCCTGGTCGAGTACTCTGGTCGGCCACGACACC <i>Lower</i> GCCGACCAGAGTACTCGACCAGGCGTTGGCCTCG	ScaI
K121F	<i>Upper</i>	ScaI



	CGCCTGGTTCAGTACTCTGGTCGGCCACGACACC <i>Lower</i> GCCGACCAGAGTACTGAACCAGGCGTTGGCCTCG	
L124Q	<i>Upper</i> GGAAGAGTACTCAGGTCGGCCACGACACCTTCACC <i>Lower</i> CCGACCTGAGTACTCTTCCAGGCGTTGGCCTCGGTG	ScaI
L124S	<i>Upper</i> GGAAGAGTACTTCGGTCGGCCACGACACCTTCACC <i>Lower</i> CCGACCGAAGTACTCTTCCAGGCGTTGGCCTCGGTG	ScaI
L124T	<i>Upper</i> GGAAGAGTACTACGGTCGGCCACGACACCTTCACC <i>Lower</i> CCGACCGTAGTACTCTTCCAGGCGTTGGCCTCGGTG	ScaI
L124V	<i>Upper</i> GGAAGAGTACTGTGGTCGGCCACGACACCTTCACC <i>Lower</i> CCGACCACAGTACTCTTCCAGGCGTTGGCCTCGGTG	ScaI
L124W	<i>Upper</i> GGAAGAGTACTTGGGTCGGCCACGACACCTTCACC <i>Lower</i> CCGACCCAAGTACTCTTCCAGGCGTTGGCCTCGGTG	ScaI
L124I	<i>Upper</i> GGAAGAGTACTATCGTCGGCCACGACACCTTCACC <i>Lower</i> CCGACGATAGTACTCTTCCAGGCGTTGGCCTCGGTG	ScaI
L124M	<i>Upper</i> GGAAGAGTACTATGGTCGGCCACGACACCTTCACC <i>Lower</i> GGCCGACCATAGTACTCTTCCAGGCGTTGGCCTCGG	ScaI
L124N	<i>Upper</i> CTGGAAGAGTACTAACGTCGGCCACGACACCTTCACC <i>Lower</i> GGCCGACGTTAGTACTCTTCCAGGCGTTGGCCTCGGCG	ScaI
L124R	<i>Upper</i> GGAAGAGTACTCGGGTCGGCCACGACACCTTCACC <i>Lower</i> CCGACCCGAGTACTCTTCCAGGCGTTGGCCTCGGTG	ScaI
L124C	<i>Upper</i> GGAAGAGTACTTGCCTCGGCCACGACACCTTCACC <i>Lower</i> CCGACGCAAGTACTCTTCCAGGCGTTGGCCTCGGTG	ScaI
L124F	<i>Upper</i> GGAAGAGTACTTTCGTCGGCCACGACACCTTCACC <i>Lower</i> CCGACGAAAGTACTCTTCCAGGCGTTGGCCTCGGTG	ScaI

L124H	Upper GGAAGAGTACTCACGTCGGCCACGACACCTTCACC Lower CCGACGTGAGTACTCTTCCAGGCGTTGGCCTCGGTG	ScaI
L124A	Upper GCCTGGGCGTCCACGCTGGTCGGCCACGACACC Lower CAGCGTGGACGCCCAGGCGTTGGCCTCGGTGG	None
L124G	Upper GGAAGTCCACGGGGGTCGGCCACGACACCTTCACC Lower CGTGGCCGACCCCCGTGGACTTCCAGGCGTTGGCC	None
L124P	Upper GGAAGAGTACTCCGGTCGGCCACGACACCTTCACC Lower GCCGACCGGAGTACTCTTCCAGGCGTTGGCCTCGG	ScaI
L124K	Upper CCAACGCCTGGAAGAGTACCAAGGTCGGCCACGACACC Lower GCCGACCTTGGTACTCTTCCAGGCGTTGGCCTCGGTGG	ScaI
L124Y	Upper GGAAGTCCACGTATGTCGGCCACGACACCTTCACC Lower CGTGGCCGACATACGTGGACTTCCAGGCGTTGGCC	None
L124E	Upper GGAAGTCCACGGAGGTCGGCCACGACACCTTCACC Lower GGCCGACCTCCGTGGACTTCCAGGCGTTGGCCTCGG	None

The PCR results were verified on a 1.2% agarose gel containing 1X Tris-Borate-EDTA (TBE) buffer. Ultra-competent XL1-Blue *E. coli* cells (in house) were transformed by PCR product and the plasmids were extracted from bacteria with a *Promega miniprep* kit (Promega®).

The successful insertion of mutations into the plasmids was verified by two methods: a restriction digest, to detect an inserted silent mutation (24/117 plasmids were analyzed), and DNA sequencing (Microsynth®, Switzerland) (14/117 different plasmids were tested). Results confirmed a successful insertion in > 90% of mutations of the sequence analyzed.

Clones were used to transform ultra-competent BL21(DE3)pLysS *E. coli* strains.

For a detailed description of molecular biology see Appendix B.

#### **2.4.4 Expression Strain**

The pET11b-Sav plasmid (provided by Prof. Santambrogio from University of Milan) was used as expression vector for recombinant T7-tagged streptavidin to transform the ultra-competent BL21(DE3)pLysS *E. coli* strain (in house).

BL21 bacterial cells were chosen because lacking of *lon* and *ompT* proteases genes. For this reason they limit proteolytic cleavage of synthesized proteins. The nomenclature DE3 suggests that bacterial host is lysogen of  $\lambda$ DE3 (*i.e.* *E. coli* cells were infected by the bacteriophage DE3) and carries a chromosomal copy of the viral T7 RNA polymerase gene.

The *lacUV5* promoter (induced by IPTG and controlled by *E. coli* RNA polymerase) directs the transcription of T7 RNA polymerase gene, which in turn transcribes the cloned gene of streptavidin as it is controlled by T7 promoter<sup>[36]</sup>.

BL21 cell strains can also contain the pLysS plasmid, conferring resistance to chloramphenicol. In the presence of pLysS, basal expression of streptavidin during the pre-induction growth is drastically reduced because of a low level expression of T7 lysozyme (*i.e.* a natural inhibitor of T7 polymerase)<sup>[37]</sup>.

## ***2.4.5 Streptavidin Production***

### *2.4.5.1 Protein Expression in 20 L of E. coli Cell Culture*

Transformed BL21(DE3)pLysS *E. coli* strain were plated on selective Luria-Bertani broth (LB) petri dishes containing ampicillin (60 µg/mL), chloramphenicol (34 µg/mL) and glucose (2% w/v) and incubated overnight at 37 °C.

300 mL of tryptone medium (20 g/L Bactotryptone; 2 g/L Na<sub>2</sub>HPO<sub>4</sub>, 1 g/L KH<sub>2</sub>PO<sub>4</sub>; 8 g/L NaCl; 15 g/L Bactoyeast extract), containing antibiotics and glucose at the same concentrations as in LB plates, were inoculated with a single colony and incubated overnight in an orbital shaker (37 °C, 250 rpm). A 20 L cell culture, inoculated with the whole pre-culture, was grown in a 30 L fermentor (Bioengineering®, Switzerland) at 37 °C, with 1000 rpm agitation speed, in the presence of glucose and antibiotics.

Cells were induced by IPTG (0.4 mM) at OD<sub>600nm</sub> = 1.8 – 2.2 (approximately 3 h after inoculation). When expression time was elapsed (~ 3 h after induction), bacterial cells were harvested and frozen at -20 °C.

For a detailed description of streptavidin expression in a 20 L bioreactor see Appendix C.

### *2.4.5.2 Protein Expression in 50 mL of E. coli Cell Culture*

5 mL of tryptone medium (20 g/L Bactotryptone; 2 g/L Na<sub>2</sub>HPO<sub>4</sub>, 1 g/L KH<sub>2</sub>PO<sub>4</sub>; 8 g/L NaCl; 15 g/L Bactoyeast extract), containing ampicillin (60 µg/mL), chloramphenicol (34 µg/mL) and glucose (2% w/v) were inoculated with a single colony or glycerol stock and incubated overnight in an orbital shaker (37 °C, 250 rpm).

A 50 mL cell culture, inoculated with the whole pre-culture, was grown in 250 mL baffled Erlenmeyer flask at 34.5 °C, with 415 rpm agitation speed, in the presence of antibiotics.

Cells were induced by IPTG (0.4 mM) 3 h after inoculation and harvested 3 h post induction. Pellet was frozen at -20 °C.

For a detailed description of streptavidin expression in 250 mL baffled flasks see Appendix D.

#### *2.4.5.3 Protein Expression in 96-Well Plate Format*

100 µL of tryptone medium (20 g/L Bactotryptone; 2 g/L Na<sub>2</sub>HPO<sub>4</sub>, 1 g/L KH<sub>2</sub>PO<sub>4</sub>; 8 g/L NaCl; 15 g/L Bactoyeast extract), containing ampicillin (60 µg/mL), chloramphenicol (34 µg/mL) and glucose (2% w/v) were transferred in each well of a 96-well plate.

After inoculation with a single colony or glycerol stock, the 96-well plate was covered with tin foil and incubated overnight in an orbital shaker (37 °C, 250 rpm).

A 500 µL cell culture, inoculated with the whole pre-culture, was grown in a 96-deep well plate at 37 °C, with 250 rpm agitation speed, in the presence of antibiotics.

Cells were induced by IPTG (0.4 mM in TP medium) 3 h after inoculation and harvested 3 h post induction. Pellet was frozen at -20 °C.

For a detailed description of streptavidin expression in 96-well plate format see Appendix E.

## ***2.4.6 Streptavidin Purification***

### *2.4.6.1 Purification on an Imino-Biotin Column*

After thawing, cell lysate was resuspended in 500 mL of resuspension buffer (Tris/HCl 20 mM, pH 7.4; PMSF 87 mg in 5 mL EtOH; mQ-H<sub>2</sub>O up to 500 mL) and incubated with DNaseI until complete degradation of nucleic acids. Afterwards, three dialysis steps performed in guanidinium hydrochloride (6 M, pH 1.5), Tris/HCl (20 mM, pH 7.4) and imino-biotin buffer (NaHCO<sub>3</sub>, 50 mM, pH 9.8; NaCl, 500 mM) preceded protein purification.

Streptavidin was applied in imino-biotin column, previously equilibrated at pH 9.8, to be successively eluted with an acetate buffer (pH 4) in a pure form. Purified protein was successively dialyzed against a neutralization solution (Tris/HCl, 10 mM, pH 7.4) and against distilled and nanopure water in order to remove salts from protein solution.

Lyophilized protein was finally titrated for biotin-fluorescein binding activity and free active sites per tetramer were calculated <sup>[26]</sup>.

For a detailed description of streptavidin purification on imino-biotin column and quantification with B4F see Appendix C.

### *2.4.6.2 Streptavidin Extraction for Immobilization*

After expression in 50 mL of *E. coli* cell culture, harvested cells were frozen-thawed and resuspended in 1 mL of extraction buffer at pH 7.4 (Tris/HCl 20 mM; NaCl 100 mM; PMSF 1 mM). After addition of 10 µl of DNaseI (10 mg/mL, from bovine pancreas; Roche, Switzerland), extracts

were incubated for 30-90 min at room temperature and micro-centrifuged (14 000 rpm, 5 min).

Pellet was re-extracted with 0.5 mL extraction buffer. Pooled supernatants (approx 1.5 mL) were titrated for biotin-fluorescein binding activity in 96-well plates, from which the concentration of free streptavidin active sites was calculated.

For a detailed description of streptavidin extraction see Appendix D.

#### *2.4.6.3 Streptavidin Purification by Thermo-Denaturation*

After expression in 50 mL of *E. coli* cell culture, harvested cells were frozen-thawed and resuspended in 1 mL of extraction buffer at pH 7.4 (Tris/HCl 20 mM; NaCl 100 mM; PMSF 1 mM). After addition of 10 µl of DNaseI (10 mg/mL, from bovine pancreas; Roche, Switzerland), extracts were incubated for 30-90 min at room temperature and micro-centrifuged (14 000 rpm, 5 min).

Pellet was re-extracted with 0.5 mL extraction buffer. Pooled supernatants were heated at 75 °C for 10 minutes and micro-centrifuged (10 000 rpm, 25 min, 4 °C).

After heat-treatment, supernatant (transparent yellow solution) was transferred in a dialysis bag and dialyzed against mQ-H<sub>2</sub>O (4 °C, 3 days). Whereafter it appeared as a cloudy solution.

In treated crude cell extract, streptavidin was quantified by B4F titration (to calculate the concentration of free streptavidin active sites) and by UV absorbance (at 280 nm). The latter strategy required a correction due to the presence of other proteins in the cell lysate. Absorbance of the empty cell

extract (non-expression of streptavidin) was subtracted from the absorbance of streptavidin-containing crude cell extract.

#### ***2.4.7 Streptavidin Refolding***

After expression in 500 mL of *E. coli* cell culture, harvested cells were frozen-thawed and resuspended in 12.5 mL of resuspension buffer at pH 7.4 (Tris/HCl 20 mM; NaCl 100 mM; PMSF 1 mM). After addition of 1 spatule of DNaseI (from bovine pancreas; Roche, Switzerland), extracts were incubated under vigorous stirring and centrifuged (4400 rpm, 30 min, 4 °C). The supernatant was kept just as negative control, whereas the pellet was resuspended in 3.25 mL of Tris/HCl (20 mM, pH 7.4). After addition of further 3.25 mL of Tris/HCl (20 mM, pH 7.4) and 225 µL of lysozyme (10 mg/mL), the solution was incubated for 5 min at room temperature (r.t.), under vigorous stirring.

Afterwards, a spatula of DNaseI was added and the solution was shaken for 10 min at r.t. In the presence of 12.5 mL of *Inclusion Wash Buffer* (Triton X-100, Cf: 0.5%; Tris/HCl pH 7.4, Cf: 20 mM; NaCl, Cf: 100 mM) the solution was mixed by inverting the tube several times and centrifuged (4400 rpm, 30 min, 4 °C). The supernatant was always kept for control.

##### *First wash:*

- The pellet was resuspended in 3.25 mL of *Inclusion Wash Buffer* and shaken vigorously.
- After addition of 12.5 mL of *Inclusion Wash Buffer*, the solution was mixed by inverting tube and centrifuged at 4400 rpm for 30 min at 4 °C (keep supernatant for control).



*Second Wash:*

- We resuspended the pellet in 3.25 mL of *Inclusion Wash Buffer* and shook vigorously.
- After adding of 12.5 mL of *Inclusion Wash Buffer*, the solution was mixed by inverting tube and centrifuged at 4400 rpm, 30 min, 4 °C (keep supernatant for control).

*Third Wash:*

- After resuspension in 3.25 mL of *Inclusion Wash Buffer*, the pellet was well shaken.
- 12.5 mL of *Inclusion Wash Buffer* were added and the solution was mixed by inverting tube.
- The solution was centrifuged (4400 rpm, 30 min, 4 °C) and the superantant was kept for control.

*Fourth Wash:*

- The pellet was resuspended in 3.25 mL of *Inclusion Wash Buffer* and shaken vigorously.
- After addition of 12.5 mL of *Inclusion Wash Buffer*, the solution was mixed by inverting tube and centrifuged at 4400 rpm for 30 min at 4 °C (keep supernatant for control).

The pellet was resuspended in 2 mL of guanidinium/HCl (6 M, pH 1.5) and centrifuged at 4400 rpm, 30 min, 4 °C, to solubilize streptavidin (soluble fraction).

Finally, protein refolding was performed in the cold room at 4 °C by adding 2 mL of supernatant into 100 mL of vortexing Phosphate Buffer Saline at

pH 7.4 (NaCl, 8 g; KCl, 0.2 g; Na<sub>2</sub>HPO<sub>4</sub> (x 12H<sub>2</sub>O), 3.58 g; KH<sub>2</sub>PO<sub>4</sub>, 0.24 g) by using a micropipette as slowly as possible.

The refolded protein was dialyzed against imino-biotin buffer at pH 9.8 and purified on imino-biotin affinity column. Before lyophilisation, the pure protein was dialyzed overnight against first Tris/HCl (10 mM, pH 7.4), then distilled water and finally nanopure water.

For a detailed description of streptavidin refolding see Appendix F.

## 2.5 Conclusions

Chemo-genetic “fine-tuning” of artificial metalloenzymes led to the creation of several hybrid variants with improved features.

This hybrid catalyst library was generated by designed evolution and a HTS system was needed to rapidly evaluate the catalytic performance. Therefore to maximize combinatorial screenings the big challenge of simplifying the lengthy streptavidin purification process was addressed <sup>[23]</sup>.

An immobilization strategy led to a successful streptavidin purification directly from crude cell extract thanks to the high affinity of the protein for biotin. This approach allowed a rapid screening of the library to identify enantioselective trends of immobilized artificial transfer hydrogenases <sup>[23]</sup>.

As future perspective, this efficient and straightforward protocol can be extended to many other catalytic reactions performed by artificial metalloenzymes, based on the biotin-streptavidin technology.

Thermo-denaturation was another strategy scrutinized to simplify streptavidin purification by exploitation of its high thermal stability <sup>[29]</sup>. Although

electrophoretic assays confirmed the efficiency of this purification approach, allylic alkylation failed in heated crude cell extracts.

Many factors may be involved in this inhibition of catalytic activity. In the cell lysate, we observed a rapid hydrolysis of the substrate, which inevitably reduced the catalytic rate of the allylic alkylation. This bottleneck could possibly be overcome by replacing the acetate leaving group with less hydrolysis prone derivatives (*e.g.* allyl-chloride derivatives).

In addition to a different substrate, a new catalytic system could also improve efficiency of allylic alkylases under physiological conditions. Ruthenium organometallic catalyst, chosen by Adriaenssens to perform C-C bond formation in *E. coli* cell lysate, could, for example, exhibit superior performance than the Pd-complex<sup>[31]</sup>.

In order to investigate the activity and the enantioselectivity of artificial metalloenzymes in crude cell extract, we can alternatively select more robust catalytic reactions towards cell debris and potential “*in vivo*” contaminants, *i.e.* the metathesis reaction.

*In vivo* catalysis is an exciting challenge, which presents many challenges. Artificial metalloenzymes with a more robust protein scaffold can be an attractive alternative to improve catalytic performance in crude cell extract.

Carbonic anhydrase is a metalloenzyme containing a zinc ion in its active site, which catalyzes the reversible conversion of carbon dioxide to bicarbonate. This enzyme could be an interesting protein scaffold for *in vivo* catalysis due to its deep binding pocket, which is suitable for protecting the catalytic moiety from inhibition<sup>[38]</sup>.

In our classical system with streptavidin as second coordination sphere, the metal complex is highly exposed to the surrounding environment and, potentially, inhibited by many external factors.

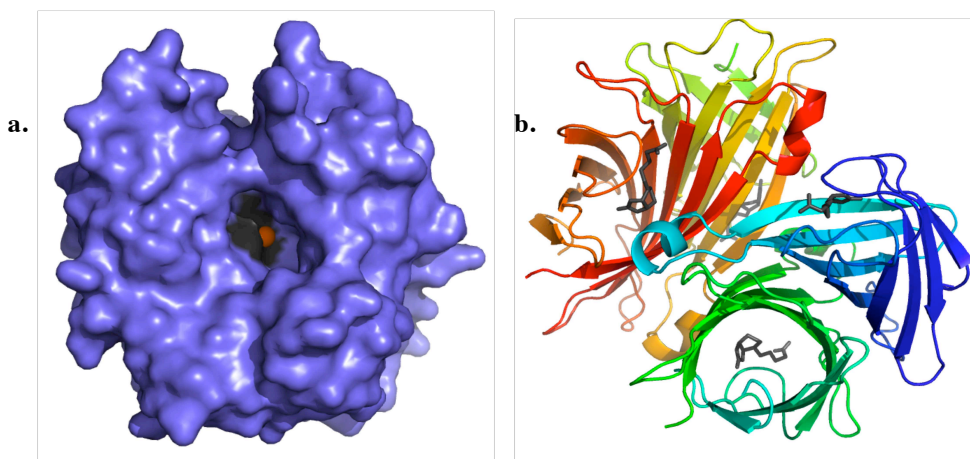


**Fig. 2.18** Close-up view of a) carbonic anhydrase and b) streptavidin active sites, highlighting a different cavity depth. In figure a) the deep pocket of carbonic anhydrase hides the zinc prosthetic group, whereas in crystallographic structure b)  $[\eta^6\text{-}(\text{benzene})\text{Ru}(\text{Biot-}p\text{-L})\text{Cl}]$  metal complex is only partially settled in the cavity of S112K Sav mutant

# REFERENCES

- [1] P. Carter, *Biochem. J.* **1986**, *237*, 1.
- [2] U. T. Bornscheuer, M. Pohl, *Curr. Opin. Chem. Biol.* **2001**, *5*, 137.
- [3] R. J. Kazlauskas, *Curr. Opin. Chem. Biol.* **2000**, *4*, 81.
- [4] a)D. W. Leung, Chen, E., and Goeddel, D.V., *Technique* **1989**, *1*, 11; b)R. Cadwell, G. Joyce, *Genome Res.* **1992**, *2*, 28.
- [5] C. Neylon, *Nuc. Acids Res.* **2004**, *32*, 1448.
- [6] M. T. Reetz, *Proc. Natl. Acad. Sci. USA* **2004**, *101*, 5716.
- [7] a)J. Brannigan, A. Wilkinson, *Nat. Cell Biol.* **2002**, *3*, 964; b)F. Arnold, *Acc. Chem. Res.* **1998**, *31*, 125.
- [8] W. Stemmer, *Nature* **1994**, *370*, 389.
- [9] J. H. Zhang, G. Dawes, W. P. C. Stemmer, *Proc. Natl. Acad. Sci. USA* **1997**, *94*, 4504.
- [10] T. Yano, S. Oue, H. Kagamiyama, *Proc. Natl. Acad. Sci. USA* **1998**, *95*, 5511.
- [11] O. May, P. T. Nguyen, F. H. Arnold, *Nat. Biotechnol.* **2000**, *18*, 317.
- [12] a)K.-E. Jaeger, M. T. Reetz, *Curr. Opin. Chem. Biol.* **2000**, *4*, 68; b)K. Liebeton, A. Zonta, K. Schimossek, M. Nardini, D. Lang, B. W. Dijkstra, M. T. Reetz, K. E. Jaeger, *Chem. Biol.* **2000**, *7*, 709.
- [13] a)P. J. Walsh, M. C. Kozlowski, *Fundamentals of Asymmetric Catalysis, University of Pennsylvania* **2009**; b)M. T. Reetz, *J. Org. Chem.* **2009**, *74*, 5767.
- [14] a)G. Klein, N. Humbert, J. Gradinaru, A. Ivanova, F. Gilardoni, U. E. Rusbandi, T. R. Ward, *Angew. Chem. Int. Ed.* **2005**, *44*, 7764; b)A. Pordea, M. Creus, J. Panek, C. Duboc, D. Mathis, M. Novic, T. R. Ward, *J. Am. Chem. Soc.* **2008**, *130*, 8085; c)J. Pierron, C. Malan, M. Creus, J. Gradinaru, I. Hafner, A. Ivanova, A. Sardo, T. R. Ward, *Angew. Chem. Int. Ed.* **2008**, *47*, 701.
- [15] M. E. Wilson, G. M. Whitesides, *J. Am. Chem. Soc.* **1978**, *100*, 306.
- [16] a)T. R. Ward, *Angew. Chem. Int. Ed.* **2008**, *47*, 7802; b)C. M. Thomas, T. R. Ward, *Chem. Soc. Rev.* **2005**, *34*, 337; c)C. Letondor, N. Humbert, T. R. Ward, *Proc. Natl. Acad. Sci. USA* **2005**, *102*, 4683.
- [17] J. Collot, J. Gradinaru, N. Humbert, M. Skander, A. Zocchi, T. R. Ward, *J. Am. Chem. Soc.* **2003**, *125*, 9030
- [18] M. Skander, N. Humbert, J. Collot, J. Gradinaru, G. Klein, A. Loosli, J. Sauser, A. Zocchi, F. Gilardoni, T. R. Ward, *J. Am. Chem. Soc.* **2004**, *126*, 14411.
- [19] a)A. Fujii, S. Hashiguchi, N. Uematsu, T. Ikariya, R. Noyori, *J. Am. Chem. Soc.* **1996**, *118*, 2521; b)K. Matsumura, S. Hashiguchi, T. Ikariya, R. Noyori, *J. Am. Chem. Soc.* **1997**, *119*, 8738.
- [20] C. Letondor, A. Pordea, N. Humbert, A. Ivanova, S. Mazurek, M. Novic, T. R. Ward, *J. Am. Chem. Soc.* **2006**, *128*, 8320.

- [21] R. Noyori, M. Yamakawa, S. Hashiguchi, *J. Org. Chem.* **2001**, *66*, 7931.
- [22] R. Noyori, S. Hashiguchi, *Acc. Chem. Res* **1997**, *30*, 97.
- [23] M. Creus, A. Pordea, T. Rossel, A. Sardo, C. Letondor, A. Ivanova, I. LeTrong, R. E. Stenkamp, T. R. Ward, *Angew. Chem. Int. Ed.* **2008**, *47*, 1400.
- [24] F. W. Studier, B. A. Moffattf, *J. Mol. Biol* **1986**, *189*, 113.
- [25] N. Humbert, P. Schürmann, A. Zocchi, J. M. Neuhaus, T. R. Ward, *Methods in molecular biology: Avidin-Biotin interactions, Totowa (NJ)* **2008**, *418*, 101.
- [26] G. Kada, H. Falk, H. J. Gruber, *Biochim. Biophys. Acta* **1999**, *1427*, 33.
- [27] M. Creus, T. R. Ward, *Org. Biomol. Chem.* **2007**, *5*, 1835.
- [28] M. T. Reetz, M. Rentzsch, A. Pletsch, A. Taglieber, F. Hollmann, R. J. G. Mondière, N. Dickmann, B. Hocker, S. Cerrone, M. C. Haeger, *ChemBioChem* **2008**, *9*, 552.
- [29] M. González, C. E. Argarana, G. D. Fidelio, *Biomol. Eng.* **1999**, *16*, 67.
- [30] C. Streu, E. Meggers, *Angew. Chem. Int. Ed. Engl.* **2006**, *45*, 5645.
- [31] L. Adriaenssens, L. Severa, J. Vávra, T. Šálová, J. Hývl, M. Čížková, R. Pohl, D. Šaman, F. Teplý, *Collect. Czech. Chem. Commun* **2009**, *74*, 1023.
- [32] a)C. G. Hartinger, A. Casini, C. Duhot, Y. O. Tsybin, L. Messori, P. J. Dyson, *J. Inorg. Biochem.* **2008**, *102*, 2136; b)F. Wang, J. Xu, A. Habtemariam, J. Bella, P. J. Sadler, *J. Am. Chem. Soc.* **2005**, *127*, 17734.
- [33] T. Sano, C. R. Cantor, *J. Biol. Chem.* **1990**, *265*, 3369.
- [34] G. P. Kurzban, E. A. Bayer, M. Wilchek, P. M. Horowitz, *J. Biol. Chem.* **1991**, *266*, 14470.
- [35] R. C. Stevens, *Structure* **2000**, *8*, R177.
- [36] F. W. Studier, A. H. Rosenberg, J. J. Dunn, J. W. Dubendorff, *Methods Enzymol.* **1990**, *185*, 60.
- [37] B. A. Moffatt, F. W. Studier, *Cell* **1987**, *49*, 221.
- [38] D. Christianson, C. Fierke, *Acc. Chem. Res.* **1996**, *29*, 331.

---

# Chapter 3

## DNA recognition *in vitro*

*Discovery consists of seeing what everyone else has seen and thinking what no one else has thought*

---

Albert Szent-Györgyi

### 3.1 Introduction

#### 3.1.1 Organometallic Compounds in Cancer Chemotherapy

DNA is the main molecular target for many drugs used as anticancer agents <sup>[1]</sup>. However, their success is limited by severe toxic side effects and the resistance mechanisms of tumor cells. Cells which are refractory to treatment and promiscuous binding to non-target molecules reduce, for example, the clinical applications of anticancer platinum drugs <sup>[2]</sup>.

For this reason, intense effort has been made to design novel anticancer metal compounds with enhanced selectivity and reduced toxicity.

More recently, new organometallic compounds have received increasing attention due to promising anticancer activity *in vitro* and *in vivo*. These compounds also display non cross-resistance with platinum drugs <sup>[3]</sup>. For example, organometallic ruthenium (II) arene complexes coordinate selectively to the electron-rich N7

nitrogen of the DNA guanine base, forming monofunctional adducts <sup>[4]</sup> and inhibiting the growth of human ovarian cancer cells <sup>[5]</sup>. The arene ligand stabilizes Ru (II) and provides a lipophilic hemisphere to the complex: this hydrophobic face allows transport of ruthenium into cancer cells through a transferrin-mediated process <sup>[6]</sup>.

Aquation – substitution of bound Cl by H<sub>2</sub>O – can activate chloro-Ru (II) arene complexes within cancer cells prior to reactions with DNA, as for the cisplatin reaction. X-ray crystal structures of anticancer Ru (II) arene complexes revealed a “piano-stool” geometry (**Fig. 3.1**), with an arene ring forming the “seat” and three other ligands forming the “legs” of the stool <sup>[7]</sup>.

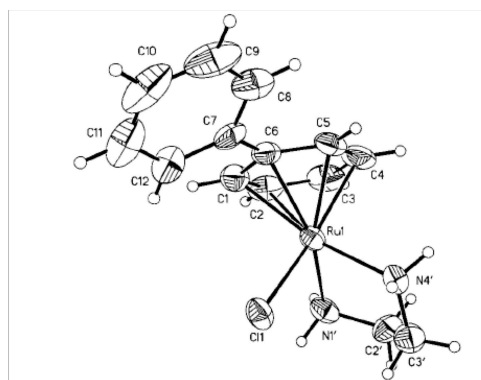


**Fig. 3.1** X-ray crystal structure of  $[(\eta^6\text{-biphenyl})\text{Ru}(1,2\text{-ethylenediamine})\text{Cl}]\text{PF}_6$  with a characteristic “piano-stool” geometry <sup>[7]</sup>

### 3.1.2 Metal Complex Binding to Cellular Thiols

The interaction of reactive metal drugs with endogenous thiols such as glutathione (GSH) can be problematic for chemotherapeutic agents. The overexpression of the tripeptide GSH ( $\gamma$ -L-Glu-L-Cys-Gly; GSH) in cancer cell plays an important role in resistance mechanisms of tumor cells against metal drugs <sup>[8]</sup>. Several binding sites are involved in the interaction between GSH and metal ions: the amino and



the carboxylate groups at the Glu terminus, the carboxylate at Gly terminus, and the thiolate sulfur of the central Cys residue (Fig. 3.2) <sup>[9]</sup>.

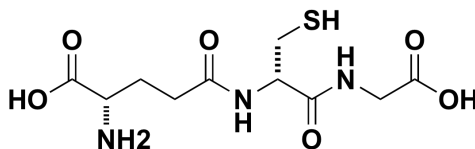


**Fig. 3.2** Tripeptide glutathione involved in the interaction with metallo-drugs

Many reactions of the anticancer Ru (II) arene complex with GSH have been investigated. Studies reveal that a large molar excess of glutathione induces the release of metals from other biological targets, such as DNA <sup>[8, 10]</sup>.

### ***3.1.3 Affinity modulation via a presenter protein***

Identifying more specific interactions between metallo-drugs and cancer-associated DNA sequences can minimize the high toxicity of metallo-complexes. However, such extensive interactions between small-molecule drugs and macromolecular targets are very difficult to achieve.

The “surface borrowing” concept may lead to effective mechanisms of small molecule delivery to preferred targets via a “presenter protein”. In a living cell, small molecules can induce the association of different intracellular macromolecules, strengthening interactions. The biological consequences of this induced proximity depend upon the macromolecules involved <sup>[11]</sup>.

In the late 90s, Crabtree and Schreiber emphasized the importance of dimerization induced by small molecules as a general control mechanism in signal transduction <sup>[12]</sup>.

Therefore, a small ligand, containing binding sites for a presenter protein and for a target, can bind to endogenous presenter protein forming a composite surface area, which improves the specificity and affinity of ligand-protein target interactions through additional surface contacts.

In the immune system, “surface enlargement” is observed for the antigenic ligand of the T cell receptor (TCR) whereby a presenter protein increases binding affinity. Antigenic peptides usually have a very low affinity for TCR. For this reason, the ligand is presented to a T cell by the major histocompatibility complex (MHC), which increases the surface area available for interactions and improves affinity, thus inducing a pronounced immune response <sup>[13]</sup> (**Fig. 3.3**).

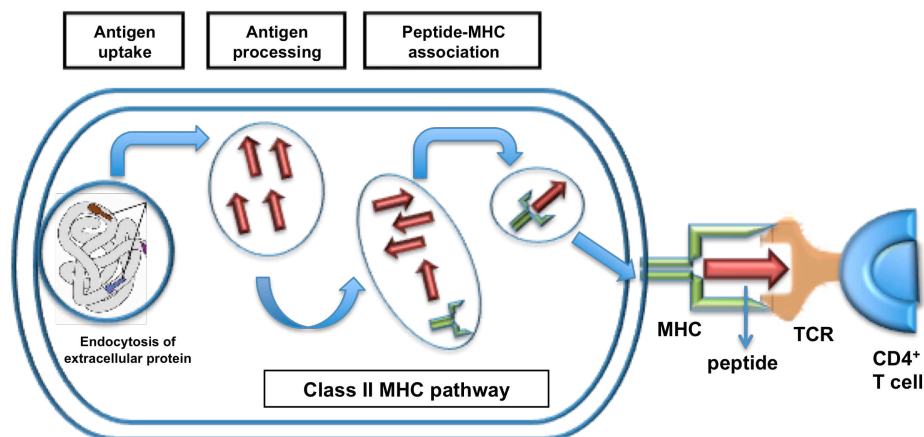


**Fig. 3.3 TCR-peptide-MHC ternary complex formation.** Proteins encoded by class II MHC are expressed on the surface of cells and display antigen peptides to T cells via T cell receptors (TCR) <sup>[14]</sup>

Certain soil microorganisms use analogous mechanisms of “surface borrowing” to present and enhance the activity of their toxins, such as the immunosuppressants cyclosporin, FK506, and rapamycin which have no affinity for their targets <sup>[11]</sup>.

The clinically useful drugs cyclosporin and FK506 are presented by two different *cis-trans* isomerases (cyclophilin and FKBP, respectively), also called

immunophilins <sup>[15]</sup>. As revealed by crystal structures, both cyclosporin-cyclophilin and FK506-FKBP complexes bind to and inhibit calcineurin with high affinity. Calcineurin is a target phosphatase involved in cytokine production. The surfaces of calcineurin and the presenter protein FKBP are involved in extensive contacts that promote the high binding affinity of ligand to its target protein <sup>[15]</sup>. Similarly, the immunosuppressive antibiotic rapamycin forms a complex with FKBP to create a composite surface area available for interactions with the target FRAP (the FKBP-Rapamycin-Associated Protein) <sup>[16]</sup> (**Fig. 3.4**).

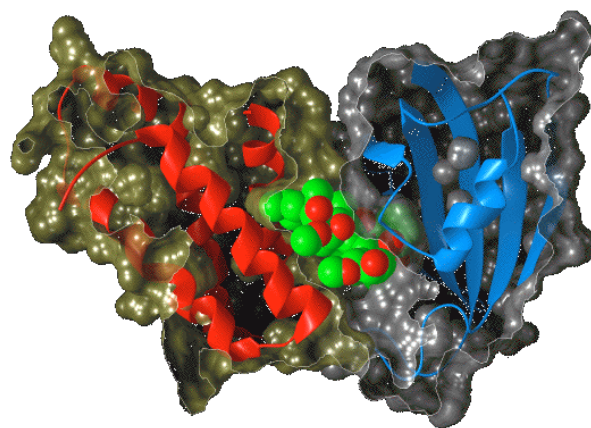


**Fig. 3.4 Three-dimensional structure of FRAP/FKBP/rapamycin complex.** The FKBP protein (blue ribbon) has five anti-parallel  $\beta$ -sheets wrapping around a short  $\alpha$ -helix. Hydrophobic parts of rapamycin (green spheres) interact with hydrophobic residues of FKBP situated between the  $\beta$ -sheet and the  $\alpha$ -helix. Rapamycin-FKBP bimolecular complex establishes only few contacts with its target FRAP (red ribbon) ([www.ch.ic.ac.uk](http://www.ch.ic.ac.uk))

As dimerizers with two distinct protein-binding surfaces, the previously described antigenic ligands of the immune system and immunophilin molecules (FKBP and cyclophilin) are the perfect examples of CIDs (Chemical Inducers of Dimerization), small molecules widely used to modulate the activity of different cellular proteins <sup>[17]</sup>. CIDs carry a protein into the close proximity of another protein, and increase *ipso facto* its activity. In general, the ternary complex between presenter protein-CID-protein target is more stable than the bimolecular complex.

Inspired by these natural examples, Pelletier *et al.* studied a new strategy to target RNA with small molecules (CIDs), designed as bifunctional ligands with a protein-binding surface and an RNA-binding portion (**Fig. 3.5**). Biotin represents the protein-binding component of CID, with high affinity for avidin and streptavidin, and tobramycin constitutes the RNA-binding moiety, specific for two RNA aptamers (J6f1 and X1) <sup>[17]</sup>.

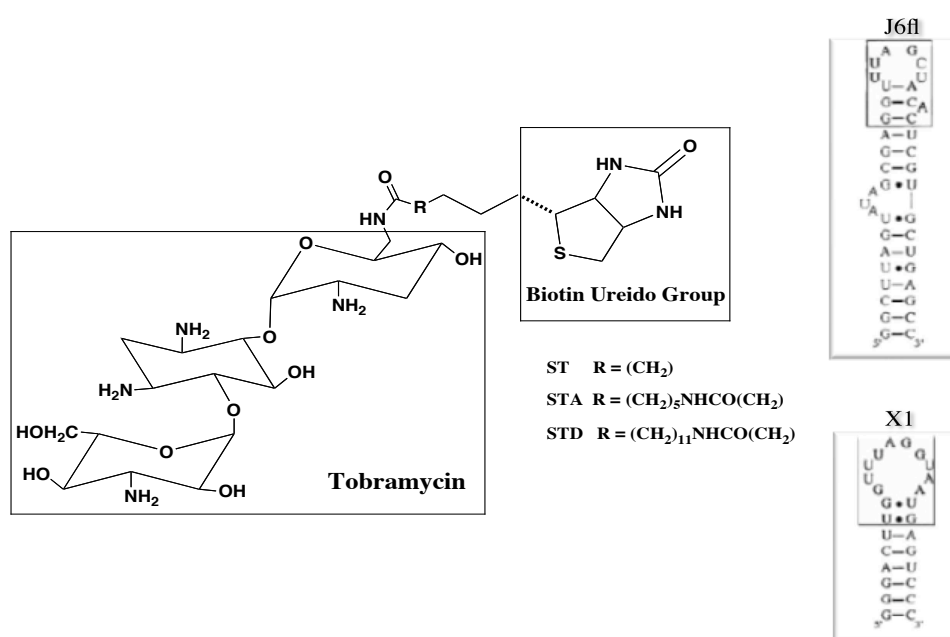


**Fig. 3.5 Biotin/Tobramycin CIDs design.** RNA-binding moiety of CID, tobramycin, is linked to biotin ureido group through a chemical spacer R of varied length. RNA aptamers (J6f1 and X1), with tobramycin-binding pocket highlighted by shaded box, are schematically depicted <sup>[17]</sup>

These bivalent molecules have been engineered to increase RNA-(strept)avidin interactions, in order to inhibit eukaryotic translation. However, the cell impermeability of biotin-tobramycin conjugate and its interactions with many other biotin-binding proteins prevent the application *in vivo* of this system. In order to overcome the limits of this strategy, Plummer *et al.* proposed a new “surface borrowing” approach for RNA targeting, in which synthetic

bifunctional ligands, known as AP1867, 2G, 4G, 8G, 2A, cross the membrane of mammalian cells and interact preferentially with an engineered presenter protein over the wild-type form (**Fig. 3.6**)<sup>[18]</sup>.

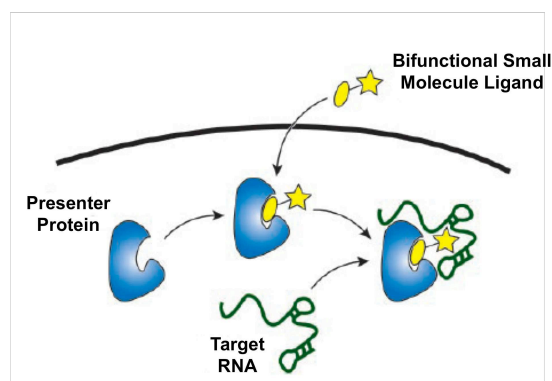


**Fig. 3.6 “Surface borrowing” approach for targeting RNA.** Upon entry into the cell, a bifunctional small molecule binds to the presenter protein, forming a bimolecular complex with a composite surface area available for specific and strong interactions with cellular RNA target<sup>[18]</sup>

The synthetic ligand AP1867 and its derivatives, containing functionalised guanine/adenine nucleobases, possess two binding moieties, which target an intracellular protein and RNA (**Fig. 3.7**).

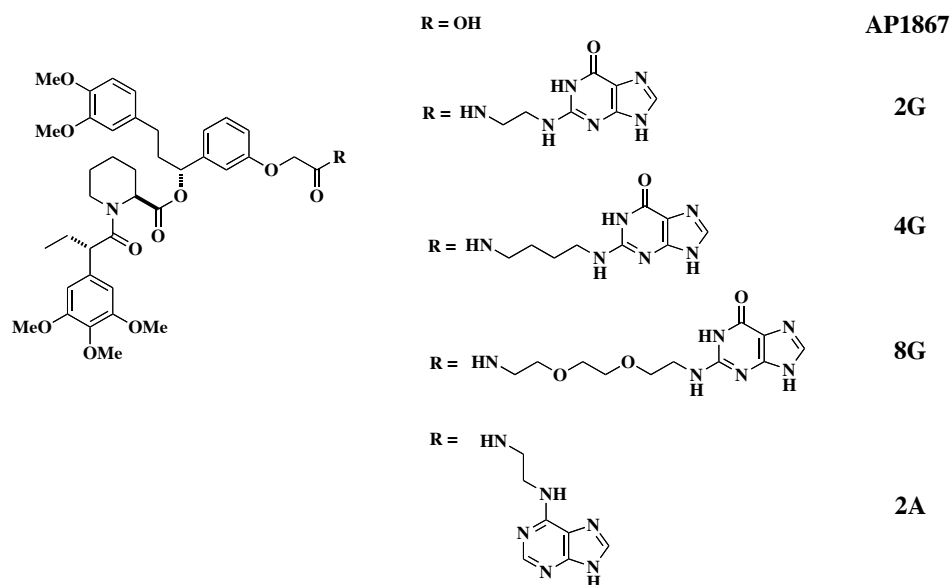


**Fig. 3.7 Small synthetic ligands for RNA targeting.** Functionalised guanine/adenine nucleobases have been conjugated to AP1867 via amide coupling to give the bifunctional ligands 2G, 4G, 8G, 2A

The presenter protein FKBP has been engineered by introducing positive charges on its binding surface in order to increase electrostatic interactions with the negatively charged surface of RNA <sup>[18]</sup>.

Upon entry into mammalian cells, the bipartite small ligand binds with high affinity to the engineered variant of FKBP, forming a composite surface area involved in electrostatic, hydrogen bonding and non-polar interactions with RNA target.

### 3.2 Aim of the Work

High toxicity of numerous anticancer drugs, due to non-specific binding to non-target molecules, is a deterrent to their clinical applications <sup>[2b]</sup>.

Recently, “surface borrowing” strategy has been proposed as a promising approach to minimize metallodrug-toxicity inasmuch as increases the specificity

of interactions between small molecule agents and macromolecule targets via presenter protein <sup>[11]</sup>.

Inspired by our previous experience on enantioselective artificial metalloenzymes <sup>[19]</sup>, we hypothesized that streptavidin could be used as a presenter protein for *in vitro*-DNA recognition.

The broad aim of this chapter was to test this hypothesis by inserting biotinylated ruthenium piano-stool complexes into streptavidin and modulating binding to model DNA targets *in vitro*.

### 3.3 Results and Discussion

#### 3.3.1 Introduction of a Biotinylated Ru (II) Complex into a Protein

Inspired by organometallic drugs with demonstrated antitumor activity, biotinylated Ru (II) piano-stool complexes **1** (*R,R*) [ $(\eta^6\text{-}p\text{-cymene})\text{Ru}(\text{Biot-L})\text{Cl}$ ] and **2** (*R,R*) [ $(\eta^6\text{-biphenyl})\text{Ru}(\text{Biot-L})\text{Cl}$ ] were synthesized within the group by Mr Malcolm Jeremy Zimbron (Fig. 3.8).

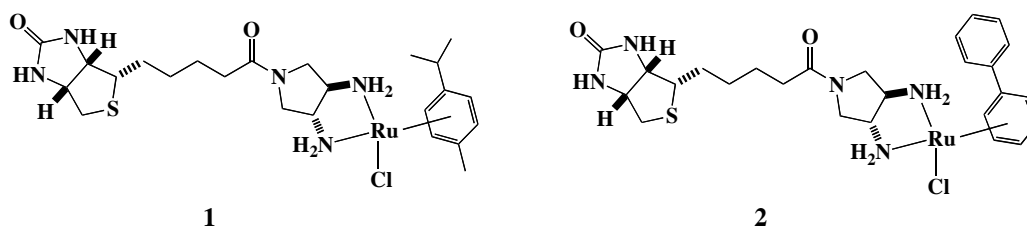


Fig. 3.8 Biotinylated Ru (II) piano-stool complexes **1** and **2**, used in this study

A second-coordination sphere was provided around the metal by embedding the biotinylated Ru (II) piano-stool moiety inside a tetrameric streptavidin in a 2 : 1 molar ratio.

It was anticipated that the resulting supramolecular complex would allow extensive interactions with macromolecules such as DNA, through metal coordination as well as through non-covalent interactions provided by the protein<sup>[20]</sup>. The streptavidin as “presenter protein”<sup>[11]</sup> provided a second coordination sphere that could enlarge the surface area available for interactions between metallo-drug and its macromolecular targets, improving specificity and affinity.

The crystal structure of the biotinylated Ru (II) complex **1**  $\subset$  streptavidin assembly, resolved by Mr Tillmann Heinisch (in collaboration with the Prof. Tilman Schirmer, Biozentrum, Universität Basel), confirmed the three-legged piano-stool geometry of the complex and provided a fascinating insight into the organization of the active site.

In light of the refined model, we focused mainly on two amino acid residues, S112 and K121, close to the active site, as being important for the assembly: the side chain hydroxyl of Ser-112, in the L7,8 loop of streptavidin, formed a hydrogen-bond with the Ru-bound amine, thus fixing the position of the metal.

The crystal structure revealed two lysines (K121 residues of the two adjacent monomers A and B) within 10 Å of the Ru, at the entrance of the largely hydrophobic biotin-binding pocket (**Fig. 3.9**).



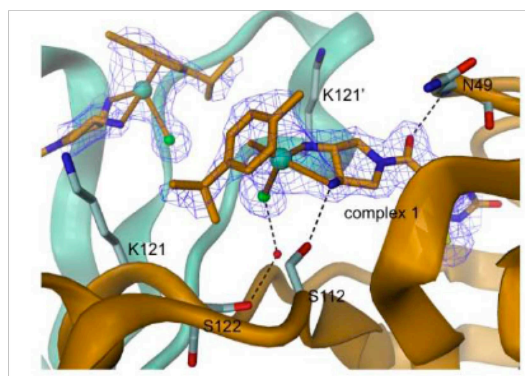


**Fig. 3.9 X-ray crystal structure of the biotinylated Ru (II) complex 1 C streptavidin assembly.** Close-up view of the ruthenium head group of complex 1 bound to a Sav monomer (orange) and partially interacting with another Sav monomer (aquamarine) also containing complex 1 (upper-left corner). Selected Sav residues are shown with side-chains and are labeled. The ruthenium atom is tetrahedrally coordinated by two amino groups of diaminopyrrolidine, the *p*-cymene and a putative chloride ion (shown in green)

In the absence of a neighboring compound **1** in *cis*, the size and charge of the pocket would allow multiple interactions with an incoming DNA molecule. Ionic interactions between DNA phosphate groups and positively charged residues on the protein surface were conceivable. The orientation of the labile Ru-Cl bond was compatible with coordination to electron-rich N1 or N7 nitrogens of the purine bases of single stranded DNA <sup>[19]</sup>.

### **3.3.2 Binding of Drug – Protein Assembly to Quadruplex DNA**

The incorporation of a metallodrug within a protein scaffold can generate an extended second coordination sphere <sup>[19]</sup>. This framework can be exploited for additional interactions with a specific macromolecular target to increase selectivity, via “surface borrowing”.

As proof-of-concept, the binding of Ru (II) metallodrug C streptavidin assembly to various DNA targets was investigated (**Fig. 3.10**). Although the target of DNA-interactive metallodrugs is generally double stranded DNA (dsDNA), 39 bases G-quadruplexes DNA represented a new class of attractive alternative therapeutic

targets <sup>[21]</sup>. These secondary DNA structures, formed by tandem repeats of short guanine tracts, occur under physiological conditions <sup>[1]</sup>. G-quadruplex structures, abundant in telomeres at the end of the chromosome, act as potential regulatory elements in genes, including oncogenes <sup>[22]</sup>.

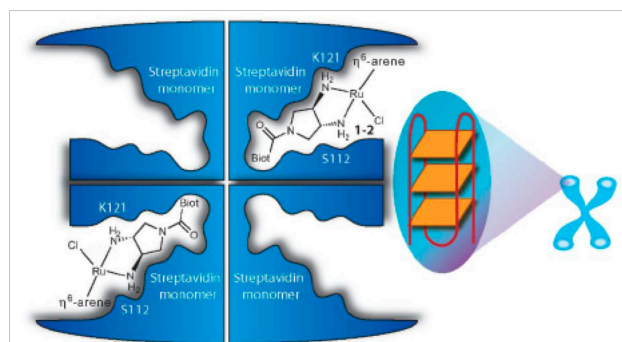


**Fig. 3.10 Concept of ruthenium metallodrug C presenter protein assembly for targeting telomeric DNA.** The ruthenium drug embedded into the tetrameric Sav in a 2 : 1 ratio forms a supramolecular complex that may allow extensive interactions with DNA (here depicted as G-quadruplex telomeric DNA). Chemogenetic optimization, performed by varying the arene cap of the Ru complex or mutating defined Sav residues (*e.g.* at position K121 and S112), can modulate the affinity of the assembly for the DNA target

The supramolecular assembly of wild-type variant streptavidin (WT) with the biotinylated Ru (II) piano-stool complexes **1** and **2** produced a concentration-dependent change in migration of quadruplex DNA (G4A) in electrophoretic mobility shift assays (EMSA).

After incubation of DNA with the drug-streptavidin assemblies, two predominant DNA species with very different mobility were identified on agarose gels: the fast migrating species coincided with unmodified G-quadruplex DNA, whereas the low mobility species was consistent with the formation of the ternary complex **1**  $\subset$  Sav · G4A or **2**  $\subset$  Sav · G4A characterized by a defined 1 : 1 stoichiometry. The affinity constant was estimated by EMSA analysis ( $K_d = < 1.6$ , entry 2, **Table 3.1**, subsection 3.3.10).

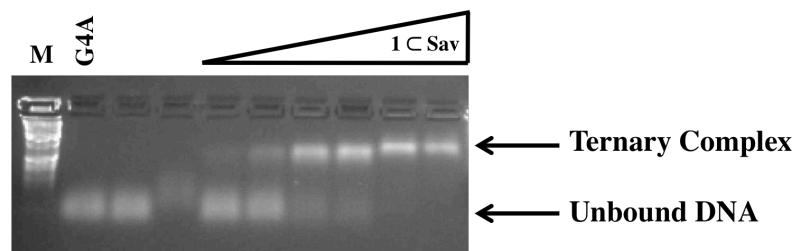


**Fig. 3.11 Binding of assembly of metallodrug and presenter protein (1 C WT-Sav) to G4A monitored by EMSA on agarose gel.** The gel was run after incubation of 1 C WT-Sav with 500 ng of telomeric G4A-DNA. Lane 1, DNA Marker. Lane 2, G4A. Lane 3, G4A (3.3  $\mu\text{M}$ ) + Sav (39.6  $\mu\text{M}$ ). Lane 4, G4A (3.3  $\mu\text{M}$ ) + **1** (85.7  $\mu\text{M}$ ). Lanes 5-10, G4A (3.3  $\mu\text{M}$ ) + **1** C Sav at increasing concentrations: 0.8  $\mu\text{M}$ , 1.6  $\mu\text{M}$ , 3.9  $\mu\text{M}$ , 7.9  $\mu\text{M}$ , 19.8  $\mu\text{M}$ , 39.6  $\mu\text{M}$ , representing a **1** C Sav : G4A ratio from 0.2 to 12

Chemical modification of the Ru complex by varying the arene-cap *p*-cymene with biphenyl changed the binding affinity of drug-presenter protein for telomeric G4A-DNA only weakly ( $K_d = 6.25$ , entry 3, **Table 3.1**).

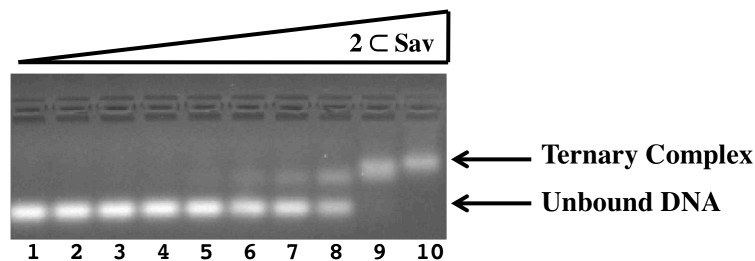


**Fig. 3.12 Binding of assembly of metallodrug and presenter protein (2 C WT-Sav) to G4A monitored by EMSA on agarose gel.** The gel was run after incubation of 2 C WT-Sav with 500 ng of telomeric G4A-DNA. Lanes 3-10, G4A (3.3  $\mu\text{M}$ ) + **2** C Sav at increasing concentrations: 0.2  $\mu\text{M}$ , 0.4  $\mu\text{M}$ , 0.6  $\mu\text{M}$ , 0.8  $\mu\text{M}$ , 1.6  $\mu\text{M}$ , 3.2  $\mu\text{M}$ , 3.9  $\mu\text{M}$ , 7.9  $\mu\text{M}$ , 19.8  $\mu\text{M}$ , 39.6  $\mu\text{M}$ , representing a **1** C Sav : G4A ratio from 0.06 to 12

During these trials, we also investigated the influence of the **1** : Sav ratio on the binding-affinity for G4A-DNA. Affinities obtained by varying the ratio of **1** : Sav from 1 : 1 to 4 : 1 were comparable (entries 2-4-5, **Table 3.1**).

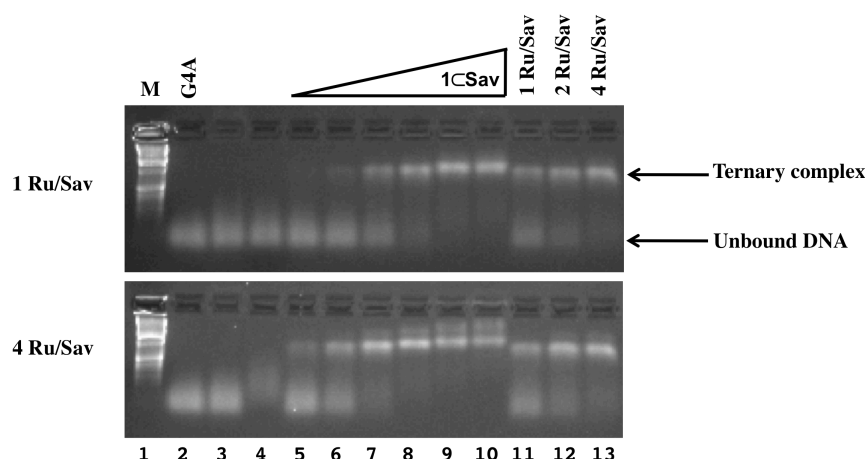


**Fig. 3.13 Binding of assembly of metallodrug and presenter protein (1 C Sav), at 1 or 4 equivalents of Ru metallodrug per tetramer, to G4A monitored by EMSA on agarose gels.** Lane 1, DNA Marker. Lane 2, G4A. Lane 3, G4A (3.3  $\mu\text{M}$ ) + Sav (39.6  $\mu\text{M}$ ). Lane 4, G4A (3.3  $\mu\text{M}$ ) + complex **1** (43  $\mu\text{M}$  for 1 Ru/Sav and 160  $\mu\text{M}$  for 4 Ru/Sav, respectively). Lane 5-10, G4A (3.3  $\mu\text{M}$ ) + **1** C Sav at increasing concentrations: 0.8  $\mu\text{M}$ , 1.6  $\mu\text{M}$ , 3.9  $\mu\text{M}$ , 7.9  $\mu\text{M}$ , 19.8  $\mu\text{M}$ , 39.6  $\mu\text{M}$ , representing a **1** C Sav : G4A ratio from 0.2 to 12. In all cases 500 ng of DNA was loaded onto the gel. Lane 11, **1** C Sav : G4A ratio of 1.2, with 1 equivalent of Ru per tetramer. Lane 12, **1** C Sav : G4A ratio of 1.2, with 2 equivalents of Ru per tetramer. Lane 13, **1** C Sav : G4A ratio of 1.2, with 4 equivalents of Ru per tetramer

The 2 : 1 ratio was selected for all subsequent studies as it yielded a well defined 1 : 1 stoichiometry (**1** C Sav : G4A) by EMSA and Isothermal Titration Calorimetry (ITC), below described.

The binding of **1** C Sav to a model quadruplex telomeric DNA (G4A) was also monitored by ITC, a powerful method for characterizing the energetics of biological interactions. All the ITC titrations presented in this chapter were performed in collaboration with Mr Malcolm Jeremy Zimbron.

The approach yielded the thermodynamic signature of binding ( $\Delta H$ ,  $\Delta S$  and  $K_d$ ) through an analysis of the heat released or absorbed as a ligand was incrementally titrated into a solution of its binding partner.

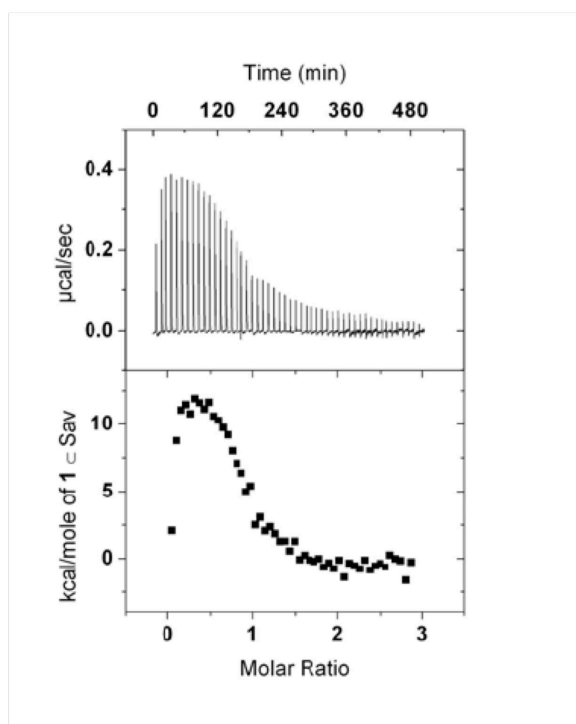


**Fig. 3.14 Binding of drug-streptavidin assembly (1 C Sav) to G-quadruplex DNA monitored by Isothermal Titration Calorimetry (ITC).** ITC profiles were fitted to a single-binding model, the simplest binding model consisting of a single set of identical independent binding sites, and provided an association constant of  $(1.35 \pm 0.28) \cdot 10^6 \text{ M}^{-1}$ . The enthalpy of binding at 25 °C was endothermic ( $\Delta H = 1.23 \cdot 10^4 \text{ kcal/mol}$ ). The stoichiometry approaching was one quadruplex bound per Sav tetramer (molar ratio = 0.90). In the upper panel the raw titration data were plotted as rate of heating *versus* time. In the lower panel the integrated heat measurements were plotted as kcal/mol of drug-streptavidin assembly injected into telomeric DNA solution

The ITC results suggested the formation of a ternary complex between the drug-presenter protein assembly and G4A-DNA, with sub-micromolar affinity ( $K_d = 0.74 \text{ } \mu\text{M}$ ). A value in the same range was observed in the extrapolated data from EMSA, where the observed  $K_d$  was  $< 1.6 \text{ } \mu\text{M}$  (entry 2, **Table 3.1**).

Thus, ruthenium metallodrug, embedded into a presenter protein, was designed to allow extensive interactions with telomeric DNA, through metal coordination as well as through non-covalent interactions provided by the protein scaffold.

### 3.3.3 Complex – DNA Interaction in the Absence of Streptavidin

Telomeric G4A-DNA incubated with complex **1** in the absence of streptavidin presented an electrophoretic mobility compatible with the formation of a mixture of fast migrating species. These species could not be resolved by EMSA (**Fig. 3.15**), presumably due to the small difference in size and charge of the adduct mixture and the binding of varying numbers of Ru moieties to each DNA quadruplex.

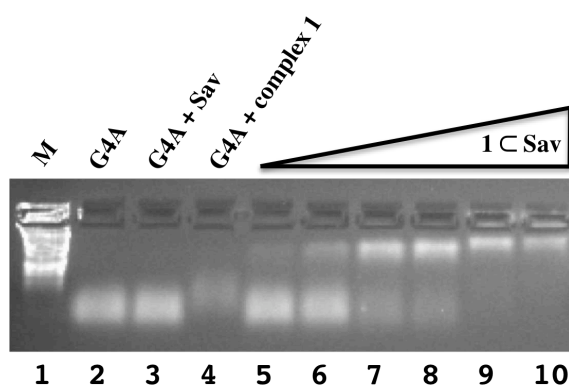


**Fig. 3.15** Different electrophoretic mobility of drug-G4A complex on agarose gel in the presence and absence of streptavidin. Lane 1, DNA Marker. Lane 2, G4A. Lane 3, G4A (3.3 μM) + Sav (39.6 μM). Lane 4, G4A (3.3 μM) + **1** (85.7 μM). Lanes 5-10, G4A (3.3 μM) + **1 C Sav** at increasing concentrations: 0.8 μM, 1.6 μM, 3.9 μM, 7.9 μM, 19.8 μM, 39.6 μM, representing a **1 C Sav** : G4A ratio from 0.2 to 12. In all cases 500 ng of DNA was loaded onto the gel.

The ITC titration of complex **1** with G4A-DNA revealed multiple binding equilibria with a large enthalpic contribution, which hampered the definition of dissociation constant (**Fig. 3.16**).

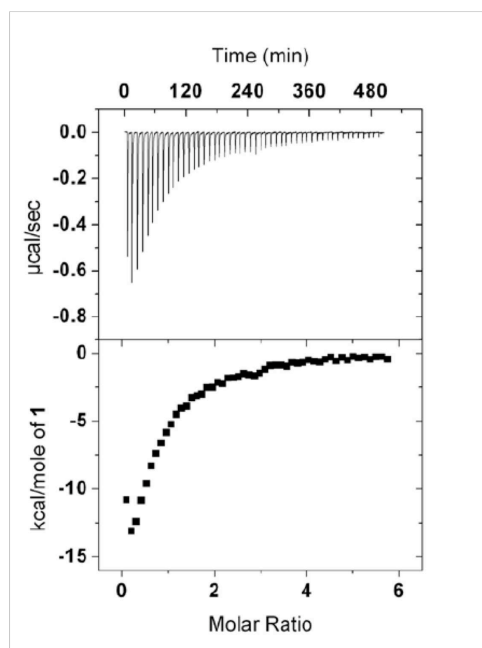


**Fig. 3.16 Binding of complex 1 to G-quadruplex DNA monitored by isothermal titration calorimetry (ITC).** ITC profiles were carried out at 25 °C in 75 mM MOPS (pH 6.5) with 10 mM KOH. In the upper panel the raw titration data were plotted as rate of heating *versus* time; in the lower panel the integrated heat measurements were plotted as kcal/mol of drug injected into telomeric DNA solution

There is ample experimental evidence for related Ru piano-stool complexes that display preferential binding to N7 guanine in DNA <sup>[23]</sup>.

Fitting the data with a single-binding model did not provide meaningful binding information, because it was difficult to interpret a 0.5 : 1 molar ratio between metal drug and telomeric DNA.

Analysis was further hampered by different factors: a model of the real stoichiometry was unclear and the equilibrium conditions were not reached (return to baseline), as it seems that an endothermic component was superimposed on an exothermic component.

However, under these experimental conditions the extrapolated results demonstrated a very different binding from that found for the complex bound to streptavidin.

In summary, it was proven that presenter protein influenced the mode of binding of complex **1** to quadruplex DNA and helped to form a defined ternary complex, by borrowing additional surface contacts, according to ITC and EMSA analysis.

### 3.3.4 Streptavidin – DNA Binding

The binding of streptavidin with quadruplex DNA was markedly weaker in the absence of Ru complex. The lack of detectable binding in EMSA (**Fig. 3.17**) confirmed the low affinity of streptavidin for G4A ( $K_d = > 145 \mu\text{M}$ , entry 1, **Table 3.1**).

Neither increasing concentrations of wild-type streptavidin nor genetic modifications of the protein altered appreciably the interaction between streptavidin and telomeric DNA, as observed in EMSA gels.

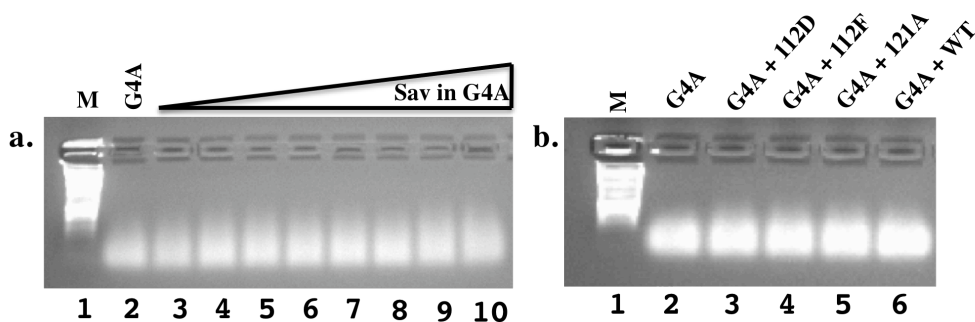


**Fig. 3.17 DNA binding of streptavidin in the absence of Ru (II) complexes monitored by EMSA on agarose gels. a)** EMSA on agarose gel of WT-Sav incubated with 500 ng of G4A-DNA. Lane 1, DNA Marker. Lane 2, G4A. Lane 3-10, G4A (3.3 μM) + WT-Sav at increasing concentrations: 39.6 μM, 47.5 μM, 55.4 μM, 63.2 μM, 71.2 μM, 79 μM, 119 μM, 146 μM, representing a Sav : DNA ratio from 12.5 to 46.2. **b)** EMSA on agarose gel of different Sav isoforms incubated with 500 ng of G4A-DNA. Lane 1, DNA Marker. Lane 2, G4A. Lane 3, G4A (3.3 μM) + S112D (7.9 μM). Lane 4, G4A (3.3 μM) + S112F (7.9 μM). Lane 5, G4A (3.3 μM) + K121A (7.9 μM). Lane 6, G4A (3.3 μM) + WT (7.9 μM)



The binding of streptavidin alone to the telomeric G4A-DNA was also monitored by ITC in the absence of metal complex. The affinity was markedly weaker than in the presence of Ru (II) complex.

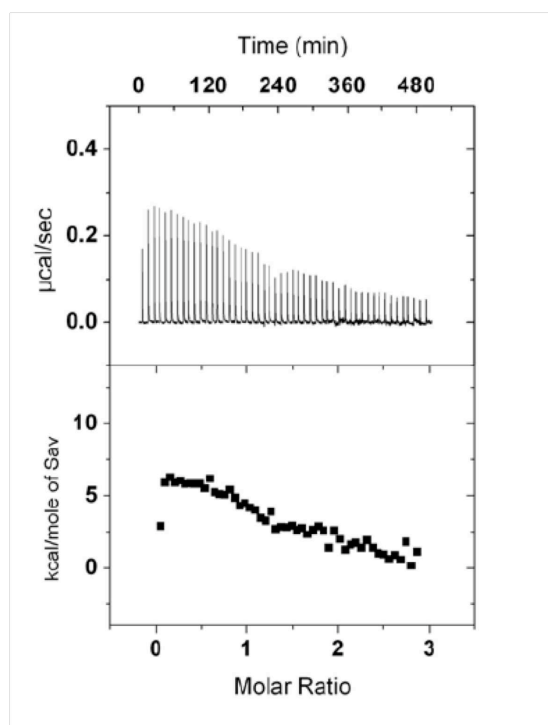


**Fig. 3.18 ITC profile for binding of WT-Sav alone to G4A.** The titration was carried out at 25 °C in 75 mM MOPS (pH 6.5) with 10 mM KOH, injecting 5 µl of streptavidin (375 µM) into DNA solution (25 µM) every 10 min. The heat values were plotted as a function of streptavidin to G4A molar ratio, to give the corresponding binding isotherms. The resulting isotherms were then fitted to a single set of identical sites model and give an association constant of  $(6.56 \pm 2.35) \cdot 10^6 \text{ M}^{-1}$ , a binding enthalpy of  $(1.055 \pm 0.124) \times 10^3 \text{ kcal/mol}$  and a stoichiometry of  $1.81 \pm 0.09$

The ITC profile revealed a weak interaction between streptavidin and telomeric DNA, as confirmed by the absence of saturation curve (within the titration window of the experiment).

The modest affinity of streptavidin (theoretical  $pI = 7$ ) for DNA in the absence of metal complex has been exploited for biotechnology applications involving biotinylated DNA, rather than using the related but very basic protein avidin (theoretical  $pI = 10.4$ )<sup>[24]</sup>.

### 3.3.5 Competition Studies with Interfering Glutathione

Glutathione has been shown to coordinate different anticancer ruthenium drugs *in vitro* [8-10] as well as our biotinylated Ru (II) complex **1**, as confirmed by mass spectrometry (see APPENDIX G). Glutathione has also been implicated in metaldrug inactivation *in vivo* [2b, 25].

To test the selectivity of the drug-presenter protein assembly towards telomeric DNA in the presence of potentially interfering macromolecules, competition studies with glutathione were carried out.

The presence of a large molar excess of GSH (300-fold excess compared to G4A), with a final concentration of 1 mM, did not appreciably affect the binding of the drug-streptavidin assembly to the telomeric G4A-DNA ( $K_d = < 1.6 \mu\text{M}$ , entry 6, Table 3.1) as evidenced by EMSA.

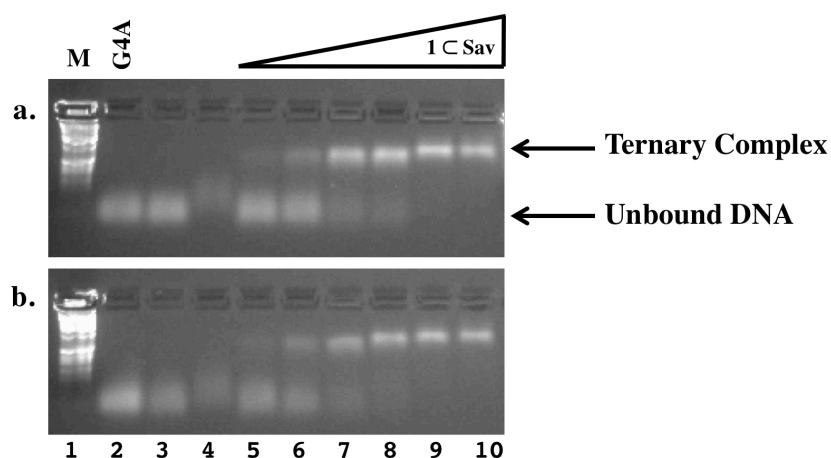


**Fig. 3.19 Binding of drug-streptavidin assembly (**1 C Sav**) to G-quadruplex DNA monitored by EMSA on agarose gels. a) Binding of **1 C Sav** in the absence of glutathione (GSH). b) Binding of **1 C Sav** in the presence of 1 mM of GSH. Lane 1, DNA Marker. Lane 2, G4A. Lane 3, G4A (3.3  $\mu\text{M}$ ) + Sav (39.6  $\mu\text{M}$ ). Lane 4, G4A (3.3  $\mu\text{M}$ ) + **1** (85.7  $\mu\text{M}$ ). Lanes 5-10, G4A (3.3  $\mu\text{M}$ ) + **1 C Sav** at increasing concentrations: 0.8  $\mu\text{M}$ , 1.6  $\mu\text{M}$ , 3.9  $\mu\text{M}$ , 7.9  $\mu\text{M}$ , 19.8  $\mu\text{M}$ , 39.6  $\mu\text{M}$ , representing a **1 C Sav** : G4A ratio from 0.2 to 12. In all cases 500 ng of DNA was loaded onto the gel**

Therefore, we hypothesized that the protein scaffold may create a steric bulk around the metal centre, providing a shielding from competing species such as glutathione.

### 3.3.6 Target Selectivity against Single Stranded DNA

To test whether metallodrug-presenter protein assemblies recognized structural features of G4A-DNA or simply its nucleotide content, we performed binding assays in the presence of G4A-Li<sup>+</sup> and “scrambled” G4A.

Since the great stabilization of G4A-DNA in the quadruplex structure requires the presence of potassium ions, we decided to perform DNA binding assays in Li<sup>+</sup> salts instead of K<sup>+</sup> in order to prevent the formation of quadruplex DNA <sup>[26]</sup>.

However, under these conditions the resulting unstructured ssDNA oligonucleotide interacted with the drug-protein assemblies with the same apparent affinity as the quadruplex G4A ( $K_d = < 1.6 \mu\text{M}$  for **1 C Sav**;  $K_d = 1.55$  for **2 C Sav**, entries 7-8, **Table 3.1**) as estimated by EMSA.

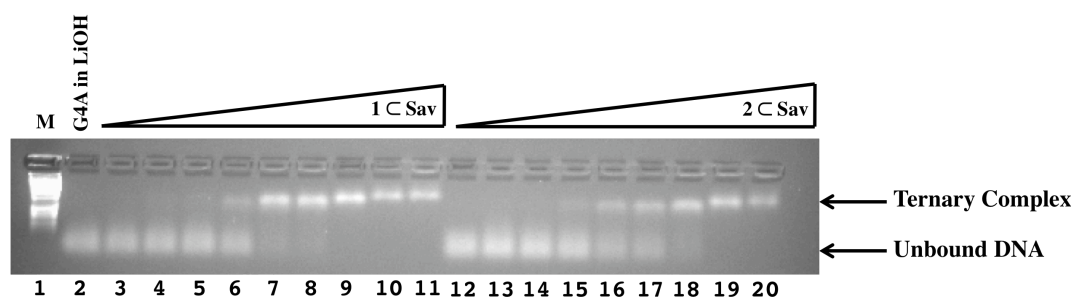


**Fig. 3.20 Binding of metallodrug-presenter protein assemblies to G4A (in MOPS/LiOH) monitored by EMSA on agarose gels. a)** Gel was run after incubation of **1 C Sav** with G4A-Li<sup>+</sup>. Lane 1, DNA Marker. Lane 2, G4A-Li<sup>+</sup>. Lanes 3-11, G4A-Li<sup>+</sup> (3.3  $\mu\text{M}$ ) + **1 C Sav** at increasing concentrations: 0.4  $\mu\text{M}$ , 0.6  $\mu\text{M}$ , 0.8  $\mu\text{M}$ , 1.6  $\mu\text{M}$ , 3.2  $\mu\text{M}$ , 3.9  $\mu\text{M}$ , 7.9  $\mu\text{M}$ , 19.8  $\mu\text{M}$ , 39.6  $\mu\text{M}$ , representing a **1 C Sav** : G4A-Li<sup>+</sup> ratio from 0.12 to 12. In all cases 500 ng of DNA was loaded onto the gel. **b)** Gel was run after incubation of **2 C Sav** with G4A-Li<sup>+</sup>. Lanes 12-20, G4A-Li<sup>+</sup> (3.3  $\mu\text{M}$ ) + **2 C WT-Sav** at the same ratio and increasing concentrations than gel a)

To investigate the interactions of metallodrug-presenter protein assemblies with other unstructured ssDNA, we performed binding assays in the presence of scrambled (Sc) G4A.

Although characterized by the same sequence as G4A, this scrambled DNA is unable to form a G-quadruplex structure.

The EMSA gel revealed that the affinities of **1 C Sav** and **2 C Sav** for the scrambled telomere was weakly lower compared to the affinities towards the structured G-quadruplex form ( $K_d = 2.25 \mu\text{M}$ , entries 9-10, **Table 3.1**), which was bound stoichiometrically in our EMSA assay.

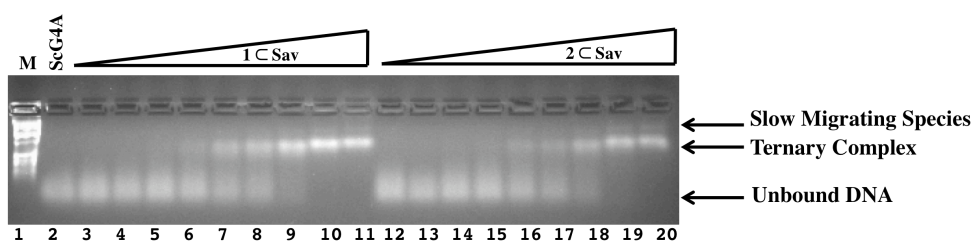


**Fig. 3.21 Binding of metallodrug-presenter protein assemblies to scrambled G4A monitored by EMSA on agarose gels. a)** Gel was run after incubation of **1 C Sav** with scrambled (Sc) G4A. Lane 1, DNA Marker. Lane 2, ScG4A. Lanes 3-11, ScG4A(3.3  $\mu\text{M}$ ) + **1 C Sav** at increasing concentrations: 0.4  $\mu\text{M}$ , 0.6  $\mu\text{M}$ , 0.8  $\mu\text{M}$ , 1.6  $\mu\text{M}$ , 3.2  $\mu\text{M}$ , 3.9  $\mu\text{M}$ , 7.9  $\mu\text{M}$ , 19.8  $\mu\text{M}$ , 39.6  $\mu\text{M}$ , representing a **1 C Sav** : ScG4A ratio from 0.12 to 12. In all cases 500 ng of DNA was loaded onto the gel. **b)** Gel was run after incubation of **2 C Sav** with ScG4A. Lanes 12-20, ScG4A (3.3  $\mu\text{M}$ ) + **2 C WT-Sav** at the same ratio and increasing concentrations than gel a)

Slow-migrating species were visible on the EMSA gel, suggesting multiple binding. The complexity of binding to unstructured and flexible ssDNA was also reflected in ITC experiments. The ITC titration curves (**Fig. 3.22**) for both unstructured ssDNA oligonucleotides could not be fitted to a single set of identical sites model, as in the **1 C Sav** into G4A (KOH) titration described previously.

Analysis was further hampered by a superimposition of an endothermic component on an exothermic component.

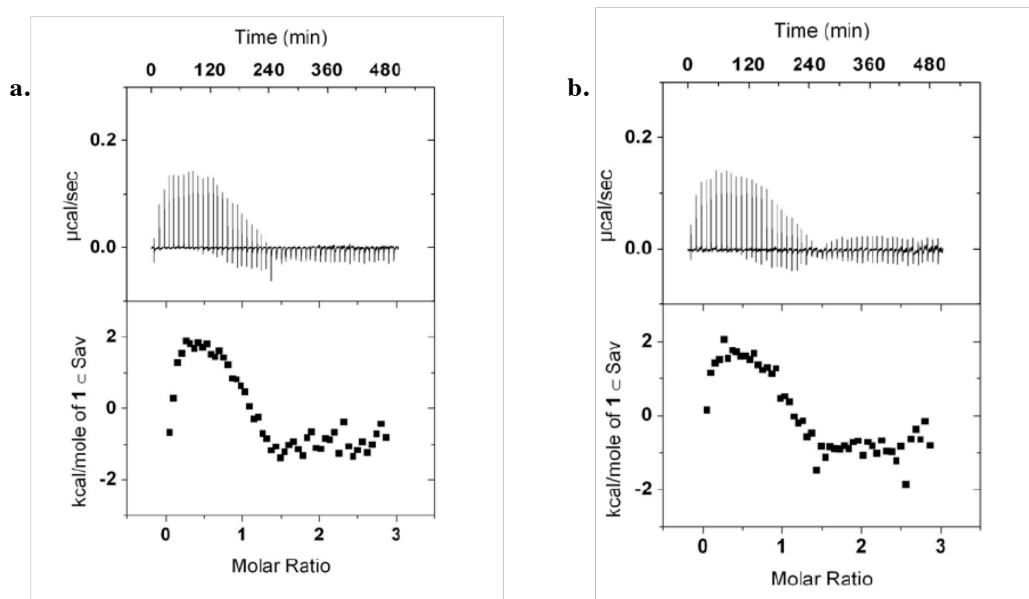


**Fig. 3.22 ITC titration of 1 C Sav assembly into a solution of unstructured ssDNA.** a) ITC profile of 1 C Sav assembly into a solution with G4A-Li<sup>+</sup>. b) ITC profile of 1 C Sav assembly into a solution containing scrambled G4A. The top panels represent the raw data for 50 sequential injections of 1 C Sav into G4A-Li<sup>+</sup> and scrambled DNA, respectively. The bottom panels show the plot of the heat evolved (kcal) per mole of drug-presenter protein added

The high similarity of these titration curves suggested comparable binding mechanisms of drug-streptavidin to each unstructured ssDNA. These mechanisms were markedly different and more complicated than the “one site model” binding of drug-presenter protein to K<sup>+</sup>-stabilized quadruplex G4A.

### ***3.3.7 Competition Studies with Single Stranded DNA***

Competition studies were also carried out in the presence of exceeded competing ssDNA co-incubated with G4A (up to 157 equivalents of ssDNA vs G4A).

We selected two different oligonucleotides: single stranded 12mer, with high guanine content, and a smaller trinucleotide GGG.

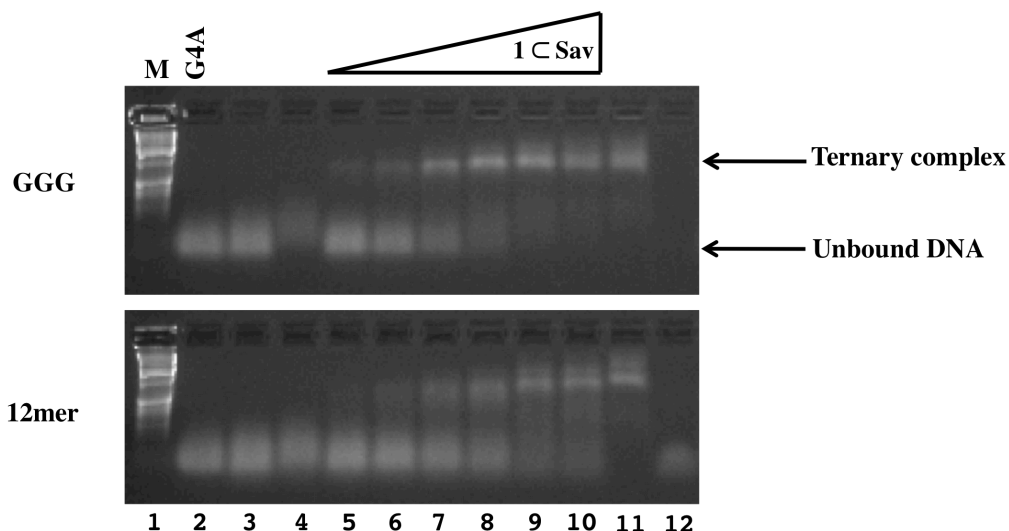


**Fig. 3.23 Binding of 1 C Sav assembly to G4A-DNA in the presence of competing ssDNA substrates monitored by EMSA on agarose gels.** Lane 1, Marker. Lane 2, G4A. Lane 3, G4A (3  $\mu\text{M}$ ) + GGG trinucleotide (206.5  $\mu\text{M}$ ) or 12mer (462  $\mu\text{M}$ ), respectively. Lane 4, G4A (3  $\mu\text{M}$ ) + GGG (206.5  $\mu\text{M}$ ) or 12mer (462  $\mu\text{M}$ ) respectively + complex **1** (76.5  $\mu\text{M}$ ). Lane 5-10, GGG (206.5  $\mu\text{M}$ ) or 12mer (462  $\mu\text{M}$ ) were incubated with G4A (3  $\mu\text{M}$ ) and the **1 C Sav** assembly at increasing concentrations: 0.7  $\mu\text{M}$ , 1.4  $\mu\text{M}$ , 3.5  $\mu\text{M}$ , 7  $\mu\text{M}$ , 17.7  $\mu\text{M}$ , 35.3  $\mu\text{M}$ . Under these conditions, the molar ratio **1 C Sav** : G4A ranges from 0.2 to 12, while GGG : G4A and 12mer : G4A ratio is 69 and 154, respectively. Lane 11, G4A (3  $\mu\text{M}$ ) + **1 C Sav** assembly (35.3  $\mu\text{M}$ ). Lane 12, GGG (206.5  $\mu\text{M}$ ) or 12mer (462  $\mu\text{M}$ ) in the presence of **1 C Sav** assembly (35.3  $\mu\text{M}$ ). GGG or 12mer are barely visible by ethidium bromide staining due to lack of intercalation of the dye in ssDNA

EMSA assays revealed that an excess of these competing ssDNA co-incubated with G4A lowered only marginally the binding of the metallodrug-protein assembly to G4A ( $K_d = 2 \mu\text{M}$  for **1 C Sav** towards G4A co-incubated with GGG;  $K_d = 5.5 \mu\text{M}$  for **1 C Sav** towards G4A co-incubated with 12mer, entries 11-12, **Table 3.1**).

As revealed by EMSA-estimated binding affinities, the single stranded 12mer was better at inhibiting G4A-binding than GGG due to the existence of a more extended interaction with the metallodrug-presenter protein assembly compared with the smaller GGG-trinucleotide. These results supported the notion that G4A was a privileged target.

### ***3.3.8 Genetic Control of the Second Coordination Sphere***

The influence of the second coordination sphere on G4A-binding was investigated through site-directed mutagenesis on the gene encoding streptavidin and monitored by EMSA.

The X-ray crystal structure of the complex **1** embedded into the WT Sav (**Fig. 3.9**) highlighted mainly on two amino acid residues, S112 and K121, close to the active site as being important for the assembly.

Mutation of two positively-charged lysines (K121A) at the entrance of the largely hydrophobic biotin-binding pocket K121 inhibited interactions of the drug-presenter protein assemblies with the telomeric DNA ( $K_d$  estimated by EMSA = 29  $\mu$ M, entry 13, **Table 3.1**).

This finding suggested that lysines might form a salt-bridge with the phosphate backbone of DNA, enhancing the interactions of the ternary complex <sup>[26]</sup>.

Similarly, the introduction of a negative charge close to the Ru head-group (S112D) equally reduced the G4A-DNA binding ( $K_d = 12.5 \mu$ M, entry 14, Table 3.1), perhaps by charge-repulsion. In contrast, mutating the same residue S112 to a large hydrophobic phenylalanine did not appreciably change the binding affinity for G-quadruplex DNA ( $K_d = < 1.6 \mu$ M, entry 15, **Table 3.1**) compared with the wild-type.

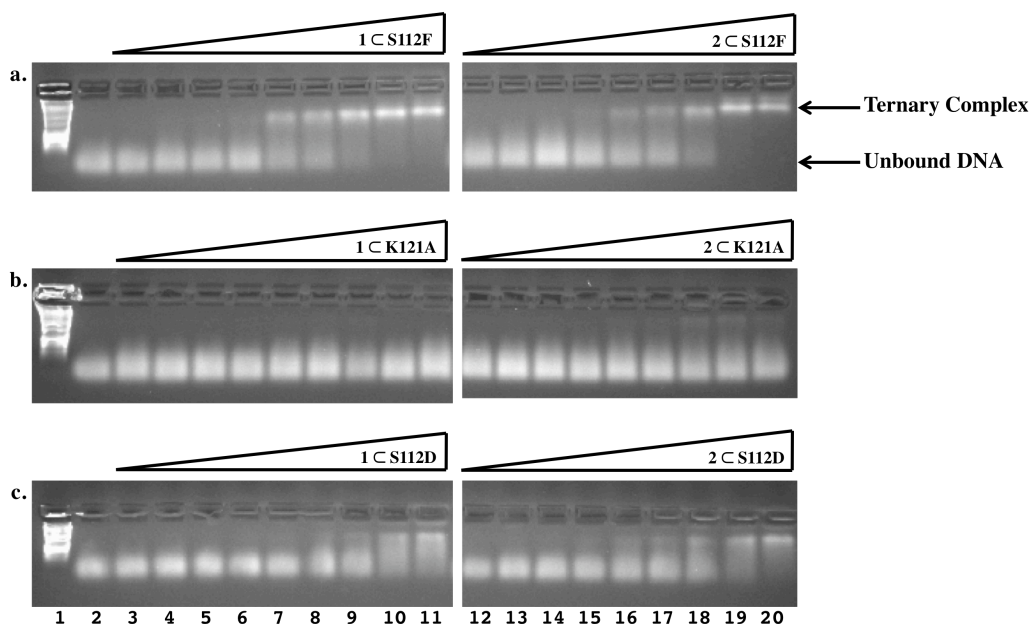


**Fig. 3.24 G4A-binding of metalldrugs embedded in different streptavidin isoforms monitored by EMSA on agarose gels.** a) Gels were run after incubation of **1** C S112F or **2** C S112F with G4A. b) Gels were run after incubation of **1** C K121A or **2** C K121A with G4A. c) Gels were run after incubation of **1** C S112D or **2** C S112D with G4A. Lane 1, DNA Marker. Lane 2, G4A. Lanes 3-11, G4A(3.3  $\mu$ M) + **1** C Sav isoforms at increasing concentrations: 0.4  $\mu$ M, 0.6  $\mu$ M, 0.8  $\mu$ M, 1.6  $\mu$ M, 3.2  $\mu$ M, 3.9  $\mu$ M, 7.9  $\mu$ M, 19.8  $\mu$ M, 39.6  $\mu$ M, representing a **1** C Sav : G4A ratio from 0.12 to 12. Lanes 12-20, G4A (3.3  $\mu$ M) + **2** C Sav isoforms at the same ratio and increasing concentrations. In all cases 500 ng of DNA was loaded onto the gel

These results were also consistent with the existence of an extended interaction between G4A-DNA and drug-protein assembly.

In light of these results we speculated that a genetic optimization of streptavidin might increase the selectivity of the metalldrug-presenter protein assembly towards the DNA target.

### 3.3.9 Chemo – Genetic Optimization with Increased dsDNA Affinity

To estimate the affinity of drug-presenter protein complex for double-stranded DNA on agarose gels, titrations of **1** C Sav and **2** C Sav were carried out with a 18 base pair dsDNA including the sequence of the common Braf V599E oncogenic mutation (dsOnc)<sup>[27]</sup>.



As estimated by EMSA, the affinity constant of **1**  $\subset$  Sav for dsOnc was significantly lower ( $K_d = 37.9 \mu\text{M}$ , entry 16, **Table 1.3**) compared to the affinity for single-stranded G4A ( $K_d = < 1.6 \mu\text{M}$ , entry 2, **Table 1.3**). We hypothesized that a different organization of functional groups as well as the reduced flexibility of dsDNA hampered efficient interactions between the ruthenium and nucleophilic sites on the bases <sup>[28]</sup>.

Chemo-genetic optimization of metallodrug-protein assembly improved the binding to dsDNA. As proof-of-the-concept, a chemical modification of the Ru (II) complex, with a *p*-cymene replaced by a biphenyl group in the arene cap, was combined with a genetic modification of the second coordination sphere, by incorporation of an aromatic residue at the position closest to Ru (S112F). The resulting drug-presenter protein complex (**2**  $\subset$  S112F) increased the affinity to dsDNA by at least a factor two from 37.9 to 18.2  $\mu\text{M}$  (entries 18-19, **Table 1.3**) compared to **1**  $\subset$  WT and **2**  $\subset$  WT ( $K_d = 37.9 \mu\text{M}$ , entries 16-17, **Table 1.3**) as best illustrated in lane 20 of **Fig. 3.25d**.

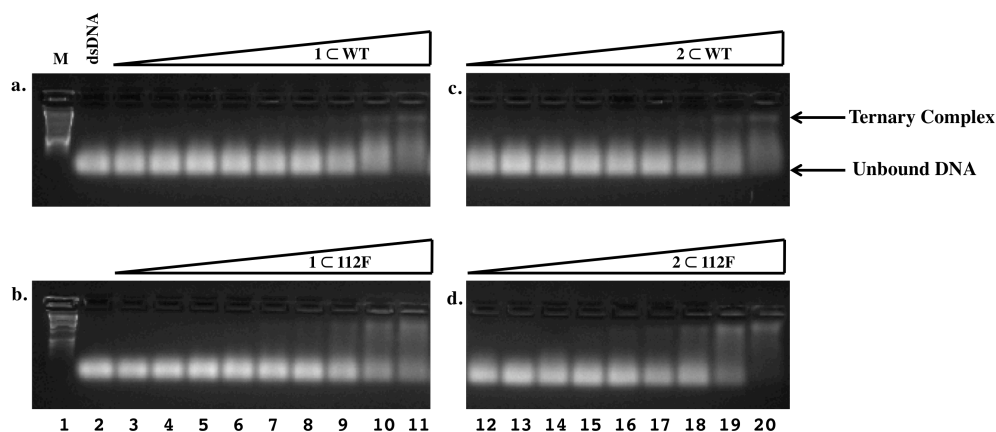


**Fig. 3.25 Chemo-genetic optimization of drug-streptavidin assemblies for improved binding to dsDNA monitored by EMSA on agarose gels.** Comparison of wildtype streptavidin (WT; **a** and **c**) to a genetic variant S112F (**b** and **d**) illustrates that the nature of the metallodrug and presenter protein can influence the binding to dsDNA. Lane 1, Marker (M). Lane 2, dsOnc. Lanes 3-11, dsOnc (3.12  $\mu$ M) + concentration increase of **1** C Sav: 0.4  $\mu$ M, 0.6  $\mu$ M, 0.8  $\mu$ M, 1.6  $\mu$ M, 3.2  $\mu$ M, 3.9  $\mu$ M, 7.9  $\mu$ M, 19.8  $\mu$ M, 39.6  $\mu$ M with a **1** C Sav : dsOnc ratio from about 0.1 to 13. Lanes 12-20, dsOnc (3.12  $\mu$ M) + concentration increase of **2** C Sav: 0.4  $\mu$ M, 0.6  $\mu$ M, 0.8  $\mu$ M, 1.6  $\mu$ M, 3.2  $\mu$ M, 3.9  $\mu$ M, 7.9  $\mu$ M, 19.8  $\mu$ M, 39.6  $\mu$ M with a **2** C Sav : dsOnc ratio from about 0.1 to 13. In all cases 500 ng of DNA was loaded onto the gel

This result suggested that a chemo-genetically engineering of drug-streptavidin assemblies, with a different arene-cap and through point mutations within the host protein, might afford more specialized binders with increased target-selectivity.

### 3.3.10 Summary of $K_d$ Estimated by EMSA and Determined by ITC

ITC titration and EMSA analysis were important tools to estimate the dissociation constants ( $K_d$ ) of ruthenium metal drug C streptavidin assemblies for various DNA targets (**Table 3.1**).

To extrapolate the affinity constants from EMSA analysis, the intensity of the bands in which DNA migrates approximately equally-distributed between the slow mobility and high mobility species, were fitted to the equation:

$$K_d = [\text{Ru-complex C Sav}]_0 - \frac{1}{2} [\text{DNA}]_0$$

with  $[\text{Ru-complex} \subset \text{Sav}]_0$  and  $[\text{DNA}]_0$  as initial concentrations of drug-presenter protein and DNA, respectively. The band intensity was assumed to be proportional to the concentration of sample when loaded on the gel.

In the case of **1**  $\subset$  Sav binding to G4A, a 1 : 1 stoichiometry of **1**  $\subset$  Sav to DNA target was observed and only an upper estimate of  $K_d$  could be determined by EMSA.

**Table 3.1 Summary of  $K_d$  of ruthenium-Sav assemblies for different DNA targets, as estimated by EMSA**

Entry	DNA Target	Metal complex	Sav	Ratio Ru:Sav	$K_d$ estimated by EMSA ( $\mu\text{M}$ )
1	G4A	None	WT	/	$> 145^a$
2	G4A	1	WT	2	$< 1.6^{b,c}$
3	G4A	2	WT	2	6.25
4	G4A	1	WT	1	2.3
5	G4A	1	WT	4	$< 1.6^c$
6	G4A (GSH) <sup>d</sup>	1	WT	2	$< 1.6^c$
7	G4A (Li <sup>+</sup> )	1	WT	2	$< 1.6^c$
8	G4A (Li <sup>+</sup> )	2	WT	2	1.55
9	ScG4A	1	WT	2	2.25
10	ScG4A	2	WT	2	2.25
11	G4A (GGG) <sup>d</sup>	1	WT	2	2
12	G4A (12mer) <sup>d</sup>	1	WT	2	5.5
13	G4A	1	K121A	2	28
14	G4A	1	S112D	2	12.2
15	G4A	1	S112F	2	$< 1.6^c$
16	dsOnc	1	WT	2	37.9
17	dsOnc	2	WT	2	37.9
18	dsOnc	1	S112F	2	37.9
19	dsOnc	2	S112F	2	18.2

<sup>a</sup>  $K_d$  determined by ITC: 15.2  $\mu\text{M}$

<sup>b</sup>  $K_d$  determined by ITC: 0.74  $\mu\text{M}$

<sup>c</sup> Binding was stoichiometric and probably beyond the sensitivity of these EMSA

<sup>d</sup> In brackets competing species: glutathione (GSH), trinucleotide GGG (GGG), ssDNA 12mer (12mer)

## **3.4 Materials and Methods**

### ***3.4.1 Chemicals***

Solvents used were all of analytical grade.

All solutions were prepared using deionised water.

**Table 3.2 List of chemical and supplier**

<b>Chemical</b>	<b>Supplier</b>
Acrylamide	
Glucose	
SDS	
Chloramphenicol	
Ampicillin	AppliChem
PMSF	
IPTG	
Glycerol	
KOH	
Tris	
Bactoyeast extract	Merck
Bactotryptone	BD
NaCl	
DMSO	
DTT	
KH <sub>2</sub> PO <sub>4</sub>	Fluka
Sucrose	
Coomassie Brilliant Blue	
TEMED	
Acetic acid	
NaOH	VWR
HCl	
LiOH	
APS	
Na <sub>2</sub> HPO <sub>4</sub>	Sigma
B4F	
DNaseI	
Guanidinium/HCl	Acros Organics
BenchMark™ Protein Ladder	Invitrogen
Bromophenol Blue	Riedel-de Haën
dNTP	Promega
Dpn1	Biolabs
DNA ladder	
Pfu Turbo	Stratagene

### ***3.4.2 Technical Equipment***

- Protein expression in 20 L of *E. coli* cell culture was performed in a fermentor NLF22 (Bioengineering®).
- PCR was performed in an eppendorf mastercycler gradient
- DNA concentration was determined by nanodrop 1000 spectrophotometer (Thermo Fisher Scientific).
- Agarose gel was analyzed with Molecular Image Gel Doc XR (Bio-Rad®, Switzerland).
- Protein was lyophilized in a lyophilizer FreeZone 2.5 L (benchtop of Labconco, USA).
- The active sites of proteins were determined with the Fluorescence Reader Safire (Tecan®).
- FPLC was performed by using äkta prime machine.
- ITC was performed in a VP-ITC titration calorimetry (*MicroCal*, Northampton, MA, USA).
- Crystallization was initially performed in high-throughput liquid-handling system (*PHOENIX*, Art Robbins Instruments, California).

### ***3.4.3 DNA***

Oligonucleotides (desalted) were purchased from MICROSYNTH (Switzerland).

DNA stocks were dissolved in mQ-water and quantified spectrophotometrically at 260 nm.

DNA was prepared for experiments by heat denaturation at 95 °C for 10 minutes, in 75 mM MOPS buffer with KOH or LiOH (10 mM) at pH 6.5, followed by cooling down to room temperature. The oligonucleotide sequences were:

*G4A*, CATGGTGGTTTGGGTTAGGGTTAGGGTTAGGGTTAACCAC;

*Scrambled-G4A*,

GTGAGTGTGCTGTGTAGGTGTAGTACGTGTGGAGTCAC;

*Onc*, CTAGCTACAGAGAAATCTCGA and complementary strand.

### ***3.4.4 Electrophoretic Mobility Shift Assay in Agarose Gel***

EMSA were carried out on 1.2% agarose gels containing ethidium bromide (5 µg per 100 mL of gel) in standard Tris-Borate-EDTA (TBE) buffer.

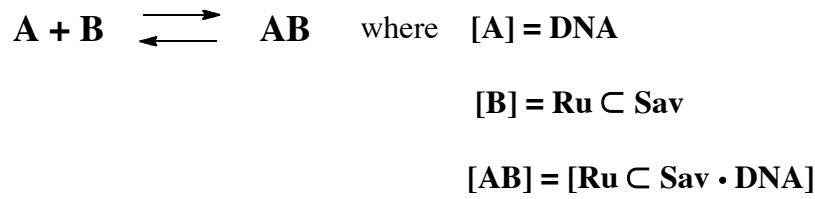
500 ng of DNA, previously refolded after heat denaturation, were incubated at 37 °C for 30 minutes with the desired amount of protein and complex mixture to give a final concentration of 13.7 µM oligonucleotide in 75 mM MOPS buffer, with KOH or LiOH (10 mM) at pH 6.5. After incubation, loading buffer consisting only of 40% sucrose was added to a final 1/6 of total volume before charging the gels. Electrophoresis was typically run at 45 V for 20-30 minutes. DNA marker with blue dye (DNA Molecular Weight Marker X, 0.07-12.2 Kb.p., Roche) was used to follow DNA migration and to confirm similar running conditions between gels.

The affinity constants, sometimes confirmed by ITC, were estimated by EMSA.

To extrapolate the affinity constants from EMSA analysis, the intensity of the bands in which DNA migrates approximately equally-distributed between the slow mobility and high mobility species, were fitted to the equation (1):

$$K_d = [\text{Ru-complex} \subset \text{Sav}]_0 - 0.5 [\text{DNA}]_0 \quad (1)$$

The equation (1) was derived from this simplified binding model:



The affinity constant was described by the equation (2):

$$K_a = \frac{[AB]}{[A][B]} \quad (2)$$

The initial concentrations were defined as:

$$C_0A = [A] + [AB] = [\text{DNA}] + [\text{Ru C Sav} \cdot \text{DNA}]$$

$$C_0B = [B] + [AB] = [\text{Ru C Sav}] + [\text{Ru C Sav} \cdot \text{DNA}]$$

By deriving:

$$[A] = C_0A - [AB] \quad [\text{DNA}] = [\text{DNA}]_0 - [\text{Ru C Sav} \cdot \text{DNA}]$$

$$[B] = C_0B - [AB] \quad [\text{Ru C Sav}] = [\text{Ru C Sav}]_0 - [\text{Ru C Sav} \cdot \text{DNA}]$$

Assuming that at 50% intensity for both bands:

$$[AB] = [A] = 0.5 \cdot C_0A$$

$$[\text{Ru C Sav} \cdot \text{DNA}] = [\text{DNA}] = 0.5 [\text{DNA}]_0$$

The affinity constant became:

$$K_a = \frac{(0.5 C_0A)}{(0.5 C_0A) \cdot (C_0B - 0.5 C_0A)}$$



$$K_a = \frac{0.5 [\text{DNA}]_0}{0.5 [\text{DNA}]_0 \cdot ([\text{Ru-complex} \subset \text{Sav}]_0 - 0.5 [\text{DNA}]_0)}$$

Finally, considering that:  $K_d = \frac{1}{K_a}$

We derived the equation (1):

$$K_d = [\text{Ru-complex} \subset \text{Sav}]_0 - 0.5 [\text{DNA}]_0 \quad (1)$$

with  $[\text{Ru-complex} \subset \text{Sav}]_0$  and  $[\text{DNA}]_0$  as initial concentrations of drug-presenter protein and DNA, respectively. The band intensity was assumed to be proportional to the concentration of sample when loaded on the gel. Values estimated for **Table 3.1** assume in all cases a 1 : 1 stoichiometry.

#### ***3.4.5 Electrophoretic Mobility Shift Assays in Acrylamide Gel***

Non-denaturing TBE-polyacrylamide gel was also performed to resolve the ternary complex drug-streptavidin-DNA from free protein, without nevertheless a defined and meaningful stoichiometric resolution of the ternary complex.

In non-denaturing gels, protein mobility is influenced by molecular weight, conformation and charge. Instead, in Sodium Dodecyl Sulphate Polyacrylamide Gel Electrophoresis (SDS-PAGE), the major determinant of protein mobility is the length of the polypeptide chain, since SDS gives all proteins equal negative charge. EMSA was carried out in 6% acrylamide gel (acrylamide, 1X TBE, APS and TEMED) in total absence of SDS. Preparation of samples was the same as described in subsection “*Electrophoretic Mobility Shift Assays (EMSA) in agarose gel*” (3.3.3).

Loading buffer consisting of Bromophenol blue and 40% sucrose was added to a final 1/6 of total volume before charging the gel.

The gel, cast between glass plates, was run at 45 V in 1X TBE running buffer and stained in Coomassie blue.

See APPENDIX D for a more detailed picture.

### ***3.4.6 Protein Expression and Purification***

Ultra-competent BL21(DE3)pLysS *E. coli* strains (in house) were transformed by pET11b-Sav plasmid (University of Milan, Prof. Paolo Santambrogio) containing a gene encoding recombinant streptavidin. Transformed bacteria, plated on selective Luria broth (LB) petri dishes containing ampicillin (60 mg/mL), chloramphenicol (34 mg/mL) and glucose (2% w/v), were incubated overnight at 37 °C.

300 mL of tryptone medium (20 g/L Bactotryptone; 2 g/L Na<sub>2</sub>HPO<sub>4</sub>, 1 g/L KH<sub>2</sub>PO<sub>4</sub>; 8 g/L NaCl; 15 g/L Bactoyeast extract), containing antibiotics and glucose at the same concentrations as in LB plates, were inoculated with a single colony and incubated overnight in an orbital shaker (37 °C, 250 rpm).

A 20 L cell culture, inoculated with the whole pre-culture, was grown in a 30 L fermentor (Bioengineering, Switzerland) at 37 °C, with 600 rpm agitation speed, in the presence of glucose and antibiotics.

For a detailed description of streptavidin expression and purification see Appendix C.

### **3.4.7 Site – Directed Mutagenesis**

Site-directed mutagenesis was carried out using Quick-Change mutagenesis kit (Stratagene, Switzerland) on the pET11b-Sav plasmid. The forward (positive) and the reverse (negative) primers (Microsynth, Switzerland) were partially overlapped with each other and fully complementary at the mutation site.

Ultra-competent XL1-Blue *E. coli* cells (in house) were transformed by PCR product. The plasmids were extracted from bacteria with a *Promega miniprep* kit (Promega®) and clones were used to transform ultra-competent BL21(DE3)pLysS *E. coli* strains.

For a detailed description of molecular biology see Appendix B.

### **3.4.8 Isothermal Titration Calorimetry (ITC)**

All ITC experiments were carried out using a VP-ITC titration calorimeter (MicroCal, Northampton, MA, USA) at 25 °C with MOPS buffer (75 mM) prepared with 10 mM KOH or LiOH at pH 6.5. Prior to each experiment, all solutions were thoroughly degassed and the ITC sample cell washed several times with MOPS buffer solution (containing KOH or LiOH).

The titration was carried out using a 300 µL syringe filled with the 1 C Sav solution or Sav solution. Injections began after baseline stability had been achieved. A typical titration experiment consisted of 50 consecutive injections of 10 µL volume and 10 s duration, with a 10 min interval between each injection and stirring at 300 rpm.

The titration was carried out with a 1 C Sav or Sav concentration of 0.375 mM. Heats of dilution of 1 C Sav solution into the buffer alone were used to adjust total observed heats of binding. At least two titration experiments were performed

for each sample set to evaluate reproducibility. The resulting data were fitted using MicroCal ORIGIN software supplied with the instrument.

### ***3.4.9 Crystallization***

Initial screening trials were set up in a high-throughput liquid-handling system (*PHOENIX*, Art Robbins Instruments, California) equipped with 96 well sitting drop plates. Classical screens in kit form, such as *Crystal Screen* and *Crystal Screen 2* (Hampton Research, California), were used as crystallization solutions. In order to optimize crystal growth, microbatch under oil crystallization experiments were carried out manually. Trials were conducted in 96-well plates, filled up with 50  $\mu\text{L}$  of mineral or paraffin oil <sup>[29]</sup>. 1 or 2  $\mu\text{L}$  of the sample, consisting of pure streptavidin (26 mg/mL in  $\text{H}_2\text{O}$ ) with biotinylated Ru (II) metal-complex **1** (0.15 mM in  $\text{H}_2\text{O}$ ), was mixed with different crystallization solutions in a ratio 1:1, 1:2, 2:2 (v/v in  $\mu\text{L}$ ).

Successful crystallizations were obtained with 2.99 M NaCl, 0.1 M Na Citrate, pH 4; 0.1 M LiBr, 0.1 M Na Citrate, PEG 8000 40%, pH 4; 0.1 M citric acid, PEG 3350 25%, pH 3.5. Crystals were not exposed to cryo solutions before freezing in liquid nitrogen. However, diffraction data were not collected due to low diffraction quality. Crystal structure of drug-streptavidin assembly (complex **1 C Sav**) was resolved by Tillmann Heinisch (in collaboration with the Prof. Tilman Schirmer, Biozentrum, Universität Basel). Apo-streptavidin was crystallized using the hanging drop vapor diffusion technique <sup>[30]</sup>. Rhombohedral crystals were obtained by mixing 5  $\mu\text{L}$  protein solution (26 mg/mL in  $\text{H}_2\text{O}$ ) with 5  $\mu\text{L}$  crystallization buffer (2 M  $(\text{NH}_4)\text{SO}_4$ , 0.1 M Na Acetate, pH 4.0) and equilibrating the droplet against a reservoir of 500  $\mu\text{L}$  crystallization buffer for 24

h at room temperature. The ligand soaking solution was prepared by mixing 9  $\mu\text{L}$  stabilization buffer (3 M  $(\text{NH}_4)\text{SO}_4$ , 0.1 M Na Acetate, pH 4.0) with 1  $\mu\text{L}$  ligand solution (50 mM  $[(\eta^6\text{-}p\text{-cymene})\text{Ru}(\text{Biot-L})\text{Cl}]\text{CF}_3\text{SO}_3$  in water). Lyophilized streptavidin (about 100-300  $\mu\text{g}$ ) was added to the ligand soaking solution subsequently to scavenge non-modified biotin. A single apo-streptavidin crystal was soaked for 24 h at room temperature. Then, the crystal was placed into cryo buffer (1.5 M  $(\text{NH}_4)\text{SO}_4$ , 0.1 M Na acetate, pH 4.0, 25% glycerol) for 30 s before to be frozen in liquid nitrogen.

### 3.5 Conclusions

The streptavidin presenter protein <sup>[11]</sup> provided an additional surface area available for interactions between metallo-drug and its macromolecular target, improving affinity and specificity for telomeric G4A. Further structural studies of ternary complexes will be of great assistance in achieving sequence selectivity by rational design.

Supramolecular assembly of a drug with a host protein may be proposed as a new attractive alternative to the current anti-cancer therapeutic agents. The binding of metal complex with a presenter protein protects the drug from unwanted interactions and chaperones its specific delivery to desired macromolecular targets.

The exploitation of an endogenous protein, such as an overexpressed protein in cancer cells, as a presenter protein for metallo-drugs can be a new outlook for rational drug-design.

Although these studies were carried out *in vitro*, it could be possible to engineer hybrid organometallic species with improved binding and selectivity *in vivo*. The intracellular delivery of chaperoned metallo-drugs still remains a challenge, due to the poor uptake of hydrophilic compounds by the cells. Over the past decade, numerous strategies to overcome the cell membrane barriers have been proposed, including electroporation, microinjection, viral vectors and liposome encapsulation, but these still have low delivery efficiencies<sup>[31]</sup>.

Therefore, naturally occurring, short, cell-penetrating peptides (CPPs) have attracted considerable interest in the field of drug delivery for their ability for direct cellular uptake. CPPs are oligopeptides containing cationic and hydrophilic residues and are able to deliver an array of pharmacological cargoes into the cells<sup>[32]</sup>.

Streptavidin and related avidins have previously been used in clinical trials as drug carriers, but unfortunately with difficult cellular uptake and low intracellular delivery<sup>[33]</sup>. In order to increase the internalization of these therapeutic proteins, a cell penetrating peptide, known as TAT, has been attached to the *N*-terminus of each streptavidin monomer. This system acted as carrier of biotinylated complexes into the nucleus of human cells to interact with the target DNA<sup>[31, 34]</sup>.

The extension of the ruthenium metallodrug-protein concept to other molecular targets, such as RNA, is an interesting perspective for future applications. RNA plays an important role in biological processes, as the carrier of necessary information for biological functions. It offers several advantages as a drug target: lack of cellular repair mechanisms, structural diversity, and direct influence on gene expression<sup>[35]</sup>.

A few years ago, Verdine <sup>[18]</sup> and Pelletier <sup>[17]</sup> developed RNA-targeting systems, in which a small molecule was presented to RNA in complex with a protein. This approach allowed modulation of gene expression.

Furthermore chaperoned metallodrugs were defined as high-affinity binders specific for ssDNA. This high affinity could be exploited to label and detect telomeric structures *in vitro* and *in vivo*, providing alternatives to antibodies <sup>[35]</sup>.

# REFERENCES

- [1] L. H. Hurley, *Nat. Rev. Cancer* **2002**, 2, 188.
- [2] a)B. Rosenberg, L. VanCamp, T. Krigas, *Nature* **1965**, 205, 698; b)L. Kelland, *Nat. Rev. Cancer* **2007**, 7, 573.
- [3] R. E. Aird, J. Cummings, A. A. Ritchie, M. Muir, R. E. Morris, H. Chen, P. J. Sadler, D. I. Jodrell, *Br. J. Cancer* **2002**, 86, 1652.
- [4] H.-K. Liu, S. J. Berners-Price, F. Wang, J. A. Parkinson, J. Xu, J. Bella, P. J. Sadler, *Angew. Chem. Int. Ed.* **2006**, 45, 8153
- [5] S. J. Dougan, A. Habtemariam, S. E. McHale, S. Parsons, P. J. Sadler, *Proc. Nat. Acad. Sci. U.S.A.* **2008**, 105, 11628.
- [6] P. Sore, Z.H. Oster, K. Matsui, G. Guglielmi, B.R.R. Persson, M.L. Pellettieri, S.C. Srivastava, P. Richards, H.L. Atkins, A. B. Brill, *Eur. J. Nucl. Med.* **1983**, 8, 491.
- [7] R. E. Morris, R. E. Aird, P. d. S. Murdoch, H. Chen, J. Cummings, N. D. Hughes, S. Parsons, A. Parkin, G. Boyd, D. I. Jodrell, P. J. Sadler, *J. Med. Chem.* **2001**, 44, 3616.
- [8] C. G. Hartinger, A. Casini, C. Duhot, Y. O. Tsybin, L. Messori, P. J. Dyson, *J. Inorg. Biochem.* **2008**, 102, 2136.
- [9] F. Y. Wang, S. Weidt, J. J. Xu, C. L. Mackay, P. R. R. Langridge-Smith, P. J. Sadler, *J. Am. Soc. Mass Spectrom.* **2008**, 19, 544.
- [10] F. Wang, J. Xu, A. Habtemariam, J. Bella, P. J. Sadler, *J. Am. Chem. Soc.* **2005**, 127, 17734.
- [11] R. Briesewitz, G. T. Ray, T. J. Wandless, G. R. Crabtree, *Proc. Nat. Acad. Sci. U.S.A.* **1999**, 96, 1953.
- [12] a)G. R. Crabtree, *Science* **1989**, 243, 355; b)S. L. Schreiber, *Science* **1991**, 251, 283.
- [13] A. C. Papageorgiou, K. R. Acharya, *Trends Microbiol.* **2000**, 8, 369.
- [14] C. A. Janeway, P. Travers, M. Walport, M. J. Shlomchik, *Immunobiology, 5th edition* **2001**.
- [15] J. B. Nielsen, F. Foor, J. J. Siekierka, M. J. Hsu, N. Ramadan, N. Morin, A. Shafiee, A. M. Dahl, L. Brizuela, G. Chrebet, K. A. Bostian, S. A. Parent, *Proc. Nati. Acad. Sci. USA* **1992**, 89, 7471.
- [16] L. A. Banaszynski, C. W. Liu, T. J. Wandless, *J. Am. Chem. Soc.* **2005**, 127, 4715.
- [17] I. Harvey, P. Garneau, J. Pelletier, *Proc. Nat. Acad. Sci. U.S.A.* **2002**, 99, 1882.
- [18] K. A. Plummer, J. M. Carothers, M. Yoshimura, J. W. Szostak, G. L. Verdine, *Nucleic Acids Res.* **2005**, 33, 5602.
- [19] M. Creus, A. Pordea, T. Rossel, A. Sardo, C. Letondor, A. Ivanova, I. LeTrong, R. E. Stenkamp, T. R. Ward, *Angew. Chem. Int. Ed.* **2008**, 47, 1400.
- [20] J. Pierron, C. Malan, M. Creus, J. Gradinaru, I. Hafner, A. Ivanova, A. Sardo, T. R. Ward, *Angew. Chem. Int. Ed.* **2008**, 47, 701.
- [21] F. Han, R. Wheelhouse, L. Hurley, *J. Am. Chem. Soc.* **1999**, 121, 3561.
- [22] S. Balasubramanian, S. Neidle, *Curr. Opin. Chem. Biol.* **2009**, 13, 345.



- [23] H.-K. Liu, S. J. Berners-Price, F. Wang, J. A. Parkinson, J. Xu, J. Bella, P. J. Sadler, *Angew. Chem. Int. Ed.* **2006**, *45*.
- [24] M. Morpurgo, A. Radu, E. Bayer, M. Wilchek, *Journal of Molecular Recognition* **2004**, *17*, 558.
- [25] a) D. Wang, S. J. Lippard, *Nat. Rev. Drug Discov.* **2005**, *4*, 307; b) J. Reedijk, *Chem. Rev.* **1999**, *99*, 2499.
- [26] P. Buczek, M. P. Horvath, *J. Mol. Biol.* **2006**, *359*, 1217.
- [27] H. Namba, M. Nakashima, T. Hayashi, N. Hayashida, S. Maeda, T. I. Rogounovitch, A. Ohtsuru, V. A. Saenko, T. Kanematsu, S. Yamashita, *J. Clin. Endocrinol. Metab.* **2003**, *88*, 4393.
- [28] D. Theobald, S. Schultz, *EMBO J.* **2003**, *22*, 4314.
- [29] J. R. Luft, R. J. Collins, N. A. Fehrman, A. M. Lauricella, C. K. Veatch, G. T. DeTitta, *J. Struct. Biol.* **2003**, *142*, 170.
- [30] A. Pahler, W. A. Hendrickson, M. A. Kolks, C. E. Argarana, C. R. Cantor, *J. Biol. Chem.* **1987**, *262*, 13933.
- [31] J. Rinne, B. Albarran, J. Jylhävä, T. O. Ihalainen, P. Kankaanpää, V. Hytönen, P. S. Stayton, M. S. Kulomaa, M. Vihinen-Ranta, *BMC Biotech.* **2007**, *7*, 1.
- [32] Y. Lee, A. Erazo-Oliveras, J. Pellois, *ChemBioChem* **2009**, *10*, 1.
- [33] B. Schechter, R. Silberman, R. Arnon, M. Wilchek, *Eur. J. Biochem.* **1990**, *189*, 327.
- [34] B. Albarran, R. To, P. S. Stayton, *Protein Eng. Des. Sel.* **2005**, *18*, 147.
- [35] C. Schaffitzel, I. Berger, J. Postberg, J. Hanes, H. J. Lipps, A. Pluckthun, *Proc. Nat. Acad. Sci. U.S.A.* **2001**, *98*, 8572.

---

## Chapter 4

# Novel Avidin from *B. pseudomallei*

*The whole of science is  
nothing more than a  
refinement of everyday  
thinking*

---

Albert Einstein

### 4.1 Introduction

#### 4.1.1 Avidins Useful in Biotechnology

Avidins have been widely exploited as important tools in a plethora of medical and biotechnological applications, owing to the exceptionally high affinity for biotin through non-covalent interactions <sup>[1]</sup>.

The extremely low dissociation constants of the interaction (avidin has a  $K_d = 1.3 \cdot 10^{-15}$  M) <sup>[2]</sup> have also proven to be an incredible useful model system for the exploration of biomolecular interactions <sup>[3]</sup>.

Over the years a wide variety of novel and engineered forms of (strept)avidin have been produced leading to their routine use in many applications, including affinity chromatography, immunoassays, cytochemistry <sup>[4]</sup>, nanotechnology <sup>[5]</sup> and drug delivery <sup>[6]</sup>.

#### ***4.1.2 Avidins from Different Organisms***

The two most widely studied avidins are Avidin (Avi) and Streptavidin (Sav), which like most avidins studied to date are homotetrameric proteins consisting of four antiparallel  $\beta$ -barrels <sup>[7]</sup>.

As widely described in the introduction, Avi is naturally glycosylated and positively charged ( $pI = 10.5$ ), whereas Sav is a non-glycosylated protein with a less basic  $pI$  than avidin.

Notwithstanding a similar organization of amino acid residues in the biotin-binding pocket, Avi and Sav differ in many aspects, which render them useful for different applications <sup>[7-8]</sup>.

Consequently, many avidins other than Avi and Sav have also been investigated for potential biotechnological applications.

Avidin-related gene (AVR), isolated in chicken, encodes protein with a different glycosylation pattern, immunological activity, isoelectric point, stability and biotin-binding pathway than chicken avidin <sup>[9]</sup>.

A novel biotin-binding protein A (BBP-A) has been recently described as an avidin-like protein with similar tetrameric structure and high affinity for biotin, but with a different stability and immunological reactivity <sup>[10]</sup>.

New bacterial avidin-like proteins, characterized by a reduced immunogenicity, were isolated from nitrogen-fixing symbiotic bacteria, such as Bradavidin and Rhizavidin. Rhizavidin is also the first dimeric member of the avidin family, which maintains high affinity towards biotin <sup>[11]</sup>.

Avian avidins, isolated from egg-white of duck, goose and ostrich, display a different immunological features and potential in pretargeting cancer treatment <sup>[6b]</sup>.

Studies of different *Streptomyces* strains led to the discovery of two novel streptavidin forms (Streptavidin v1 and Streptavidin v2), purified from *Streptomyces venezuelae*. As revealed from sequence alignment, these new biotin-binding proteins shared a sequence homology of 98% with streptavidin <sup>[12]</sup>.

Tamavidin <sup>[13]</sup> and Xenavidin <sup>[14]</sup> were isolated from fungi and frogs, respectively.

Many other genes, probably encoding biotin-binding proteins, have been identified over the years.

## **4.2 Aim of the Work**

The broad aim of this chapter was to express novel bacterial avidins recombinantly in *E. coli* and to purify and characterize the proteins in view of their potential in biotechnological applications.

We aimed to characterize novel avidins in term of their biotin-binding activity and their stability over temperature ranges and in the presence of proteases and chaotropic reagents.

Inspired by our previous experience on artificial metalloenzymes, we hypothesized that novel biotin-binding proteins could be used as scaffold for hybrid catalysts.

## 4.3 Results and Discussion

### 4.3.1 Overexpression and Purification of Novel Avidins

Homology searches in DNA databases can be used to identify many putative avidin-like proteins. Of these, three candidates from bacteria were chosen for further investigation following recombinant expression in *E. coli*: one from *Rhodopseudomonas palustris*<sup>[15]</sup>, here called Rhod, and two from the human pathogen *Burkholderia pseudomallei*<sup>[16]</sup>, named Burk1 and Burk2.

The natural functions of these novel avidins remained speculative, although they might have a similar antimicrobial function to other avidins, through biotin depletion<sup>[17]</sup>.

To study the characteristics of these novel biotin-binding proteins, the genes were cloned by PCR from genomic bacterial DNA into pET11b for recombinant overexpression of the native (untagged) open reading frames in *E.coli*.

Envisaging the existence of either *N*-terminal secretion peptides or alternative start codons, several truncated forms of the genes were chosen. Protein extracts were analyzed with a functional screening assay for biotin-binding proteins<sup>[18]</sup>, which revealed functional expression of one construct of each protein.

Whereas Rhod and Burk2 migrated in the SDS-PAGE as functional and stable tetramers, Burk1 tended to form dimers.

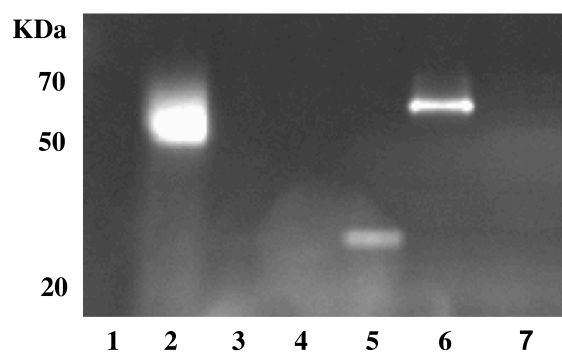


**Fig. 4.1 Functional assay of biotin-binding, monitored by SDS-PAGE in the presence of B4F.** Lane 1, protein ladder (220 KDa). Lane 2, Rhodavidin (good expression). Lane 3, Burk1 (MARPA isoform; no expression). Lane 4, Burk1 (MTGAP isoform; no expression). Lane 5, Burk1 (MQRLE isoform; (modest expression and probably dimeric). Lane 6, Burk2 (MPIQE, good expression). Lane 7, Burk2 (MDTSTA, no expression)

Visible leaching of the biotinylated fluorophore (B4F) from Rhod and Burk1 (Fig. 4.1, Lanes 2 and 5) during electrophoresis probably suggested fast dissociation and weak B4F-binding activity. Low affinity for biotin of these two proteins was confirmed by their inability to bind on iminobiotin-sepharose.

By contrast, Burk2 was the only protein purified successfully by means of its strong iminobiotin-binding, following protocols previously established for Sav<sup>[19]</sup>. About 5 mg of purified lyophilized protein per liter of culture were obtained, without further protocol optimization.

### ***4.3.2 Sequence Alignments and 3D-Modelling***

These three novel avidins presented a very low sequence similarity with each other or with either Sav or Avi. The paired-alignments revealed less than 25% sequence identity and only 12 residues from the five proteins (including Sav and Avi) aligned perfectly overall. These conserved residues were mostly implicated in biotin-binding in Sav and Avi<sup>[11a]</sup>.

A conserved tryptophan residue (Trp-120 of Sav) on a loop was involved in an inter-monomeric contact, effectively “closing” the lid of the active site upon biotin-binding <sup>[20]</sup>. However, not all biotin-binding residues were perfectly conserved and, for example, Burk2 had a leucine (Leu-106) at the equivalent position of Trp-108 of Sav, both presumably providing a hydrophobic lining inside the biotin pocket.



**Fig. 4.2 Multiple sequence alignment of novel biotin-binding proteins.** Primary structures of burkavidin-2 (Burk2), T7-tagged streptavidin (T7-Sav), avidin (Avi), burkavidin-1 (Burk1) and rhodavidin (Rhod) are lined. Black arrows indicate the positions of the eight  $\beta$ -strands. The secretory signal peptide of Burk2 is written in italic. The T7-tag peptide of recombinant streptavidin (T7-Sav) is underlined <sup>[21]</sup>. The residues directly involved in biotin-binding, identified in the crystal structure of “core” Avi and T7-Sav, are shaded in blue. The cysteines of Burk2 and Avi, which form a disulphide bridge, are circled. Perfectly conserved residues are marked by stars

By comparing these novel avidins that we expressed recombinantly in *E. coli*, only Burk2 appeared to bind biotin and its derivatives with sufficient affinity. The reasons for the low biotin-binding of Rhod and Burk1 were not pursued

further, but sequence alignments of the new avidins could provide some clues.

For example, Burk1 was the only avidin having an alanine (Ala-76) at the equivalent position of Ser-88 in Sav, thus potentially losing hydrogen bonding with the carboxylic group of biotin (or with the carbonyl group of an amide in biotinylated derivatives).

Burk1 also appeared to have shorter loop around the active site, thus probably providing a more “open” biotin-binding pocket.

Finally, the presence of an alanine (Ala-108), at the inter-monomeric surface, rather than valine at the equivalent position of Sav (Val-125) could contribute to this protein’s tendency to dissociate into dimers.

In contrast, Burkavidin (Burk2) bound biotin strongly and formed tetramer of very pronounced structural stability, as judged by thermal and chemical denaturation assays (see below).

In addition to important inter-monomeric contacts of residues (*e.g.* Val-123 and Trp-118), that are also conserved in Sav, a homology model of Burkavidin based on the Sav structure suggested the presence of additional hydrophobic residues at the inter-monomeric interfaces in Burkavidin, which probably stabilized the tetramer (*e.g.* Trp-54, Tyr-56, Tyr-107, Tyr-109, Val-121).



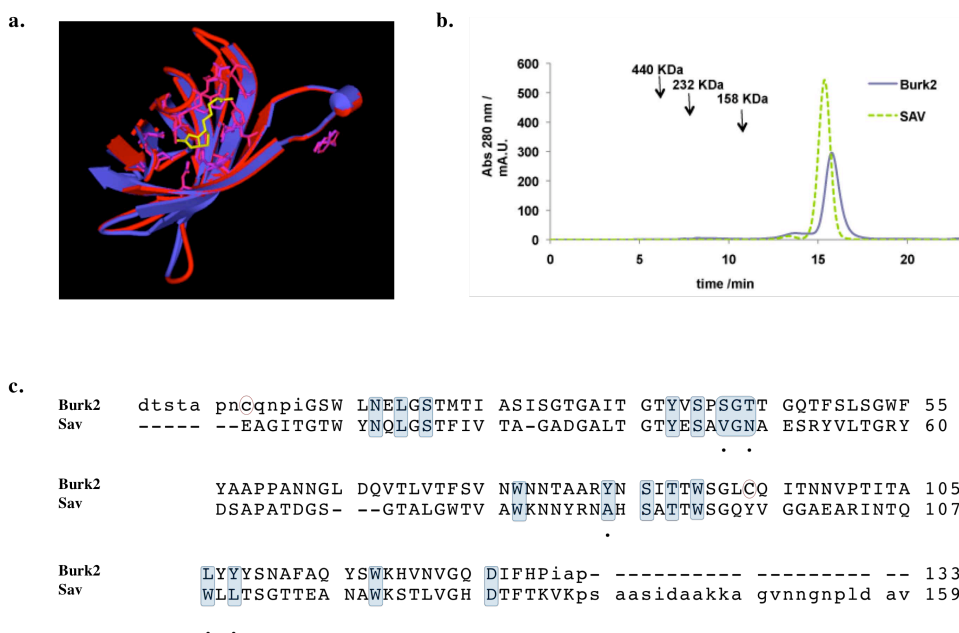


**Fig. 4.3 Structural comparisons of Burkavidin (Burk2) and Streptavidin (Sav).** **a)** Superposition of the crystal structure of Sav monomer bound to biotin (1MK5:A) with a structural model of Burk2. The same residues highlighted in the sequence alignment in **4.3c** (within 4 Å of biotin) are shown in full. Sav: red (backbone) and magenta (residues in full); biotin: yellow; Burk2 blue (backbone) and purple (residues in full). Residues W120 in Sav and W118 in Burk2 are also highlighted because W120 is known to make a contact with the biotin in the neighbouring monomer. The superposition has a RMSD of 0.41 Å over 114 aminoacids. **b)** Comparison of quaternary structures of Sav and Burk2 by gel-filtration chromatography. Both proteins are tetrameric in solution. **c)** Sequence alignment of Sav and Burk2. The highlighted residues are those contacting biotin (within 4 Å) in the crystal structure of streptavidin (pdb code 1MK5:A). Those putative biotin-binding residues that are not perfectly conserved are indicated with a dot (•). The cysteines, which form a disulphide bridge (conserved in avidin), are circled. In lower case are amino acids not included in the structural model

### 4.3.3 Biotin-Binding Activity

The facile expression and purification of Burk2, simply called Burkavidin, warranted a further exploration of its features, such as, for example, biotin-binding activity and stability over temperature ranges and in the presence of proteinases and chaotropic reagents.

Despite a very different primary aminoacid sequence compared with Avi and Sav, Burkavidin bound biotin strongly, as monitored by Isothermal Titration Calorimetry (ITC) analysis and 2-[(4-hydroxyphenyl)azo]benzoic acid

(HABA) titration.

The dissociation constant of Burkavidin, determined by ITC ( $K_d < 10^{-7}$  M, in the sub-micromolar range), was modest. For comparison, the values of  $K_d$  that we obtained for T7-tagged Sav were only an order of magnitude lower. Therefore, these data were likely to be an underestimate considering that they approach the sensitivity of the instrumentation.

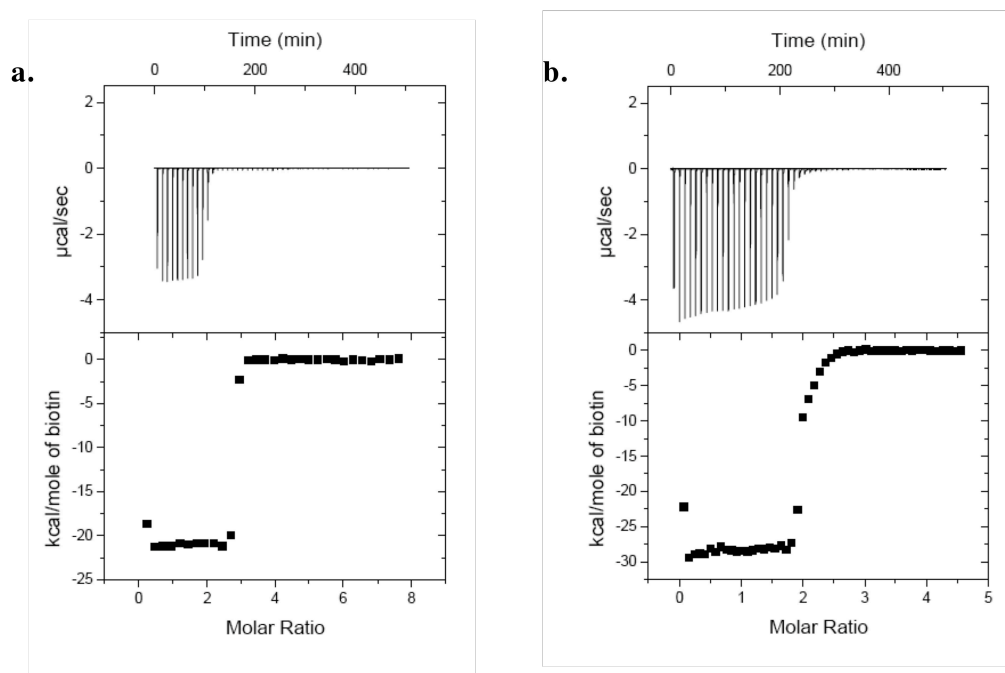


**Fig. 4.4 Binding of biotin to Burkavidin (Burk2) and Sav monitored by Isothermal Titration Calorimetry (ITC).** ITC for the binding of biotin onto **a)** Sav and **b)** Burkavidin, respectively. Titrations were carried out at 25 °C in 50 mM HEPES, pH 6.5. In the upper panels the raw titration data were plotted as heat versus time. In the lower panels, the integrated heat measurements are plotted as Kcal/mol of biotin injected into **a)** tetrameric Burkavidin or **b)** Sav. The data were fitted to a single set of one site model. For Burkavidin, the association constant is  $(1.14 \pm 0.319) \times 10^7 \text{ M}^{-1}$ , an enthalpy of  $(-2.83 \pm 296.2) \times 10^4 \text{ Kcal/mol}$ , and a stoichiometry of 1.95. For Streptavidin, the association constant is  $1.09 \times 10^8 \text{ M}^{-1}$ , an enthalpy of  $-2.102 \times 10^4 \text{ Kcal/mol}$  and a stoichiometry of 3.16

The stoichiometric value determined by ITC suggested around two free-biotin binding sites per tetramer of Burkavidin.

Evidence of strong-binding of biotin was also provided by a spectrophotometric HABA titration of Burkavidin, which gave a clear equivalent point upon biotin addition.

Displacement of the chromophore HABA from Burkavidin upon titration with biotin caused a decreased absorbance at 506 nm <sup>[22]</sup>. However, the HABA absorption changed only moderately upon biotin-binding to Burkavidin compared with Sav or Avi <sup>[22]</sup>.

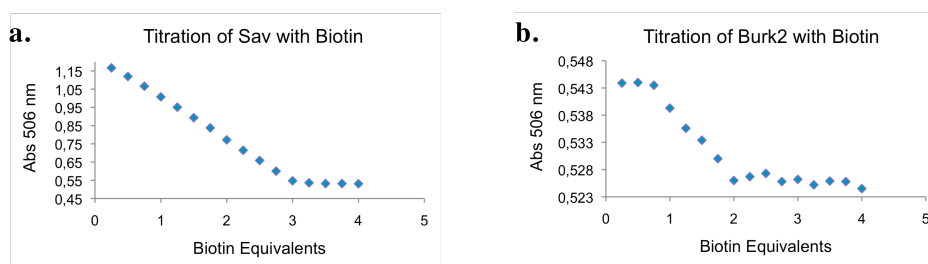


**Fig. 4.5. Binding of biotin to Burkavidin (Burk2) and Sav monitored by HABA titration.** HABA titration of **a)** Streptavidin and **b)** Burkavidin, respectively. Displacement of the chromophore HABA upon titration with biotin causes a decreased absorbance at 506 nm <sup>[22]</sup>. Three free active sites per tetramer of Sav and two free active site per tetramer of Burkavidin are quantified by HABA titration

A low dissociation constant of Burkavidin was confirmed by additional findings:

- i. The protein could be purified easily by iminobiotin-affinity.
- ii. Traces of a biotinylated enzyme from *E. coli* (acetyl CoA carboxylase) were present in some batches, suggesting co-purification of the minor contaminant due to the tetrameric nature of Burkavidin.
- iii. Only about two biotin-binding sites per tetramer were quantified, suggesting that biotin from yeast extract in rich medium remained bound, although this was apparently not a problem encountered when recombinant secreted avidin was expressed in rich medium in *E. coli*

<sup>[23]</sup>.

iv. In contrast to Rhod and Burk1, no leaching of B4F was observed in SDS-PAGE (**Fig. 4.1**).

#### ***4.3.4 Protein Stability***

##### *4.3.4.1 Resistance to Proteinase Digestion*

A further characterization round of Burkavidin was aimed to assess its stability in the presence of chaotropic agents and proteinases .

During purification, Burkavidin was dialyzed against 6 M guanidinium chloride at pH 1.5 at room temperature, remaining active in SDS-PAGE analysis.

We also performed B4F-binding analysis to test the resistance of Burkavidin to Proteinase K digestion (**Fig. 4.6**).

In this assay, active Avi did not migrate into the gel, probably due to its very high *pI*, although the inactive monomer in the preparation was visible degraded by proteinase K.

In contrast, both Sav and Burkavidin resisted Proteinase K treatment in an active form either in the presence or absence of B4F, albeit with slight changes in migration pattern.

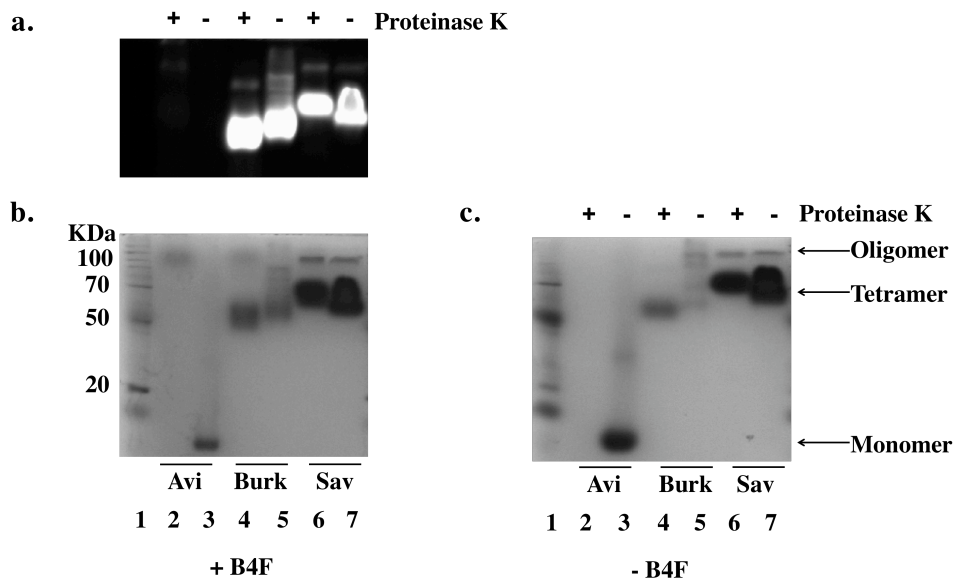


**Fig. 4.6. Burkavidin resistance to proteolysis by Proteinase K monitored by SDS-PAGE.** Gel a) and b) were run following incubation in the presence of B4F (assaying for functional activity). Gel c) was run in absence of B4F (and only Coomassie stained). Lane 1, protein ladder (220 KDa). Lanes 2, 4, and 6, Avi, Burkavidin and Sav with Proteinase K, respectively. Lanes 3, 5 and 7, Avi, Burkavidin and Sav without Proteinase K, respectively. The functional assay (panel a) shows that Burkavidin and Sav remain active upon incubation with Proteinase K. Functional Avi does not migrate into the gel under these conditions. Binding of the biotin-fluorophore B4F alters sensitivity of Burkavidin against Proteinase K (panels b and c). Comparison of lane 5 suggests that oligomerization domains responsible for apparent heterogeneity are sensitive to proteolytic cleavage, especially in the presence of B4F (panel b)

In certain Burkavidin preparations, high-molecular weight species (probably aggregated oligomers) were observed in addition to the tetramer, particularly in the absence of B4F (Fig. 4.6c).

A change in migration of Burkavidin upon Proteinase K treatment, leading towards a single species formation, was more evident in more heterogeneous preparations. We ascribed this different migration of active Sav and Burkavidin to the formation of a “core” (active) tetramer [24]. Then, the terminal sequences that were cleaved upon proteolysis in Burkavidin probably induced oligomerization in the non-treated species.

Increased formation of the tetramer from oligomers in the presence of B4F suggested the presence of the apo-protein termini into the biotin-binding site, as described for the C-terminus of Sav<sup>[25]</sup>.

#### 4.3.4.2 Thermal Stability

The high stability of Burkavidin in the presence of denaturing agents was an attractive property for its use in biotechnological applications, in particular as a catalytic artificial enzyme. However, many catalytic reactions are carried out in the presence of organic solvents or at high temperature.

Thus, we also explored the thermal stability of Burkavidin through electrophoretic assays.

Burkavidin resisted incubation in an active B4F-bound form upon heat treatment up to 99 °C for 10 minutes.

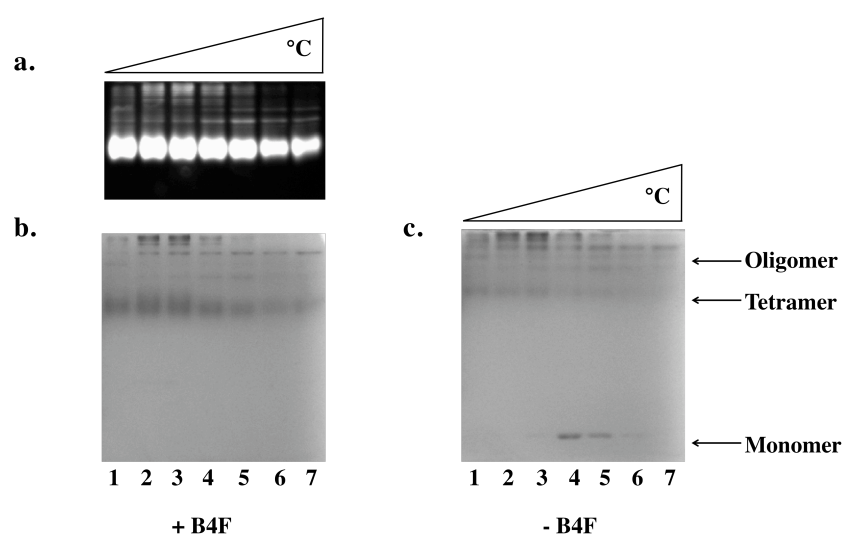


**Fig. 4.7. Thermal stability of Burkavidin (Burk2) assessed by SDS-PAGE.** Purified Burkavidin samples were electrophoresed after heating at 50 °C to 99 °C for 10 minutes, either in the presence of B4F (a and b) or in the absence of B4F (c). a) Activity assay: fluorescence of B4F is strongly associated to tetramers and only more weakly to oligomers. Disaggregation oligomers occurs with higher temperatures. b) and c) Coomassie-blue staining of gels reveals that denaturation into monomers only occurs (weakly) in the absence of B4F above at higher temperature (80°C and above). Lanes 1-7, supernatants from heat treatment at different temperatures: 50°C, 60°C, 70°C, 80°C, 85°C, 90°C, 99°C, respectively. Samples were loaded in the same order in all gels

A small amount of monomeric species was observed at the highest temperatures tested only in the absence of B4F, in agreement with the notion protein stabilization upon ligand-binding <sup>[26]</sup>.

Whether in the presence or absence of B4F, dissociation of oligomers towards a more defined tetrameric species was observed with higher temperatures.

#### 4.3.4.3 Resistance to Reducing Agents

As revealed by the sequence alignments, the cysteines that form an intramonomeric disulphide bridge in Avi were also conserved in Burkavidin.

Consequently, to assess the stability of Burkavidin in the presence of reducing agents, we carried out denaturing SDS-PAGE analysis in the presence and absence of DTT as reductant.

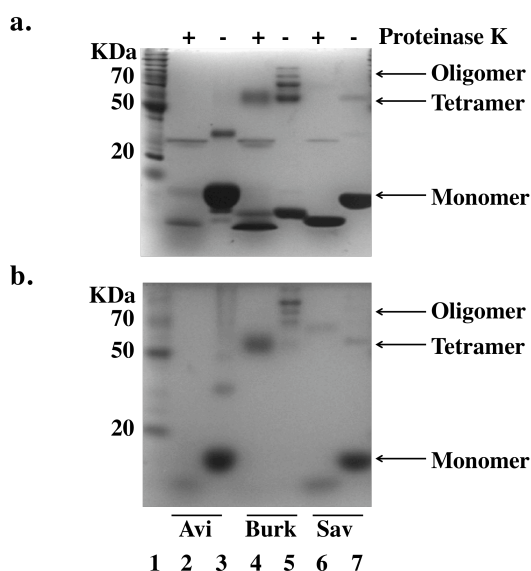


**Fig. 4.8 Burkavidin (Burk2) stability in presence of reducing agents assessed by denaturing SDS-PAGE.** In all cases, proteins were electrophoresed in the absence of B4F. **a)** Heating at 95 °C for 10 min in DTT. **b)** Heating at 95 °C for 10 min in absence of DTT. Lane 1, protein ladder (220 KDa). Lanes 2, 4 and 6, Avi, Burkavidin and Sav in the presence of Proteinase K, respectively. Lanes 3, 5 and 7, Avi, Burkavidin and Sav in the absence of Proteinase K, respectively. Samples were loaded in the same order in all gels

Remarkably, Burkavidin remained tetrameric upon treatment with Proteinase K, following by 10 minutes incubation at 95 °C. In contrast, both Avi and Sav were degraded mostly into monomers under these conditions.

Adding a reducing agent to Burkavidin in these assays led to partial denaturation into dimers and monomers, although tetrameric Burkavidin remained.

The destabilization of the tetramer upon incubation with a reducing agent suggested that the presence of an intra-monomeric disulphide bridge, found also in Avi <sup>[2]</sup>, contributed to the extreme stability of Burkavidin to thermal, proteolytic and chemical denaturation of the protein.

To confirm the importance of this disulphide bridge for Burkavidin expression, we produced Burkavidin mutant C8A (numbering refers to position following the signal peptide). This single point mutation did not lead to any detectable expression of active protein, as monitored by SDS-PAGE analysis.



**Fig. 4.9 Expression of Burkavidin mutant C8A monitored by SDS-PAGE.** Functional assay of mutant C8A to assess importance of disulphide-bond formation. Lane 1, cell-extract of wildtype Burkavidin (WT). Lane 2, C8A-mutant of Burkavidin



The presence of the disulphide bridge was crucial for Burkavidin expression in an active form as well as contributing to its extremely high stability.

#### ***4.3.5 Protein Secretion into the Periplasm of *E. coli****

##### *4.3.5.1 Secretory Signal Peptide*

Sequencing of purified Burkavidin by Edman degradation confirmed the sequence DTSTA at the *N*-terminal, in line with signal-peptide predictions <sup>[27]</sup>. In some cases, the sequence MDIRK was also detected as a minor species (less than 10 %), corresponding to the *N*-terminal of acetyl CoA carboxylase of *E. coli*.

The principal ESI-MS peak was 14249.71 Da (theoretical for Burkavidin monomer: 14250.74 Da) and in some cases a peak of 16913.23 Da was also detected and attributed to the biotinylated contaminant acetyl CoA carboxylase (theoretical mass: 16669 + 244 biotin = 16913 Da), as previously found in recombinant avidin preparations <sup>[28]</sup>.

##### *4.3.5.2 Periplasmic Expression in *E. coli**

Since protein sequencing and mass spectra showed a cleavage of the *N*-terminus, we sought to explore whether Burkavidin was secreted into the periplasm of *E. coli*, due to the presence of a secretory signal peptide from *B. pseudomallei* <sup>[27]</sup>.

Periplasmic extracts of *E. coli* expressing Burkavidin were enriched in B4F-binding protein compared with those containing recombinant T7-tagged Sav, which was found mostly intracellularly in *E. coli* in an active form <sup>[21]</sup>.

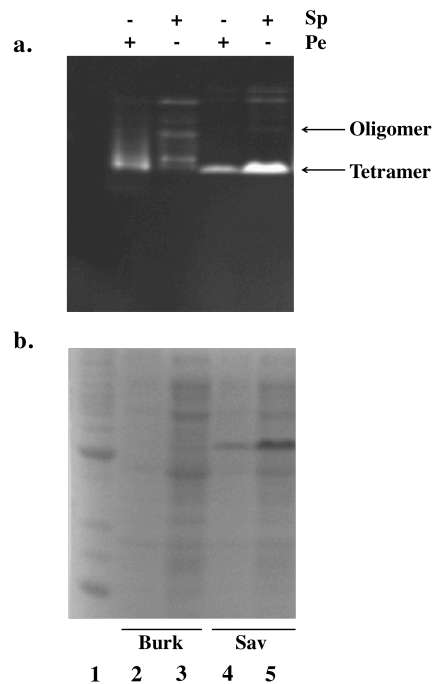


**Fig. 4.10 Functional analysis of Burkavidin (Burk2) periplasmic secretion into the periplasm of *E.Coli*.** **a)** Functional analysis of Burkavidin and Sav expression into the periplasmic (Pe) or spheroplasmic (Sp) fractions of *E. Coli*. Lane 1, protein ladder (220 KDa). Lanes 2 and 4, Burkavidin and Sav periplasmic extracts, respectively. Lanes 3 and 5, Burkavidin and Sav spheroplasmic extracts, respectively. **b)** Coomassie-blue staining of gel a)

As reported for secreted avidin in *E. coli*, a large fraction of the protein was associated with the non-periplasmic fraction<sup>[23]</sup>. However, unlike reported for Avi, the cellular Burkavidin fraction contained active protein with high propensity to form oligomers, while the secreted form tended to be only tetrameric.

We speculated that the presence of the hydrophobic signal peptide, which was only cleaved upon secretion, might contribute to Burkavidin oligomerization. Expression of a construct lacking the signal peptide, with *N*-terminal sequence MDTSTA led to absence of active protein in *E. coli*, suggesting that the less reducing environment of the periplasm was necessary for S-S bond formation and the correct folding of the protein (**Fig. 4.1**).

These experiments suggested that secretion into the periplasm, using Burkavidin's native secretory signal, and the presence of the disulphide bridge were crucial for Burkavidin expression in an active form and protein stability.

#### ***4.3.6 Burkavidin Homogeneity***

Further optimization of expression and purification conditions of Burkavidin may lead to higher yield, more efficient secretion and improved properties, such as a decreased oligomerisation propensity and a lower biotin content of preparations.

The best batches of periplasmic Burkavidin showed a single main species in isoelectric focusing (IEF) analysis, performed in collaboration with Prof. Zoller (Medical University of Innsbruck). Surprisingly, the highly-purified T7-tagged Sav was much more heterogeneous than Burkavidin with several unidentified isoforms, as judged by IEF <sup>[29]</sup>.

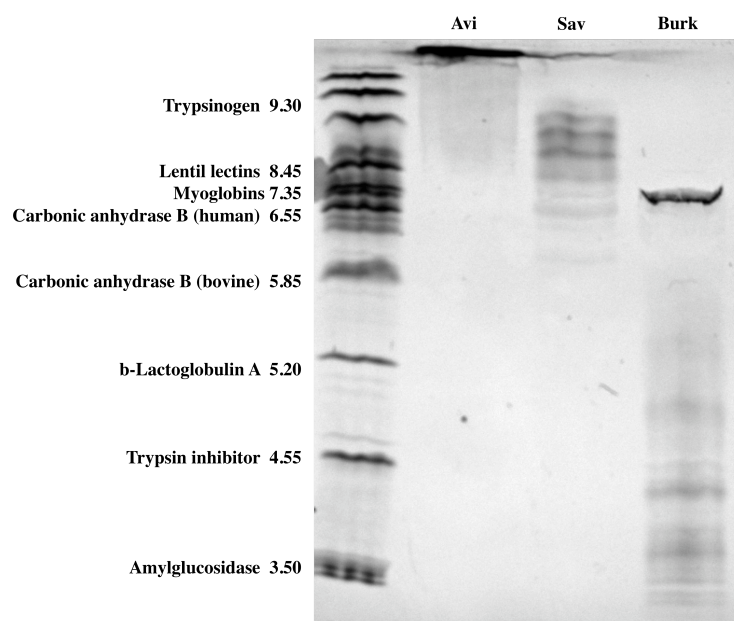


**Fig. 4.11 Isoelectric focusing (IEF) of Avidin (Avi), T7-tagged Streptavidin (Sav) and Burkavidin (Burk2).** Marker (left lane), PhastGel IEF 3-9 (GE-Healthcare). Whereas the highly-purified T7-Streptavidin (Sav) shows several unidentified isoforms, Burkavidin is comparatively homogeneous and with a dominant species that has a lower isoelectric point ( $pI$ ) than either Avi (very basic) or most isoforms of Sav

It was noteworthy that the  $pI$  of the T7-tagged Sav tested here was higher than expected. Both heterogeneity and the presence of Sav preparations with high  $pI$  have also been reported previously by others for untagged streptavidin<sup>[30]</sup>.

The low  $pI$  of Burkavidin compared with Avi and T7-Sav may render this novel protein also useful for specific binding of biotinylated DNA, since the negatively charged DNA can bind strongly to avidin non-specifically due to electrostatic interactions.

#### ***4.3.7 Burkavidin as an Artificial Metalloenzyme***

To begin exploring the potential of Burkavidin in biotechnology, we chose to use the protein for enantioselective hydrogenation of *N*-acetamidoacrylic acid

and *N*-acetamidocinnamic acid using  $[\text{Rh}(\text{COD})(\mathbf{Biot-1})]^+$  or  $[\text{Rh}(\text{COD})(\mathbf{Biot-}(\mathbf{R})\text{-Pro-1})]^+$  as artificial cofactors for the hydrogenation of *N*-protected dehydroamino acids <sup>[31]</sup>, in collaboration with Mr. Lo.

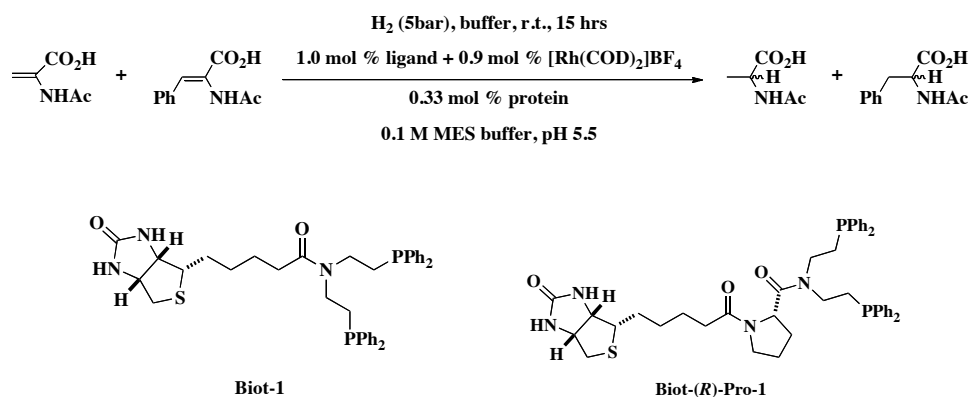


**Fig. 4.12 Enantioselective reduction of *N*-acetamidoacrylic acid and *N*-acetamidocinnamic acid catalyzed by artificial hydrogenases.** The reaction was catalyzed by  $[\text{Rh}(\text{COD})(\mathbf{Biot-1})]^+$  or  $[\text{Rh}(\text{COD})(\mathbf{Biot-}(\mathbf{R})\text{-Pro-1})]^+$  in the presence of 50 equiv of each substrate with respect to the ligand and using T7-Streptavidin (Sav) or Burkavidin (Burk2) as protein host. Results are summarized in Table 1. MES buffer is composed of 4-morpholineethanesulfonic acid that is pH adjusted with sodium hydroxide

The catalyst in the absence of protein catalyzed hydrogenation leading to racemic mixture of products. In contrast, the placement of the catalyst within the chiral environment of the Burkavidin, through biotin-anchoring, led to enantioselective enrichment of the reduced species: up to 39% *ee* in favour of the (*R*)-product for *N*-AcAla using  $[\text{Rh}(\text{COD})(\mathbf{Biot-1})]^+$  catalyst and up to 65% *ee* for the (*S*)-product for *N*-AcPhe using  $[\text{Rh}(\text{COD})(\mathbf{Biot-}(\mathbf{R})\text{-Pro-1})]^+$ .

**Table 4.1 Numeric summary of results from catalytic experiments**

Entry	Protein	Ligand	<i>N</i> -AcPhe <sup>[1]</sup>		<i>N</i> -AcAla <sup>[2]</sup>	
			<i>ee</i> [%]	Conv [%]	<i>ee</i> [%]	Conv [%]
1	Burkavidin	<b>Biot-1</b>	-65	18	39	52
2	Burkavidin	<b>Biot-(<i>R</i>)-Pro-1</b>	-35	21	15	100
3	WT Sav	<b>Biot-1</b>	93	84	94	100
4	S112W Sav	<b>Biot-(<i>R</i>)-Pro-1</b>	-95	100	-95	100

<sup>[1]</sup>*N*-AcPhe = *N*-acetamidophenylalanine; <sup>[2]</sup>*N*-AcAla = *N*-acetamidoalanine

Catalytic hydrogenation conditions are as detailed in **Fig. 4.12**.

WT Sav = wildtype Streptavidin; S112W = mutant S112W of Sav; Burkavidin refers to Burk2

The results revealed that:

- i. Conversion in Burkavidin was higher for the smaller substrate *N*-AcAla regardless of the metal complex employed (entries 1-2).
- ii. For both ligands used, *N*-AcAla was enriched for the (*R*)-product, whereas *N*-acPhe was enriched for the (*S*)-product (entries 1-2). Such opposite enantioselectivities for both substrates were never observed before using either Sav or Avi isoforms <sup>[31b]</sup>.

These observations suggested very different discrimination events for both substrates <sup>[31a,32]</sup>. The different conversions further supported this hypothesis.

The finding of enantiomeric enrichment and discrimination against the larger substrate when using Burkavidin in hydrogenation was strongly indicative that catalysis occurred within the defined-biotin-binding pocket <sup>[31a]</sup>.

Further, the large differences in catalytic results in term of *ee* and conversion when compared Burkavidin to Sav suggested that the chiral environment provided by Burkavidin or Sav around the metal-catalyst were markedly different.

Importantly, the successful use of Burkavidin as an enantioselective artificial metalloenzyme for Rh-catalyzed hydrogenation provided proof-of-principle that the biotin-binding affinity of Burkavidin was sufficient for its use in biotechnological applications.

## **4.4 Materials and Methods**

### ***4.4.1 Chemicals***

Solvents used were all of analytical grade.

All solutions were prepared using deionised water.

**Table 4.2 List of chemical and supplier**

<b>Chemical</b>	<b>Supplier</b>
Acrylamide	
Glucose	
SDS	
Chloramphenicol	
Ampicillin	AppliChem
PMSF	
IPTG	
Glycerol	
Tris	
Bactoyeast extract	Merck
Bactotryptone	BD
NaCl	
DMSO	
DTT	
KH <sub>2</sub> PO <sub>4</sub>	Fluka
Coomassie Brilliant Blue	
Triton X-100	
Lysozyme (from egg white)	
TEMED	
Acetic acid	VWR
Urea	
APS	
Na <sub>2</sub> HPO <sub>4</sub>	Sigma
B4F	
DNaseI	
Guanidinium/HCl	Acros Organics
BenchMark™ Protein Ladder	Invitrogen
Bromophenol Blue	Riedel-de Haën
dNTP	Promega
Dpn1	Biolabs
DNA ladder	
Pfu Turbo	Stratagene



#### **4.4.2 Technical Equipment**

- Protein expression in 20 L of *E. coli* cell culture was performed in a fermentor NLF22 (Bioengineering®).
- PCR was performed in an eppendorf mastercycler gradient
- DNA concentration was determined by nanodrop 1000 spectrophotometer (Thermo Fisher Scientific).
- SDS-PAGE was analyzed with Molecular Image Gel Doc XR (Bio-Rad®, Switzerland).
- Protein was lyophilized in a lyophilizer FreeZone 2.5 L (benchtop of Labconco, USA).
- The active sites of proteins were determined with the Fluorescence Reader Safire (Tecan®).
- FPLC was performed by using äkta prime machine.
- ITC was performed in a VP-ITC titration calorimetry (*MicroCal*, Northampton, MA, USA).
- IEF was performed in a PhastGel IEF, 3-9 (GE-Healthcare).

#### **4.4.3 Vector Generation**

For cloning Burkavidin isoform 2 (Burk2), the following primers were designed: GC AGC GCG *cat atg* CCA ATA CAA GAG ATC (upstream primer for expression of full-length isoform translated as MPIQE...); AA CCT GCG *cat atg* GAC ACT TCA ACC GCC C (upstream primer for expression of putative mature isoform MDTSTA..., starting at D36 according to signalp); CACGTTCAAAT*ggatcc*TACCGCTTTATGC (downstream primer). For cloning Burkavidin isoform 1 (Burk1): G CCG ATA AAA GAA

*cat atg* GCG CGC CC (upstream primer for expression of full-length isoform translated as MARPA...); GG AGG CGA *catatg* CAG CGA TTG GAA C (isoform translated as: MQRLE...); TC AAG *cat atg* ACC GGC GCG CCG ATC GAT TTC (isoform translated as: MTGAP...); *ccgttgatcctcaagtcttcacgaatatatc* (downstream primer for all Burk1 isoforms). For cloning Rhodavidin (Rhod): A TGG AGT TTT *cat atg* CTC CGT ATC (upstream primer for expression of full-length isoform translated as: MLRIV...); TCC GCT GCA *cat atg* GCG CAA GTC AG (upstream primer for expression of putative mature isoform MAQVSW..., starting at aa27 according to signalp); GACg gatccGCGACGATGTTATTTTC (downstream primer for Rhod isoforms).

Genomic DNA from *R.palustris* strain BisB18 was a kind gift from Dr. Caroline Harwood at the University of Washington (US). Genomic DNA from *Burkholderia pseudomallei* strain K96243 was kindly provided by Prof. Richard Titball from the Defence Science Technology Laboratory, Porton Down, Salisbury (UK). In all cases, PCR was carried out using genomic DNA as a template and the amplified genes were cloned into expression plasmid pEt11b (Novagen) using *Nco*I and *Bam*H1 as cloning sites. DNA sequencing was carried out by Microsynth (Switzerland) or StarSEQ® GmbH (Germany).

#### **4.4.4 Expression and Purification** <sup>[19]</sup>

Ultra-competent BL21(DE3)pLysS *E. coli* strains (in house) were transformed by pET11b-burkavidin plasmid containing a gene encoding recombinant burkavidin. Transformed bacteria, plated on selective Luria

broth (LB) petri dishes containing ampicillin (60 mg/mL), chloramphenicol (34 mg/mL) and glucose (2% w/v), were incubated overnight at 37 °C.

300 mL of tryptone medium (20 g/L Bactotryptone; 2 g/L Na<sub>2</sub>HPO<sub>4</sub>, 1 g/L KH<sub>2</sub>PO<sub>4</sub>; 8 g/L NaCl; 15 g/L Bactoyeast extract), containing antibiotics and glucose at the same concentrations as in LB plates, were inoculated with a single colony and incubated overnight in an orbital shaker (37 °C, 250 rpm).

A 20 L cell culture, inoculated with the whole pre-culture, was grown in a 30 L fermentor (Bioengineering, Switzerland) at 37 °C, with 1000 rpm agitation speed, in the presence of glucose and antibiotics.

Isopropyl- $\beta$ -D-1-thiogalactopyranoside (IPTG) (0.4 mM as final concentration) was added to the culture when the OD<sub>600</sub> reached a value between 1.8 and 2.0. Three hours after induction, the bacterial pellet was collected by centrifugation and stored at -20 °C until purification. On the next day, the pellet was thawed and resuspended in 20 mM Tris/HCl pH 7.4, 1 mM PMSF and 2-3 mg DNaseI under vigorous shaking.

The sample was dialysed against 6 M guanidine chloride at pH 1.5 for 24 h, against 20 mM Tris/HCl pH 7.4 for another day and finally against 50 mM NaHCO<sub>3</sub>/500 mM NaCl pH 9.8 for 24 h. The protein extract was loaded onto a 2-iminobiotin agarose column, pre-equilibrated with 50 mM NaHCO<sub>3</sub>/500 mM NaCl buffer. At this step, it was observed that Rhod (MAQVS isoform) and Burk1 (MQRLE isoform) did not bind to the column, as judged by SDS-PAGE of elution fractions. Only Burk2 (containing the signal peptide starting with MPIQE) had sufficiently-strong binding to iminobiotin-sepharose for affinity purification. The protein was washed with the same buffer and eluted with 1% acetic acid.

Purified Burkavidin was immediately dialysed against 10 mM Tris/HCl pH 7.4 for 24 hrs and twice in mQ-water, before lyophilisation.

For a detailed description of burkavidin expression and purification see Appendix C.

N-terminal sequencing (on an Applied Biosystems Procise Sequencer) and mass spectrometry by electrospray ionisation (ESI-MS) were carried out by Analytical Research and Services, University of Bern.

#### ***4.4.5 Preparation of Periplasmic Proteins from Bacterial Culture***

One mL of a bacterial cell culture, inoculated with 200 µL of pre-culture, was grown at 37 °C in a 15 mL Falcon tube for 2 hrs. The cells, induced by IPTG, were harvested by centrifugation at the log phase, one hour after induction.

The fresh culture was immediately processed as described in the *PeriPreps<sup>TM</sup> Periplasting* protocol (Connectorate AG, Switzerland). Spheroplastic and periplasmic fractions were analysed by a 12% acrylamide gel.

#### ***4.4.6 Site – Directed Mutagenesis***

For generating Burk C8A, site-directed mutagenesis was carried out using the Quick-Change mutagenesis kit (Stratagene, Switzerland) on the pET11b-burkavidin plasmid. The forward (positive) and the reverse (negative) primers were partially overlapped with each other and fully complementary at the mutation site.

**Table 4.3 List of mutagenic primers used for generating Burk C8A**

MUTATION	PRIMERS (5'– 3')
C8A	Forward
	TTCAACCGCCCCGAATGCTCAGAACCCGATC
	Reverse
	GTTCTGAGCATTTCGGGGCGGTTGAAGTGTC

The PCR results were verified on a 1.2% agarose gel containing 1X Tris-Borate-EDTA (TBE) buffer. Ultra-competent XL1-Blue *E. coli* cells (in house) were transformed by PCR product. Finally the plasmids were extracted from bacteria with a *Promega miniprep* kit (Promega) and clones, sequenced by *StarSEQ® GmbH* (Germany), were used to transform ultra-competent BL21(DE3)pLysS *E. coli* strains.

For a detailed description of molecular biology see Appendix B.

#### ***4.4.7 Structural Modeling***

Structural models were carried out by automated homology modeling with SWISS-MODEL <sup>[33]</sup>.

#### ***4.4.8 Thermostability***

The thermostability of burkavidin was assessed by SDS-PAGE assay. The samples (26  $\mu$ M tetramer) were solubilised in 10 mM CaCl<sub>2</sub>/50 mM Tris pH 8 and incubated for 10 minutes at selected temperature (from 50 °C to 99 °C) in the presence or absence of biotin-4-fluorescein (B4F).

After heat treatment, the samples were loaded onto 12% acrylamide gels, prepared as described by Laemmli <sup>[34]</sup>.

The gels were run at 200 V for 40 minutes and stained in Coomassie Brilliant Blue. The BenchMark Protein Ladder (Invitrogen), containing 10 proteins ranging in apparent molecular weight from 10 to 220 kDa, was used to compare the different oligomeric states of the protein.

#### ***4.4.9 Sensitivity to Proteinase Treatment***

The stability of Burkavidin against Proteinase K was assessed in the presence and absence of B4F by SDS-PAGE assay.

The samples were incubated with 386  $\mu$ M Proteinase K (Promega) for 2 hrs at 37 °C. Loading buffer (300 mM Tris/HCl pH 6.8; 6% SDS; 30% glycerol; 0.036% Bromophenol-Blue; optional 50 mM DTT) was added to a final 1/3 of total volume before charging the gels.

#### ***4.4.10 Isothermal Titration Calorimetry (ITC)***

ITC profile for the titration of biotin onto Burkavidin was carried out using a VP-ITC titration calorimetry (*MicroCal*, Northampton, MA, USA) at 25 °C in HEPES buffer (50 mM, pH 8).

Prior to each experiment, all solutions were thoroughly degassed and the ITC sample cell washed several times with HEPES buffer solution.

The titration was carried out injecting biotin (1 mM in HEPES buffer) in the reaction cell ( $V_{\text{CELL}} = 1.5$  ml) filled with burkavidin (40  $\mu$ M in HEPES buffer). Injections were started after the stability of the baseline had been achieved. A typical titration experiment normally consisted of 50 consecutive injections of 5  $\mu$ L and 10 s each, with 10 min interval between each injection and stirring at 300 rpm.

Heats of dilution of biotin into the buffer alone were used to adjust total observed heats of binding. The resulting data were fitted using *MicroCal ORIGIN* software supplied with the instrument.

#### **4.4.11 Titration by HABA**

2-(4'-hydroxyphenylazo)benzoic acid (HABA) forms with Burkavidin a dyed complex, which can be detected spectrophotometrically at 506 nm <sup>[22]</sup>. Competitive displacement of HABA by biotin resulted in the decrease of absorbance and provided a spectroscopic assay to assess the free biotin-binding sites in burkavidin.

The host protein (8  $\mu$ M, 2.4 mL, 0.0192  $\mu$ mol) was loaded with a large excess of a 9.6 mM HABA solution (584 eq *versus* burkavidin monomer). Aliquots of 0.25 eq (*versus* Burkavidin monomer) up to 7.0 eq of biotin (0.96 mM) were added to HABA  $\subset$  Burkavidin complex under stirring.

#### **4.4.12 Isoelectric Focusing (IEF)**

Purified proteins at 1mg/ml in water were analysed using a PhastGel IEF – 3-9 (GE-Healthcare) and compared against a kit of Broad pI Standards (pI 3.5-9.3) according to supplier's instructions.

#### **4.4.13 Gel Filtration**

Proteins were dissolved in 50 mM TRIS-HCl, pH 7.4, 100 mM NaCl at 1 mg/ml. A Superose-20 column (GE-Healthcare) was loaded with 0.5 ml of sample and ran at 0.5 ml/ml.

## 4.5 Conclusions

The natural function of secreted Burkavidin in *B. pseudomallei* remains speculative. The native host *B. pseudomallei* was recognized as a causative agent of melioidosis <sup>[35]</sup>.

We hypothesized that Burkavidin's strong biotin-binding activity might contribute to virulence, as secreted proteins were important for *Burkholderia* pathogenicity <sup>[36]</sup> and biotin deficiency was associated with immunodepression <sup>[37]</sup>.

However, the presence of closely-related isoforms in the relatively avirulent *B. thailandensis* and *B. oklahomensis* suggested that Burkavidin was not a virulent factor in these organisms <sup>[36]</sup>.

On the other hand, the finding that Burkavidin was a secreted avidin suggested its potential use in vaccines <sup>[38]</sup>. Alternatively, its strong biotin-binding activity could be exploited as diagnostic for *Burkholderia* <sup>[38]</sup> and as a means of targeting biotinylated antimicrobials.

In summary, this study represented, to our knowledge, the first demonstration of an avidin in a human pathogen with strong biotin-binding activity. This avidin may have potential implications in the medical field.

The low *pI* of Burkavidin may render this novel protein also useful for specific binding of biotinylated DNA, in contrast to avidin that is involved in non-specific electrostatic interactions with the negatively charged DNA <sup>[39]</sup>.

In combination with a biotinylated metal complex Burkavidin has been shown to perform the enantioselective hydrogenation of *N*-protected dehydroamino acids. Further chemogenetic optimization or evolution could improve conversion and selectivity <sup>[40]</sup>.



*In vivo* catalysis remains an exciting challenge and Burkavidin represents a milestone in this direction as the creation of hybrid enzymes within the cell periplasm may allow catalytic reactions to be carried out *in vivo*.

# REFERENCES

- [1] M. Wilchek, E. A. Bayer, *Methods Enzymol.: Avidin-Biotin Technology*, Academic Press, San Diego **1990**, 184, 5.
- [2] O. Livnah, E. Bayer, M. Wilchek, J. Sussman, *Proc. Natl. Acad. Sci. USA* **1993**, 90, 5076.
- [3] a)P. S. Stayton, S. Freitag, L. A. Klumb, A. Chilkoti, V. Chu, J. E. Penzotti, R. To, D. Hyre, I. L. Trong, T. P. Lybrand, R. E. Stenkamp, *Biomol. Eng.* **1999**, 16, 39; b)P. C. Weber, D. H. Ohlendorf, J. J. Wendoloski, F. R. Salemme, *Science* **1989**, 243, 85.
- [4] M. Wilchek, E. A. Bayer, O. Livnah, *Immunol. Lett.* **2006**, 103, 27.
- [5] K. K. Caswell, J. N. Wilson, U. H. F. Bunz, C. J. Murphy, *J. Am. Chem. Soc.* **2003**, 125, 13914.
- [6] a)D. S. Wilbur, P. S. Stayton, R. To, K. R. Buhler, L. A. Klumb, D. K. Hamlin, J. E. Stray, R. L. Vessella, *Bioconjugate Chem.* **1998**, 9, 100; b)V. P. Hytönen, O. H. Laitinen, A. Grapputo, A. Kettunen, J. Savolainen, N. Kalkkinen, A. T. Marttila, H. R. Nordlund, T. K. M. Nyholm, G. Paganelli, *Biochem. J.* **2003**, 372, 219.
- [7] O. H. Laitinen, V. P. Hytönen, H. R. Nordlund, M. S. Kulomaa, *Cell. Mol. Life Sci.* **2006**, 63, 2992.
- [8] O. H. Laitinen, H. R. Nordlund, V. P. Hytonen, M. S. Kulomaa, *Trends Biotechnol.* **2007**, 25, 269.
- [9] O. H. Laitinen, V. P. Hytönen, M. K. Ahlroth, O. T. Pentikäinen, C. Gallagher, H. R. Nordlund, V. Ovod, A. T. Marttila, E. Porkka, S. Heino, M. S. Johnson, K. J. Airene, M. S. Kulomaa, *Biochem. J.* **2002**, 363, 609.
- [10] V. P. Hytönen, J. A. E. Määttä, E. A. Niskanen, J. Huuskonen, K. J. Helttunen, K. K. Halling, H. R. Nordlund, K. Rissanen, M. S. Johnson, T. A. Salminen, M. S. Kulomaa, O. H. Laitinen, T. T. Airene, *BMC Struct. Biol.* **2007**, 7, 1.
- [11] a)H. R. Nordlund, V. P. Hytonen, O. H. Laitinen, M. S. Kulomaa, *J. Biol. Chem.* **2005**, 280, 13250; b)S. H. Helppolainen, K. P. Nurminen, J. A. E. Maatta, K. K. Halling, J. P. Slotte, T. Huhtala, T. Limatainen, S. Yla-Herttuala, K. J. Airene, A. Narvanen, J. Janis, P. Vainiotalo, J. Valjakka, M. S. Kulomaa, H. R. Nordlund, *Biochem. J.* **2007**, 405, 397.
- [12] E. A. Bayer, T. Kulik, R. Adar, M. Wilchek, *Biochim. Biophys. Acta* **1995**, 1263, 60.
- [13] Y. Takakura, M. Tsunashima, J. Suzuki, S. Usami, Y. Kakuta, N. Okino, M. Ito, T. Yamamoto, *FEBS Journal* **2009**, 276, 1383.
- [14] J. A. E. Määttä, S. H. Helppolainen, V. P. Hytönen, M. S. Johnson, M. S. Kulomaa, T. T. Airene, H. R. Nordlund, *BMC Struct. Biol.* **2009**, 9, 63.
- [15] F. W. Larimer, P. Chain, L. Hauser, J. Lamerdin, S. Malfatti, L. Do, M. L. Land, D. A. Pelletier, J. T. Beatty, A. S. Lang, F. R. Tabita, J. L.

- Gibson, T. E. Hanson, C. Bobst, J. L. T. Y. Torres, C. Peres, F. H. Harrison, J. Gibson, C. S. Harwood, *Nat. Biotechnol.* **2004**, *22*, 55.
- [16] M. T. G. Holden, R. W. Titball, S. J. Peacock, A. M. Cerdeno-Tarraga, T. Atkins, L. C. Crossman, T. Pitt, C. Churcher, K. Mungall, S. D. Bentley, M. Sebahia, N. R. Thomson, N. Bason, I. R. Beacham, K. Brooks, K. A. Brown, N. F. Brown, G. L. Challis, I. Cherevach, T. Chillingworth, A. Cronin, B. Crossett, P. Davis, D. DeShazer, T. Feltwell, A. Fraser, Z. Hance, H. Hauser, S. Holroyd, K. Jagels, K. E. Keith, M. Maddison, S. Moule, C. Price, M. A. Quail, E. Rabbinowitsch, K. Rutherford, M. Sanders, M. Simmonds, S. Songsivilai, K. Stevens, S. Tumapa, M. Vesaratchavest, S. Whitehead, C. Yeats, B. G. Barrell, P. C. F. Oyston, J. Parkhill, *Proc. Nat. Acad. Sci. U.S.A.* **2004**, *101*, 14240.
- [17] H. A. Elo, S. Räsänen, P. J. Tuohimaa, *Cell. Mol. Life Sci.* **2005**, *36*, 312.
- [18] G. Kada, H. Falk, H. J. Gruber, *Biochim. Biophys. Acta* **1999**, *1427*, 33.
- [19] N. Humbert, P. Schürmann, A. Zocchi, J. M. Neuhaus, T. R. Ward, *Methods in Molecular Biology: Avidin-Biotin Interactions, Totowa (NJ)* **2008**, *418*, 101.
- [20] A. Chilkoti, P. S. Stayton, *J. Am. Chem. Soc.* **1995**, *117*, 10622.
- [21] A. Gallizia, C. d. Lalla, E. Nardone, P. Santambrogio, A. Brandazza, A. Sidoli, P. Arosio, *Protein Expression Purif.* **1998**, *14*, 192.
- [22] N. M. Green, *Methods Enzymol.* **1970**, *18*, 418.
- [23] V. P. Hytönen, O. H. Laitinen, T. T. Airene, H. Kidron, N. J. Meltola, E. J. Porkka, J. Hörhä, T. Paldanius, J. A. E. Määttä, H. R. Nordlund, *Biochem. J.* **2004**, *384*, 385.
- [24] T. Sano, M. W. Pandori, X. Chen, C. L. Smith, C. R. Cantor, *J. Biol. Chem.* **1995**, *270*, 28204.
- [25] L. Le Trong, N. Humbert, T. R. Ward, R. E. Stenkamp, *J. Mol. Biol.* **2006**, *356*, 738.
- [26] O. H. Laitinen, A. T. Marttila, K. J. Airene, T. Kulik, O. Livnah, E. A. Bayer, M. Wilchek, M. S. Kulomaa, *J. Biol. Chem.* **2001**, *276*, 8219.
- [27] J. D. Bendtsen, H. Nielsen, G. von Heijne, S. Brunak, *J. Mol. Biol.* **2004**, *340*, 783.
- [28] W. W. S. Wang, D. Das, M. R. Suresh, *Mol. Biotechnol.* **2005**, *31*, 29.
- [29] A. Han, M. Creus, G. Schurmann, V. Linder, T. R. Ward, N. F. de Rooij, U. Staufer, *Anal. Chem.* **2008**, *80*, 4651.
- [30] G. P. Kurzban, E. A. Bayer, M. Wilchek, P. M. Horowitz, *J. Biol. Chem.* **1991**, *266*, 14470.
- [31] a) M. E. Wilson, G. M. Whitesides, *J. Am. Chem. Soc.* **1978**, *100*, 306;  
b) G. Klein, N. Humbert, J. Gradinaru, A. Ivanova, F. Gilardoni, U. E. Rusbandi, T. R. Ward, *Angew. Chem. Int. Ed.* **2005**, *44*, 7764.
- [32] M. Creus, T. R. Ward, *Org. Biomol. Chem.* **2007**, *5*, 1835.
- [33] N. Guex, M. C. Peitsch, T. Schwede, *Electrophoresis* **2009**, *30*, s162.
- [34] U. K. Laemmli, *Nature* **1970**, *227*, 680.
- [35] T. Dharakul, S. Songsivilai, S. Viriyachitra, V. Luangwedchakarn, B. Tassaneetritap, W. Chaowagul, *J. Clin. Microbiol.* **1996**, *34*, 609.

- [36] P. J. Brett, D. DeShazer, D. E. Woods, *Int. J. Systematic Bacteriology* **1998**, *48*, 317.
- [37] M. J. Cowan, D. W. Wara, S. Packman, A. J. Ammann, *Lancet* **1979**, *2*, 115.
- [38] P. L. Felgner, Kayala, M. A., Vigil, A., Burk, C., Nakajima-Sasaki, R., Pablo, J., Molina, D. M., Hirst, S., Chew, J. S. W., Wang, D. L., Tan, G., Duffield, M., Yang, R., Neel, J., Chantratita, N., Bancroft, G., Lertmemongkolchai, G., Davies, D. H., Baldi, P., Peacock, S., Titball, R. W., *Proc. Natl. Acad. Sci. USA* **2009**, *106*, 13499.
- [39] M. Morpurgo, A. Radu, E. A. Bayer, M. Wilchek, *J. Mol. Recognit.* **2004**, *17*, 558.
- [40] M. Creus, A. Pordea, T. Rossel, A. Sardo, C. Letondor, A. Ivanova, I. LeTrong, R. E. Stenkamp, T. R. Ward, *Angew. Chem. Int. Ed.* **2008**, *47*, 1400.

---

# Chapter 5

## General Conclusions

*This is not the end. It is not even the beginning of the end. But it is, perhaps, the end of the beginning*

---

Winston Churchill

The *ex nihilo* creation of an artificial metalloenzyme, through the construction of the entire polypeptide sequence with metal-ions affinity, remains a challenging task<sup>[1]</sup>. For this reason, many efforts have been devoted towards the creation of catalytic activity by engineering a novel catalytic site into a native scaffolds, such as protein<sup>[2]</sup> and DNA<sup>[3]</sup>.

In the aftermath of the pioneering work of Wilson and Whitesides<sup>[2a]</sup>, hybrid catalysts have been generated by introducing a new metal-binding site within biotin-binding proteins (*i.e.* streptavidin and burkavidin)<sup>[4]</sup>.

Biotinylated organometallic fragments are anchored into the proteins within a supramolecular approach<sup>[5]</sup>. A genetic “fine-tuning” of the second coordination sphere can improve the “fitness” of hybrid catalysts in term of *ee* and substrate specificity.

In this study, the influence of the protein scaffold on enantioselectivity and catalytic performance of artificial transfer hydrogenases was widely investigated and optimized through a “designed” evolution scheme<sup>[6]</sup>.

Inspired by the X-ray crystal structure of a (*S*)-selective catalyst for the reduction of acetophenone derivatives, we selected two close lying residues (K121 and L124) for further mutagenesis studies, with the creation of several hybrid variants with improved features <sup>[5]</sup>. We implemented a straightforward protein production and purification scheme, amenable to HTS. This high-throughput strategy, described as immobilization approach, led to a successful streptavidin purification directly from crude cell extract thanks to the high affinity of the protein for biotin, with a simplified screening effort towards a larger hybrid-catalyst library investigation <sup>[5]</sup>. In this context, we also scrutinized thermo-denaturation as another strategy to simplify streptavidin purification by exploitation of its high thermal stability. Preliminary screening for Pd-mediated allylic alkylation using crude cell extract was disappointing. However, many efforts can be focused in this direction to improve the catalytic activity in cell lysate.

Artificial metalloenzymes were also generated using burkavidin as novel protein-scaffold. In combination with a biotinylated metal complex burkavidin has been shown to perform the enantioselective hydrogenation of *N*-protected dehydroamino acids <sup>[7]</sup>. Further chemogenetic optimization or evolution could improve conversion and selectivity.

At this stage, *in vivo* catalysis remains an exciting challenge and burkavidin represents a milestone in this direction as the creation of hybrid enzymes within the cell periplasm may allow catalytic reactions to be carried out *in vivo* <sup>[8]</sup>.

The well-defined binding pocket of biotin-binding proteins could be also exploited to accommodate small molecule drugs and generate supramolecular assemblies.

The incorporation of a biotinylated ruthenium piano-stool into streptavidin using a supramolecular approach can modulate the macromolecular-target recognition

through additional non-covalent interactions. This “surface borrowing” strategy *via* a presenter protein allows to modulate the affinity and the selectivity towards DNA telomeres, even in the presence of competing species <sup>[9]</sup>.

Accordingly, supramolecular assemblies of drugs within host proteins can be proposed as a promising alternative to the current anti-cancer therapeutic agents inasmuch as chaperone drug specific delivery to a desired macromolecular target <sup>[10]</sup>.

In the present form, such hybrid organometallic species cannot be delivered to a cell. Nevertheless, a chemo-genetic engineering could improve binding and selectivity *in vivo*. As future perspective, the challenging intracellular delivery of supramolecular metallodrugs can be addressed differently, either by appending a cell-penetrating peptide sequence to the presenter protein <sup>[11]</sup> or by exploiting an overexpressed protein in cancer cells (i.e. carbonic anhydrase) as presenter scaffold <sup>[12]</sup>.

Potential important implications in the medical field have been also attributed to burkavidin, the first demonstration of an avidin in a human pathogen. Its strong biotin-binding activity could be exploited as diagnostic for *Burkholderia* and as a means of targeting biotinylated antimicrobials <sup>[13]</sup>, while its low pI may render this novel protein also useful for specific binding of biotinylated DNA, in contrast to avidin that is involved in non-specific electrostatic interactions with the negatively charged DNA <sup>[14]</sup>.

# REFERENCES

- [1] a)W. F. DeGrado, C. M. Summa, V. Pavone, F. Nastro, A. Lombardi, *Annu. Rev. Biochem.* **1999**, *68*, 779; b)L. Jiang, E. A. Althoff, F. R. Clemente, L. Doyle, D. Rçthlisberger, A. Zanghellini, J. L. Gallaher, J. L. Betker, F. Tanaka, C. F. Barbas III, D. Hilvert, K. N. Houk, B. L. Stoddard, D. Baker, *Science* **2008**, *319*, 1387; c)F. Xu, L. Zhang, R. L. Koder, V. Nanda, *Biochemistry* **2010**, *49*, 2307.
- [2] a)M. E. Wilson, G. M. Whitesides, *J. Am. Chem. Soc.* **1978**, *100*, 306; b)J. Collot, J. Gradinaru, N. Humbert, M. Skander, A. Zocchi, T. R. Ward, *J. Am. Chem. Soc.* **2003**, *125*, 9030 ; c)T. Kokubo, T. Sugimoto, T. Uchida, S. Tanimoto, M. Okano, *J. Chem. Soc. Chem. Commun.* **1983**, 769; d)M. Ohashi, T. Koshiyama, T. Ueno, M. Yanase, H. Fuji, Y. Watanabe, *Angew. Chem. Int. Ed.* **2003**, *42*, 1005; e)K. Okrasa, R. J. Kazlauskas, *Chem. Eur. J.* **2006**, *12*, 1587.
- [3] a)A. J. Boersma, R. P. Megens, B. L. Feringa, G. Roelfes, *Chem. Soc. Rev.* **2010**, *39*, 2083; b)S. Park, H. Sugiyama, *Angew. Chem. Int. Ed.* **2010**, *49*, 3870
- [4] C. M. Thomas, T. R. Ward, *Chem. Soc. Rev.* **2005**, *34*, 337.
- [5] M. Creus, A. Pordea, T. Rossel, A. Sardo, C. Letondor, A. Ivanova, I. LeTrong, R. E. Stenkamp, T. R. Ward, *Angew. Chem. Int. Ed.* **2008**, *47*, 1400.
- [6] C. Letondor, A. Pordea, N. Humbert, A. Ivanova, S. Mazurek, M. Novic, T. R. Ward, *J. Am. Chem. Soc.* **2006**, *128*, 8320.
- [7] G. Klein, N. Humbert, J. Gradinaru, A. Ivanova, F. Gilardoni, U. E. Rusbandi, T. R. Ward, *Angew. Chem. Int. Ed.* **2005**, *44*, 7764.
- [8] S. Voss, A. Skerra, *Protein Eng.* **1997**, *10*, 975.
- [9] a)R. Briesewitz, G. T. Ray, T. J. Wandless, G. R. Crabtree, *Proc. Nat. Acad. Sci. U.S.A.* **1999**, *96*, 1953; b)G. R. Crabtree, *Science* **1989**, *243*, 355; c)S. L. Schreiber, *Science* **1991**, *251*, 283; d)I. Harvey, P. Garneau, J. Pelletier, *Proc. Nat. Acad. Sci. U.S.A.* **2002**, *99*, 1882; e)K. A. Plummer, J. M. Carothers, M. Yoshimura, J. W. Szostak, G. L. Verdine, *Nucleic Acids Res.* **2005**, *33*, 5602.
- [10] L. Kelland, *Nat. Rev. Cancer* **2007**, *7*, 573.
- [11] a)J. Rinne, B. Albarran, J. Jylhävä, T. O. Ihalainen, P. Kankaanpää, V. Hytönen, P. S. Stayton, M. S. Kulomaa, M. Vihinen-Ranta, *BMC Biotech.* **2007**, *7*, 1; b)B. Albarran, R. To, P. S. Stayton, *Protein Eng. Des. Sel.* **2005**, *18*, 147.
- [12] Ö. Türeci, U. Sahin, E. Vollmar, S.Siemer, E. Göttert, G. Seitz, A.-K. Parkkila, G. N. Shah, J. H. Grubb, M.Pfreundschuh, W. S. Sly, *Proc. Nat. Acad. Sci. U.S.A.* **1998**, *95*, 7608.
- [13] P. L. Felgner, Kayala, M. A., Vigil, A., Burk, C., Nakajima-Sasaki, R., Pablo, J., Molina, D. M., Hirst, S., Chew, J. S. W., Wang, D. L., Tan, G., Duffield, M., Yang, R., Neel, J., Chantratita, N., Bancroft, G.,



- Lertmemongkolchai, G., Davies, D. H., Baldi, P., Peacock, S., Titball, R. W., *Proc. Natl. Acad. Sci. USA* **2009**, *106*, 13499.
- [14] M. Morpurgo, A. Radu, E. A. Bayer, M. Wilchek, *J. Mol. Recognit.* **2004**, *17*, 558.

# APPENDIX A

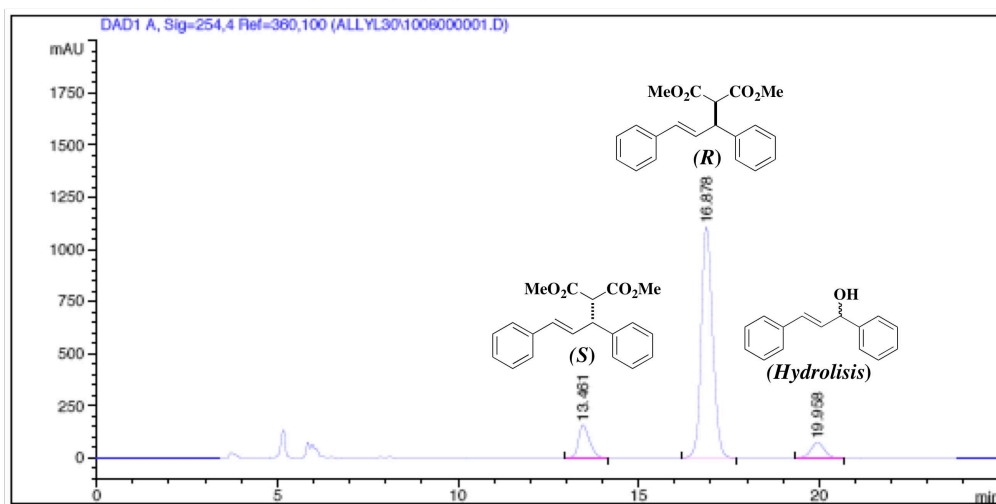
## HPLC Analysis of Allylic Product

(performed by Mr Cheikh Lo)

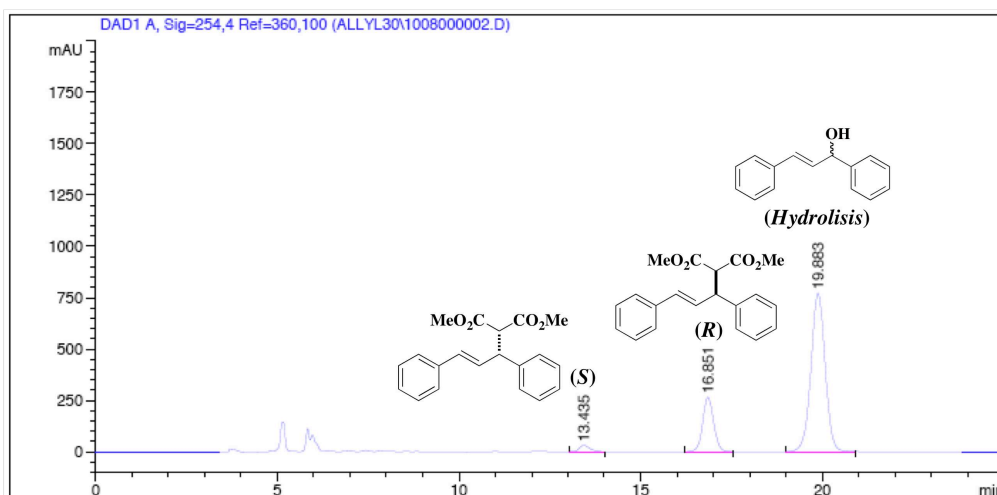
*OD-H column*

*Hexane : iPrOH = 95 : 5; 0.3 mL/min*

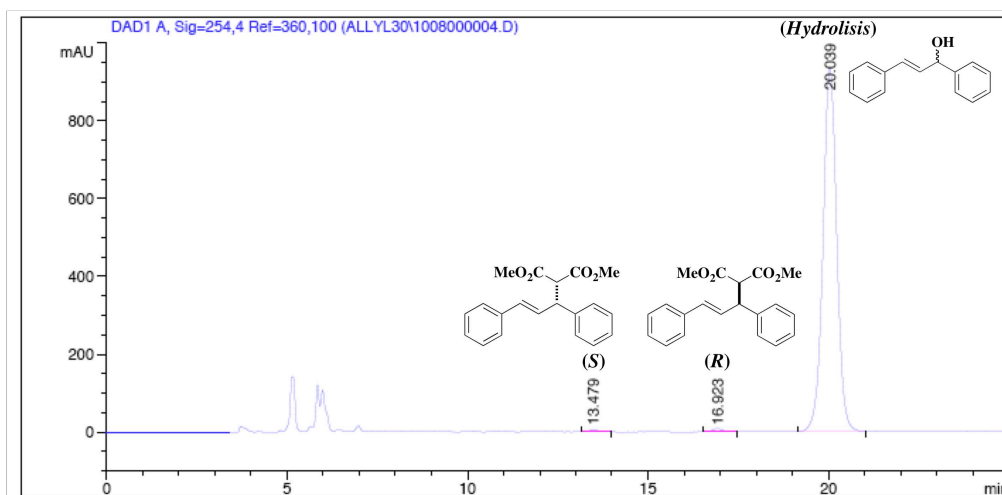
*207 nm*



Scaffold	Vol reaction	Retention Time	Area [%]
Pure Sav WT	440 $\mu$ L	13.461	11,4323
		16.878	81,9812
		19.958	6,5864



Scaffold	Vol reaction	Retention Time	Area [%]
Pure Sav WT	2800 $\mu$ L	13.461	2,1648
		16.887	20,7713
		19.951	77,0639



Scaffold	Vol reaction	Retention Time	Area [%]
Cell Extract WT	2800 $\mu$ L	13.479	0,4307
		16.923	0,6585
		20.039	98,9108



# APPENDIX B

## Molecular Biology Protocol

(written in collaboration with Mr Narasimha Rao Uda)

### DAY ONE:

#### **PCR Mutagenesis on ice: (50 $\mu$ L total volume)**

- *Template* (5-25 ng/ $\mu$ L) = 1  $\mu$ L
- *Primer +* (10  $\mu$ M) = 1.5  $\mu$ L ( $C_F$  300 nM)
- *Primer -* (10  $\mu$ M) = 1.5  $\mu$ L ( $C_F$  300 nM)
- *dNTP* (10 mM total) = 2  $\mu$ L ( $C_F$  0.4 mM)
- *10X Buffer* = 5  $\mu$ L
- *DMSO* (100%) = 2.5  $\mu$ L ( $C_F$  5%)
- *H<sub>2</sub>O* (sterile) = 35  $\mu$ L
- *Pfu Turbo* (2.5 u/  $\mu$ L) = 1.5  $\mu$ L ( $C_F$  0.075 u/  $\mu$ L)

#### **Program:**

- 95 °C – 5 ’
- **START 16X:**
  - *Start cycle*
  - 95 °C – 1’
  - 60 °C – 1’ (or 50 °C-1’; or 55 °C-1’)
  - 68 °C – 10’
  - *End cycle*
  - 68 °C – 60’
- 4 °C – overnight

### DAY TWO:

#### **Agarose gel 1.2%**

#### **DpnI Treatment (for positive sample):**

- 1  $\mu$ L of DpnI in each tube
- Incubation for 1 h @ 37 °C

#### **Transformation of cloning cells (DH5 $\alpha$ or XL-Blue):**

#### **Prepare LB-AGAR plate:**

- *Bactotryptone*: 8 g
- *Bactoyeast extract*: 4 g

- NaCl: 8 g
- Agar: 12 g
- H<sub>2</sub>O: make-up to 800 mL
- At 50 °C, add antibiotics: AMP (960 µL of 50 mg/mL)

Transformation of ultra-competent XL-Blue strain:

- Take the ultra-competent cells out of freezer (- 80 °C)
- Thaw on ice (always treat cells carefully)
- Pre-warm LB-agar plate on the bottom shelf of incubator (@ 37 °C)
- Wait until DTT is completely thawed
- Add 8 µL of DTT (200 mM frozen stock) into 100 µL of cells
- Add 5 µL (or 10 µL if of a weak spot) of PCR product to 100 µL of competent cells and mix gently: no up and down!
- Leave on ice for 15'
- Plating into the pre-warmed plates (LB/AMP) and incubation overnight.

## DAY THREE:

**Pre-culture for minipreps:**

- In 14 mL Falcon tube:
  - AMP ( 50 mg/mL) = 3.6 µL (C<sub>F</sub> 60 µg/mL)
  - Glucose (20%) = 15 µL (C<sub>F</sub> 0.1%)
  - LB = 3 mL (also 5 mL)
  - Inoculation: 1 colony from plate (or glycerol stock)
  - Incubation overnight (37 °C, 250 rpm)

## DAY FOUR:

**Minipreps DNA Purification:**

- Centrifuge Falcon tube = 4400 rpm, 4 °C, 5'
- Discard supernatant
- Resuspend pellet with 250 µL "CELL RESUSPENSION SOLUTION" and transfer in eppendorf (1.5ml)
- Add 250 µL "CELL LYSIS SOLUTION" to each sample: invert 8 times to mix (1 eppendorf for time)
- Add 10 µL "ALKALINE PROTEASE SOLUTION": invert 8 times to mix. Incubate 5' at r.t. (to time from the first)
- Add 350 µL "NEUTRALIZATION SOLUTION": invert 8 times to mix.
- Centrifuge at top speed for 10' at r.t.
- Insert "SOIN COLUMN" into "COLLECTION TUBE"

- Decant cleared lysate into Spin Column
- Centrifuge at top speed for 1' at r.t. : discard flow-through and reinsert column into collection tube (without cover in centrifuge: no problem)
- Add 750  $\mu\text{L}$  "WASH SOLUTION" (ethanol added). Centrifuge at top speed for 1' at r.t. : discard flow-through and reinsert column into collection tube
- Add 250  $\mu\text{L}$  "WASH SOLUTION". Centrifuge at top speed for 3' at r.t. : discard flow-through and reinsert column into collection tube
- Transfer Spin Column to a sterile 1.5 ml eppendorf.
- Add 40  $\mu\text{L}$  of "NUCLEASE-FREE WATER" to the spin column: wait 5'.
- Centrifuge at top speed for 1' at r.t
- Discard column and measure concentration in NANODROP (the ratio 260/280 is very important: only if it's  $>1.8$ , the DNA is very pure and the concentration in ng/  $\mu\text{L}$  is real)
- Finally store DNA @  $-20^{\circ}\text{C}$ .

## DAY FIVE:

### **Transformation of expression strain: BL21(DE3)pLysS**

#### Prepare LB-AGAR plate:

- Bactotryptone: 8 g
- Bactoyeast extract: 4 g
- NaCl: 8 g
- Agar: 12 g
- H<sub>2</sub>O: make-up to 800 mL
- At 50 °C, add antibiotics: AMPICILINE (960  $\mu\text{L}$  of 50 mg/mL; Cf: 60  $\mu\text{g}/\text{mL}$ ), CHLORAMPHENICOL (800  $\mu\text{L}$  of 34 mg/mL; Cf: 34  $\mu\text{g}/\text{mL}$ ), GLUCOSE (80 mL of 20%; Cf: 2%)

#### Transformation of ultra-competent BL21(DE3)pLysS:

- Take the ultra-competent cells out of freezer ( $-80^{\circ}\text{C}$ )
- Thaw on ice (always treat cells carefully)
- Pre-warm LB-agar plate on the bottom shelf of incubator (@  $37^{\circ}\text{C}$ )
- Wait until DTT is completely thawed
- Add 8  $\mu\text{L}$  of DTT (200 mM frozen stock) into 100  $\mu\text{L}$  of cells
- Add 3  $\mu\text{L}$  of plasmid (0.2-0.5  $\mu\text{g}$  of DNA) to 100  $\mu\text{L}$  of competent cells and mix gently: no up and down!
- Leave on ice for 15'
- Plating into the pre-warmed plates (LB+AMP+CP+GLU) and incubation overnight.

# APPENDIX C

## Streptavidin Expression in 20 L of *E. coli* Cell Culture

(written in collaboration with Ms Elisa Nogueira)

### DAY ONE:

*In the morning:*

Prepare TP MEDIUM		
PRODUCT	20 L Culture	300 mL Preculture
Bactotryptone	400 g	6 g
Na <sub>2</sub> HPO <sub>4</sub>	26 g	0.39 g
KH <sub>2</sub> PO <sub>4</sub>	20 g	0.3 g
NaCl	160 g	2.4 g
Bactoyeast extract	300 g	4.5 g
d-H <sub>2</sub> O	Make-up to 5 L	Make-up to 300 mL

#### ***Sterilization in Autoclave:***

1. 300 mL TP medium in 3L flask
2. 100 mL ANTIFOAM in anti-foam bottle + magnet
3. 900 mL mQ-H<sub>2</sub>O for antifoam dilution (then keep at 4 °C)
4. Inoculation bottle
5. Glucose 20% (100 g in 500 mL) – *Final concentration: 0.4%*
6. 400 mL NaOH 1 M
7. Air filter (from fermentor)

#### ***Prepare:***

- Sterile IPTG 0.8 M: 1.9 g in 10 mL H<sub>2</sub>O (sterile filter under hood) – *Final concentration: 0.4 mM*
- Sterile CHLORAMPHENICOL (34 mg/mL): 680 mg in 20 mL Ethanol (sterile filter under hood) – *Final concentration: 34 µg/mL*
- Sterile AMPICILIN (50 mg/mL): 1.2 g in 24 mL H<sub>2</sub>O (sterile filter under hood) – *Final concentration: 50 µg/mL*
- Prepare concentrated 20 L of TP medium (quantities for 20 L but add only 5 L H<sub>2</sub>O)

*In the early afternoon:*

#### **IMPORTANT PRECAUTIONS:**

1. High temperature (do not get burned!)



2. Lamp vessel (be careful!)
3. Moving pieces under vessel (do not touch!)
4. High pressure: **!!! NEVER OPEN VESSEL UNDER HIGH PRESSURE !!!**
5. Read instructions, get help.

***Sterilisation of 20 L TP medium:***

- Turn on the cryostat – ensure that the level of refrigerant inside the cryostat is OK. If not, add a mixture of 10% EtOH/ H<sub>2</sub>O;
- Turn on the ventilator in the fermentation room. Close the doors.
- Empty and clean fermentor (which is kept in 50% ethanol in between fermentations) – rinse it twice with water to get rid of ethanol traces;
- Ensure all septa are intact: if necessary, change the old septa with new ones;
- pH calibration:
  - **Connect pH-meter**
  - Cali on MENU
  - Cali meas.
  - 1° ref: pH 4.00
  - When the value is stable: Calibrate
  - 2° ref: pH 7.00
  - When the value is stable: Calibrate
  - Calibration is done
- Pour the 5 L of concentrated TP medium in the vessel and top-up with 15 L of water, making a total volume of 20 L. Before pouring the medium, make sure that the pH-probe is connected on the bottom of the vessel and all the entrances/tap are closed!
- Check the level of antifoam probe (approx. 10 cm above liquid level);
- Switch on fermentor (main switch);
- Agitation speed 600 rpm: ▲▼ CTRL.M. OFF ◀▶ Controlled: OK (◀▶ OFF OK to stop)
- Open air: put 1 beaker at the end of air outlet;
- Start sterilisation on Temperature panel: ▲▼ CTRL.M. OFF ◀▶ Sterilize: OK (◀▶ OFF OK to stop); at start of fermentation, the vessel should be closed and air-outlet open;
- At 95 °C (more or less after 40 minutes) close the air outlet and press OK to continue;
- Sterilise at 121 °C for 30 minutes;
- Then the temperature comes down;
- At 100 °C, open air outlet and connect air-filter (verify that pressure inside vessel is zero!);
- At 50 °C add ANTIBIOTICS: 10 mL CP (34 mg/mL) and 12 mL AMP (50 mg/mL), through septum;
- Add 1.5 bar by opening the air inlet (air tap on the wall, and tap on the air tubing), close air outlet and air inlet;
- Switch off the fermentor and cryostat.

***Pre-Culture: (under hood)***

- Sterile 300 mL TP medium in 3 L flask
- Sterile Glucose 20%: 15 mL
- Sterile CP (34 mg/mL): 300 µL
- Sterile AMP (50 mg/mL): 360 µL
- Inoculation with glycerol stock (in -80 °C): keep the glycerol stock in dry-ice
- Incubation at 37 °C, 250 rpm, overnight.

## DAY TWO:

*In the early morning:*

### **Culture:**

- Switch on the cryostat and the ventilation in the room;
- Turn on fermentor and programme the temperature to 37 °C;
- Add ANTIBIOTICS: 10 mL CP (34 mg/mL) and 12 mL AMP (50 mg/mL) (open air outlet to bring pressure inside the vessel to zero, check on the manometer): release pressure
- Take blank (40 mL)
- Under hood prepare:
  - Mix pre-culture + 400 mL glucose 20% (in the sterile inoculation bottle)
  - Antifoam 10%: add 900 mL of cold water to 100 mL of sterile antifoam and keep on ice
- Connect acid/base bottles. Leave one free just for the inoculation. Set it up to pH 2.0 if you use the Acid pump for inoculation. Afterwards, remember to set it up back to 6.5!
- At 37 °C, inoculate the medium with pre-culture (open air outlet to bring pressure inside the vessel to zero, check on the manometer); use one of the acid/base pumps to inoculate medium or the antifoam one. Be sure that the antifoam probe touches the top of the liquid and set up the pump to 100%. At the end, pull the probe up again (10 cm above the liquid level) and set the pump back to 20%.
- Connect Antifoam bottle and set it up on the “Antifoam” panel – 20%, use “controlled” set-up. Put the antifoam bottle in a beaker with ice (to keep it cool) and on a stirring plate;
- Set up agitation to 600 rpm and use “controlled” set-up;
- Open **air inlet to 1.5 bar** and leave the **air outlet open**, so air can circulate through the vessel;
- Each hour take sample to check **OD<sub>600</sub>** and keep them on ice.
  - Use an UV cuvette (1 mL – BIOLOGIST USE ONLY)
  - SIMPLE READS Program → Setup → Read at Wavelength: 600 nm
  - Y-Mode → Abs x F = 10.0000 **OK**
  - Blank the Spec → add 1 mL of the blank sample (medium before inoculation) → Zero
  - Add 900 µl of Blank + 100 µl of your sample (10x dilution)
  - Mix covering the cuvette with parafilm (be careful with the air bubbles)
  - Read at 600 nm (Abs · 10)
  - Print Report at the end of the fermentation
- When the OD is between 1.8 and 2, induce – close air inlet, verify that there is no air inside the vessel (manometer at 0, air outlet open) and with a syringe add 10ml IPTG 0.8 M (Cf: 0.4 mM) (from one of the septum on top of the fermentor)
- Stop the culture when the **OD<sub>600</sub>** starts to decrease by closing the air (in and out).
- Set programme temperature to 4 °C and decrease agitation to 250 rpm.

### **Harvest:**

- Cool down the centrifuges to 4 °C
- Centrifugation programme:
  - 4400 rpm, 4 °C, 10 minutes for the small centrifuge
  - 4400 rpm, 4 °C, 10 minutes for the ultracentrifuge (big one)
- Discard the supernatant and inactivate the waste (supernatant) with NaClO (bleach)
- Repeat as much as necessary, i.e. the same centrifuge bottle can be reused over and over again, until the 20 L of culture are centrifuged
- Freeze the pellet at –20 °C.
- Switch off cryostat
- Wash the fermentor – rinse it twice with water with the agitation on (maximum speed – 1500 rpm)
- Add 10L H<sub>2</sub>O and 10 L ethanol (you can find the container in the yellow cabinet in the basement)
- Switch off fermentor

- Make sure that nothing is left on the way (hallway to the library) / everything is turned off (cryostat, main switch of the fermentor, taps (air and water), ventilator...) / biological waste disposed in proper containers as well as needles, etc.
- Rinse the bottles and tubing first with water, second with ethanol, and with water again; finally wash them in the dishwasher. DO NOT put them as they are in the dishwasher as the tubes burst/caramelize if they're not previously rinsed.
- Finally, spin down 1mL of each sample (1 h before induction and all samples after induction), discard supernatant and keep labelled pellet at -20 °C to run a SDS-Page gel next day.

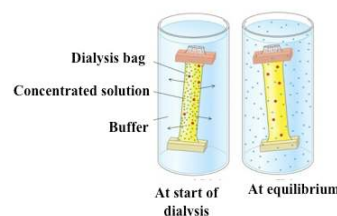
## DAY THREE:

### ***Resuspension of cell lysate:***

- Thaw the bacterial pellet at room temperature. DO NOT warm them up!
- Prepare a resuspension buffer:
  - **Tris/HCl** (pH 7.4, 1 M): 10 mL (Cf : 20 mM)
  - **PMSF**: 87 mg in 5 mL EtOH (freshly prepared)
  - **mQ-H<sub>2</sub>O**: bring volume up to 500 mL
- Resuspend the pellet in 500 mL of resuspension buffer
- Add 2-3 mg of DNase1 powder (the tip of a spatula) and incubate at room temperature under vigorous stirring (until the nucleic acids are totally degraded – no more slimy strings inside the bottles). Add more DNase1 if necessary.

### ***Dialysis in guanidinium hydrochloride 6 M, pH 1.5:***

- Prepare a large dialysis bag (Spectra/Por, 6-8.000 MWCO), capable of containing at least 800 mL of liquid and let it soak in distilled water (15 min)
- Prepare 15 L of denaturation buffer:
  - **Guanidinium hydrochloride 6 M**: 8597.7 g in 15 L of distilled water (pH 1.5 with HCl)
- Pour the bacterial extract into the dialysis bag
- Place the bag in a tank containing denaturation buffer
- Dialyse under gentle stirring for 24 h at room temperature
- The dialysis solution can be reused 2-3 times



### ***Electrophoresis SDS-PAGE:***

#### **Gel preparation:**

#### **SDS – loading gel**

#### **12% gel – 15 mL for 2 gels**

- 5 mL of ddH<sub>2</sub>O
- 6 mL of 30% acrylamide
- 3.8 mL of 1.5 M Tris pH 8.8
- 75 μL of 20% SDS
- 100 μL of 15% APS
- 6 μL of TEMED

*Pour ± 7 mL of gel in each cassette. Add ethanol on top of the gel, until gel is ready (1mL left in the falcon tube serves as control). Wash it thoroughly with dH<sub>2</sub>O before loading the stacking gel.*

### SDS – stacking gel

#### 5% gel – 6 mL for 2 gels

3.4 mL of ddH<sub>2</sub>O

1 mL of 30% acrylamide

1.5 mL of 0.5 M Tris pH 6.8

30  $\mu$ L of 20% SDS

40  $\mu$ L of 15% APS

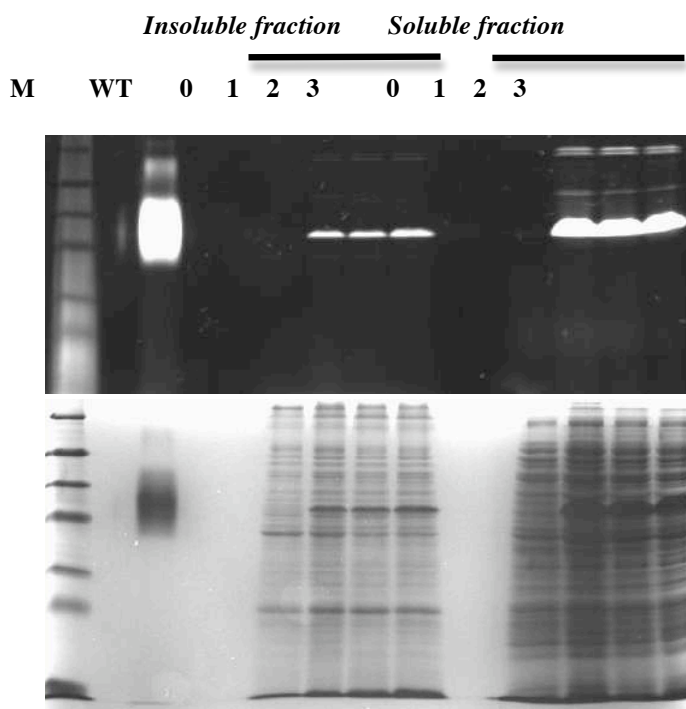
6  $\mu$ L of TEMED

*Pour  $\pm$  3 mL of gel in each cassette. Carefully place the comb into the cassette (use goggles, as some of the gel solution can splash out of the cassette). Use the remaining 1 mL as control. When ready, remove the comb carefully (don't put too much pressure on it as it can break the gel easily). Wash thoroughly with dH<sub>2</sub>O. Place it into the tank, and add 1X SDS buffer immediately to prevent dryness of the gel.*

#### Samples preparation:

- Thaw the bacterial pellet at r.t.
- Multiply by 40 the OD of each sample you've taken during the fermentation. Then add the corresponding result in  $\mu$ L of dH<sub>2</sub>O.
- Add 1  $\mu$ L of DNase (10 mg/mL) and incubate for 30 minutes
- Vortex for 5 minutes
- Centrifuge the samples: 14000 rpm, 4 °C, 5'
- Transfer the supernatant in a new eppendorf: this is the **SOLUBLE FRACTION**
- Resuspend the pellet in the same volume of H<sub>2</sub>O as previously and vortex for 5 minutes: this is the **INSOLUBLE FRACTION**
- Transfer 20  $\mu$ L of each sample in a new tube
- Add 1  $\mu$ L of B4F (0.6 mM) and incubate for 10' at r.t.
- Add 10  $\mu$ L of LB (3X, without DTT)
- Mix up and down with the pipette
- Positive control **SAV-WT**: 18  $\mu$ L of H<sub>2</sub>O; 2  $\mu$ L of WT (10 mg/mL); 1  $\mu$ L of B4F; 10  $\mu$ L 3X LB
- Load 20  $\mu$ L on the gel
- Protein Marker: 8  $\mu$ L

Gel picture:



## DAY FOUR:

***Dialysis in Tris/HCl 20 mM, pH 7.4:***

- Prepare 15 L of renaturation buffer:
  - **Tris/HCl (pH 7.4, 1 M):** 300 mL
  - **d-H<sub>2</sub>O:** bring volume up to 15 L
- Transfer the dialysis bag to the renaturation buffer
- Dialyze under gentle stirring for 16 h at room temperature

## DAY FIVE:

***Dialysis in imino-biotin binding buffer, pH 9.8:***

- Prepare 15 L of imino-biotin binding buffer, to equilibrate the protein in buffer pH 9.8
  - **NaHCO<sub>3</sub> (1 M, pH 9.8):** 750 mL (Final concentration: 50 mM)
  - **NaCl (5 M):** 1.5 L (Final concentration: 500 mM)
  - **dH<sub>2</sub>O:** bring volume up to 15 L
- Transfer the dialysis bag to the imino-biotin binding buffer
- Dialyze under gentle stirring for 16 h at 4 °C (in the cold room)

## DAY SIX:

### *Centrifugation*

- Cool down the centrifuges to 4 °C;
- Open membranes and transfer all the content of the membranes to a centrifugation bottle (500 mL);
- Centrifugation programme: 10000 rpm, 4 °C, 30 minutes;
- Keep the supernatant in a new centrifugation bottle and inactivate the waste (pellet) with NaClO (bleach);
- If particles are present, filter the supernatant using Whatman filters,
- Freeze the supernatant at –20 °C if you don't purify on the same day.

### *Purification on an imino-biotin column:*

Defrost your sample. Do not forget that a big volume takes a long time to defrost. Plan your day so you won't start the washing of the FPLC too soon! You will need 2 L of imino-biotin buffer Ph 9.8 and 2 L of Acetic Acid 1%.

Be sure that all tubes are at the bottom of each bottle, so no air bubbles are created inside the system!

**POS 1:** Imino-biotin Buffer, pH 9.8 (50 mM NaHCO<sub>3</sub>, 500 mM NaCl)

**POS 2:** Sample

**Buffer B:** Acetic Acid 1%

- Software: *Prime View*
  - UV: 280 nm
  - Cond: conductivity (salt concentration)
  - pH: no probe
  - Pressure: 1MPa (limit)
  - Temperature
  - Conc: % B
- Use *Esc* in order to come back and ▲▼ to move in the same level
- **SET PARAMETERS:** OK
  - To switch on the UV lamp:
- **Turn ON – Lamp: Lamp Off – OK - ▲▼ - On – OK**
- **Esc**
- First wash of the system:
  - The whole system has to be washed with water to wash out the ethanol.
  - Plunge the three inlet tubes in a bottle of mQ-H<sub>2</sub>O and make sure that the three outlet tubes are in the waste bottle
  - Perform Programme 5 (Quick-Wash):
- Run Stored Method → **OK** → from System → **OK** – From System No 5 (*Data Transfer to PC*) → Press OK to Start RUN
- **OK**
- Initial washing of the system:
  - Three inlet tubes (Red-B, White-A2, Blue-A1) in acetic acid 1%
  - Empty the waste
  - Three outlet tubes in the waste flask
  - Verify that the arm (to collection tubes) is in the correct position
  - Template: **OK** → Application template: **OK** → System wash method: **OK** → B, A, 2...: **OK** → Press OK to Start RUN
  - Method is done: no memory

- Washing of A2 Line and equilibration of the column:
  - Place A2 and A1 tubes in the equilibration buffer (imino-biotin buffer)
  - Go to “Manual Run”
- Set flow rate → **10 mL/min**
- Set buffer valve position → **Pos2**
- Start Run → **OK → OK**
  - Leave it run for ±50 mins (5 columns volume).
- Press END → **OK → OK**
  - Empty the Waste bottle and put a clean one to collect the waste of your protein.
  
- Streptavidin purification on an imino-biotin column:
  - Add some Tris/HCl 1 M, pH 8.8 to each collection tube on the collector;
  - Measure the volume of your sample in a cylinder and change the programme according to the total volume you want to be purified (subtract ±50 mL to the total volume to be sure that air is not pumped into the system)
  - Changing the value in the **3<sup>rd</sup> Breakpoint** (in this case, 380 mL – 350 mL total volume) will change automatically the values of the other breakpoints.
- Run Stored Method → **OK** → from System → **OK** – From System No 1 (*Data Transfer to PC*) → Press OK to Start RUN
- **OK**
  
- **PROGRAMME 1:**
- **Breakpoint 30 mL (equilibration of column with imino-biotin buffer pH 9.8):**
  - ◆ *Set method base (mL)*
  - ◆ *Set fraction base (mL)*
  - ◆ *Pressure: 1 MPa*
  - ◆ *Set alarm: no*
  - ◆ *Show: no*
  - ◆ *Edit breakpoint: OK*
    - ml (0.0)
    - B %: 0
    - Set flow: 10 mL/min
    - Set fraction size: 0.0 mL
    - Set buffer: pos 1
    - Set inject: load
    - Set peak collect: no
    - Autozero: no
    - Event mark: no
    - Edit time vol: 30.0 mL
    - Save breakpoint: OK
  
- **Breakpoint 30.1 mL (loading of sample):**
  - B %: 0
  - Set flow: 10 mL/min
  - Set fraction size: 0.0 mL
  - Set buffer: pos 2
  - Set inject: load
  - Set peak collect: no
  - **Autozero: yes**
  - Event mark: yes
  - Edit time vol: 30.1 mL
  - Save breakpoint: OK

- **\*\*Breakpoint 380 mL (end of loading of sample (350 mL total volume) + start column washing with imino-biotin buffer pH 9.8):**
  - B %: 0
  - Set flow: 10 mL/min
  - Set fraction size: 0.0 mL
  - Set buffer: pos 1
  - Set inject: load
  - Set peak collect: no
  - Autozero: no
  - Event mark: yes
  - Edit time vol: 380.0 mL
  - Save breakpoint: OK
- ◆ **To change this value: Edit time → Change → Save**
- **Breakpoint 1400 mL (washing with imino-biotin buffer pH 9.8)**
  - B %: 0
  - Set flow: 10 mL/min
  - Set fraction size: 0.0 mL
  - Set buffer: pos 1
  - Set inject: load
  - Set peak collect: no
  - Autozero: no
  - Event mark: yes
  - Edit time vol: 1400.0 mL
  - Save breakpoint: OK
- **Breakpoint 1400.1 mL (start elution with acetic acid 1%).**
  - B %: 100
  - Set flow: 10 mL/min
  - **Set fraction size: 10.0 mL**
  - Set buffer: pos 1
  - Set inject: load
  - Set peak collect: no
  - Autozero: no
  - Event mark: yes
  - Edit time vol: 1400.1 mL
  - Save breakpoint: OK
- **Breakpoint 2000 mL (gradient – elution with acetic acid 1%):**
  - B %: 100
  - Set flow: 10 mL/min
  - Set fraction size: 10.0 mL
  - Set buffer: pos 1
  - Set inject: load
  - Set peak collect: no
  - Autozero: no
  - Event mark: yes
  - Edit time vol: 2000.0 mL
  - Save breakpoint: OK
- **Breakpoint 2000.1 mL (washing with imino-biotin buffer pH 9.8):**
  - B %: 0
  - Set flow: 10 mL/min
  - Set fraction size: 0.0 mL



- Set buffer: pos 1
  - Set inject: load
  - Set peak collect: no
  - Autozero: no
  - Event mark: yes
  - Edit time vol: 2000.1 mL
  - Save breakpoint: OK
- **Breakpoint 2400 mL (washing with imino-biotin buffer pH 9.8):**
    - B %: 0
    - Set flow: 10 mL/min
    - Set fraction size: 0.0 mL
    - Set buffer: pos 1
    - Set inject: load
    - Set peak collect: no
    - Autozero: no
    - Event mark: yes
    - Edit time vol: 0.0 mL
    - Save breakpoint: OK
    - End method
    - Save method

Rinse the system with mQ-H<sub>2</sub>O, and wash it with 75% EtOH. Leave column and tubing in EtOH to prevent the growth of foreign microorganisms.

## DAY SEVEN:

### ***Dialysis in Tris/HCl 1 0mM, pH 7.4:***

- Prepare 15 L of neutralisation buffer:
  - **Tris/HCl** (1 M, pH 7.4): 150 mL
  - **dH<sub>2</sub>O**: bring volume up to 15 L
- Dialyse the pure protein under gentle stirring against the neutralisation solution for 16 h at 4 °C.

## DAY EIGHT:

### ***Dialysis in distilled water (d-H<sub>2</sub>O):***

- Transfer the dialysis bag in a tank containing distilled water (15 L) and dialyse under gentle stirring for 16 h at 4 °C.

## DAY NINE:

### ***Dialysis in nanopure water (mQ-H<sub>2</sub>O):***

- Transfer the dialysis bag in a tank containing mQ-H<sub>2</sub>O (15 L) and dialyse under gentle stirring for 16 h at 4 °C.

## DAY TEN:

### ***Protein lyophilisation:***

*A lyophiliser creates a very low temperature and low-pressure environment in which aqueous solvents will sublime, leaving only solute(s) behind. To have this to work the most efficiently, samples should be 'shell' frozen to maximize surface area.*

*Do not use a lyophiliser to remove organic solvents, as they can damage the vacuum pump.*

- Place your samples in tubes (such as 15 mL or 50 mL Falcon tubes, or even glass test tubes) or directly into a thoroughly cleaned lyophiliser vessel
- Secure a double layer of Kimwipe/Whatman filter over the tube with a rubber band or parafilm; pierce it 5-10 times with a needle.
- Freeze your sample in one of 3 ways:
  - a. You can simply put your samples at an angle at -80 °C overnight and lyophilize them the next day. While this works, it will take quite a bit of extra time. I recommend this method if you have a bunch of samples and you don't care that it might take the extra time to lyophilise.
  - b. Or you can simply put your samples at an angle in liquid nitrogen. Take all the precautions when handling it.
  - c. You can put a small amount of dry ice (about 2 cups) in the bottom of an ice bucket, and then slowly pouring methanol onto the dry ice. You will need enough methanol to completely immerse your sample. Hold the sample container at an angle and turn it slowly and steadily as it freezes, continuing until it is all frozen in layers (or a 'shell') up the sides of the container.
- Turn on the lyophiliser (switch on the right side of the equipment), switch on the manual refrigeration and wait until the temperature reaches -50 °C. The light on the sigmoidal graph should be green.
- After covering, and being sure that the temperature is OK, place the frozen samples into the lyophiliser main vessel, and close the lid. Press the button to turn on the vacuum pump.
- At this point, note that the vacuum gauge will be close to atmospheric pressure, but should be creeping back down. The temperature gauge shouldn't have moved too much. You can now walk away, but I recommend coming back in an hour or so to make sure that your sample is still frozen and that the vacuum is still creeping back down.
- When there is no more ice in your sample (typically 24 h or more depending on the size of your sample), turn off the vacuum pump and carefully remove the vessel.
- Keep your lyophilised samples in the 4°C fridge.
- Put a bucket under the "cleaning valve" (bottom left) to collect the water.
- Clean the vessel with paper towel and ethanol.

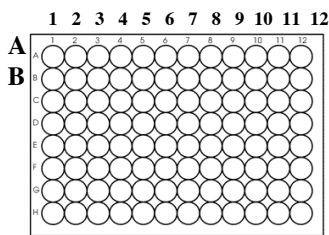
## DAY ELEVEN:

### *Streptavidin quantification by B4F:*

#### *Prepare:*

1. Phosphate buffer Ph 7.0 + BSA (0.1 mg/mL): dissolve 5 mg BSA (at 4 °C) in 50 mL phosphate buffer pH 7.0 (Na<sub>2</sub>HPO<sub>4</sub> 0.2 M/NaH<sub>2</sub>PO<sub>4</sub> 0.2 M, pH 7.0)
2. SAV stock solution 10 mg/mL (152 µM): 5 mg of pure protein in 500 µL mQ-H<sub>2</sub>O (this solution can be stored at -20 °C for a long time)
3. Dilution of protein in buffer pH 7/BSA (Final concentration: 0.131 mg/mL = 2 µM):
  - **Buffer pH 7.0/BSA**: 1973.8µL
  - **Protein 10 mg/mL**: 26.2 µL
4. B4F 40 µM in buffer pH 7/BSA: (for one 96-well plate)
  - **Buffer pH 7.0/BSA**: 2333.4 µL
  - **B4F 0.6mM (in DMSO)**: 166.6 µL

## METHOD



### STREPTAVIDIN

**A (1-12) Front line:** BLANK

Add 100  $\mu\text{L}$  of phosphate buffer/BSA in each well using a multichannel pipette.

**B (1-12) Second line:** SAV

Add 100  $\mu\text{L}$  of 2 $\mu\text{M}$  SAV in each well.

#### **B4F**

**1st column, n°1 (lines A-B):** 40  $\mu\text{M}$  B4F

Add 8  $\mu\text{L}$  of B4F in each well using a multichannel pipette and mix (up and down)

**2nd column, n°2 (lines A-B):** 40  $\mu\text{M}$  B4F

... 10  $\mu\text{L}$

**3rd column, n°3 (lines A-B):** 40  $\mu\text{M}$  B4F

... 12  $\mu\text{L}$

**4th column, n°4 (lines A-B):** 40  $\mu\text{M}$  B4F

... 14  $\mu\text{L}$

**5th column, n°5 (lines A-B):** 40  $\mu\text{M}$  B4F

... 16  $\mu\text{L}$

**6th column, n°6 (lines A-B):** 40  $\mu\text{M}$  B4F

... 18  $\mu\text{L}$

**7th column, n°7 (lines A-B):** 40  $\mu\text{M}$  B4F

... 20  $\mu\text{L}$

**8th column, n°8 (lines A-B):** 40  $\mu\text{M}$  B4F

... 22  $\mu\text{L}$

**9th column, n°9 (lines A-B):** 40  $\mu\text{M}$  B4F

... 24  $\mu\text{L}$

**10th column, n°10 (lines A-B):** 40  $\mu\text{M}$  B4F

... 26  $\mu\text{L}$

**11th column, n°11 (lines A-B):** 40  $\mu\text{M}$  B4F

... 28  $\mu\text{L}$

**12th column, n°12 (lines A-B):** 40  $\mu\text{M}$  B4F

... 30  $\mu\text{L}$

Centrifuge for 1 min at 1000 rpm to remove air bubbles.

## TECAN READER

### Measurement Parameters:

Measurement mode: Fluorescence Top

Excitation wavelength: 485 nm

Emission wavelength: 520 nm

Excitation bandwidth: 12.0 nm

Emission bandwidth: 12.0 nm

Gain: 50

Number of flash: 10

Lag time: 0  $\mu$ s

Integration time: 40  $\mu$ s

Plate definition file: NUN96ft.pdf

Z-Position: 6900  $\mu$ m

Shake duration (Linear Normal): 30 s

Unit: RFU

### Program: MAGELLAN 6

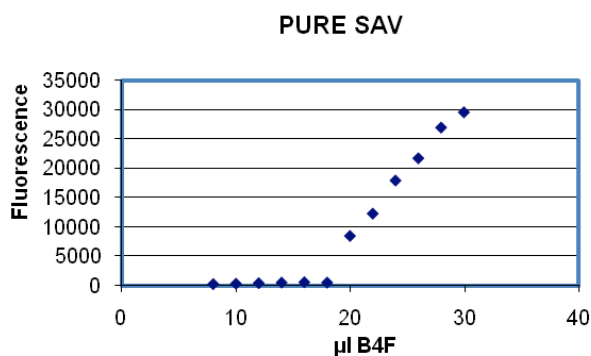
- Start Measurement
- Use Predefined Method
- Folder **Mth**
- Thibaud

### Calculation:

Activity % =  $\frac{V_{B4F}(\text{equivalent point})}{V_{B4F}(\text{theoretical} = 20)}$

$$\text{Activity (\%)} = \frac{V_{B4F}(\text{equivalent point})}{V_{B4F}(\text{theoretical} = 20)} \cdot 100$$

$$\text{Active sites} = \frac{V_{B4F}(\text{equivalent point})}{V_{B4F}(\text{theoretical} = 20)} \cdot 4$$



# APPENDIX D

## Streptavidin Expression in 50 mL of *E. coli* cell culture

### DAY ONE:

Sterilize 250 mL flask with 50 mL TP

#### *Pre-culture in 14 mL Falcon tube for culture:*

- TP Medium: 5 mL
- Glucose 20%: 500  $\mu$ L (Cf: 2%)
- Chloramphenicol (34 mg/mL): 5  $\mu$ L (Cf: 34 $\mu$ g/mL)
- Ampicilin (50 mg/mL): 6  $\mu$ L (Cf: 60 $\mu$ g/mL)
- Inoculation with glycerol stock
- Incubation @ 37°C, 250 rpm, overnight

### DAY TWO:

#### *Culture in 250 mL flask:*

- TP Medium: 50 mL
- Chloramphenicol (34 mg/mL): 50  $\mu$ L (Cf: 34  $\mu$ g/mL)
- Ampicilin (50 mg/mL): 60  $\mu$ L (Cf: 60  $\mu$ g/mL)
- Inoculation with 5 mL of pre-culture
- Incubation @ 34.5 °C, 415 rpm, for 6 hours

⇒ **Induction with IPTG (0.8 M): 75  $\mu$ L** 3h after inoculation

- Stop the culture 3 h after induction
- Centrifugation: 4400 rpm, 10 minutes, @ 4 °C
- Discard the supernatant and inactivate the waste with NaClO
- Freeze the pellet @ -20 °C

#### *Extraction:*

- Harvested cells are frozen-thawed
- Cells are resuspended in 1mL of extraction buffer pH 7.4 (Tris/HCl 20 mM; NaCl 100 mM, PMSF 1mM)
- After addition of 10  $\mu$ L of DNase1 (10 mg/mL), extracts are incubated for 30-90 min @ room temperature
- When DNA is completely destroyed, extracts are microcentrifuged at 14000 rpm for 5 min
- The pellet is re-extracted with 0.5 mL extraction buffer

For 32 flasks prepare **50 mL** of extraction buffer with:

- Tris/HCl 1M pH 7.4: 1 mL
- NaCl 5 M: 1 mL

- PMSF: 8.6 mg in 0.5 mL of EtOH
- H<sub>2</sub>O: qqb 50 mL
- DNase1: 5 mg in 0.5 mL of H<sub>2</sub>O
- MgCl<sub>2</sub> 1M: 250 µL

Transfer 1 mL of the extraction buffer in each tube for the first extraction and 0.5 mL for the second extraction.

# APPENDIX E

## Streptavidin Expression in 96-Well Plate Format

### DAY ONE:

#### *Pre-Culture in 96-well plate:*

Mix for 96-wells:

- Sterile TP medium: 8618.88  $\mu\text{L}$
- Sterile Glucose 20%: 960  $\mu\text{L}$
- Sterile CP (34 mg/mL): 9.6  $\mu\text{L}$
- Sterile AMP (50 mg/mL): 11.52  $\mu\text{L}$

Transfer 100  $\mu\text{L}$  in each well with multichannel pipette

- Inoculation with glycerol stock (in  $-80^{\circ}\text{C}$ ): keep the glycerol stock in dry-ice
- Cover with tin foil
- Incubate at  $37^{\circ}\text{C}$ , 250 rpm, overnight

### DAY TWO:

#### *Culture in 96-deep well plate:*

Mix for 96-wells:

- Sterile TP medium: 48000  $\mu\text{L}$
- Sterile CP (34 mg/mL): 48  $\mu\text{L}$
- Sterile AMP (50 mg/mL): 57.6  $\mu\text{L}$

Transfer 500  $\mu\text{L}$  in each well with multichannel pipette

- Inoculation with 100  $\mu\text{L}$  of pre-culture (leave tips inside – help aeration and for further steps)
- Cover with tin foil
- Incubate at  $37^{\circ}\text{C}$ , 250 rpm, overnight

Induce with IPTG (14.4 mM in TP medium) 3 hrs after inoculation:

- Transfer 100  $\mu\text{L}$  of IPTG in a new 96-well plate
- Add 50  $\mu\text{L}$  of IPTG in each well, by using the same tips you've left inside previously

Stop the culture 3 hrs after induction

Centrifuge at 4400 rpm, 10 minutes,  $4^{\circ}\text{C}$

Discard the supernatant and inactivate the waste with NaClO

Freeze the pellet @  $-20^{\circ}\text{C}$ .

### DAY THREE:

#### *Resuspension of cell lysate:*

- Thaw the bacterial pellet at room temperature.
- Prepare a resuspension buffer:
  - HEPES (500 mM, pH 7.5) : 1920  $\mu\text{L}$
  - DNase (10 mg/mL): 480  $\mu\text{L}$
  - mQ-H<sub>2</sub>O: 16800  $\mu\text{L}$
- Resuspend the pellet in 200  $\mu\text{L}$  of resuspension buffer

- Mix up and down with pipette
- Shake for ½ h
- Centrifuge at 4400 rpm, 10 minutes, 4 °C
- Load the supernatant in the gel

***Electrophoresis SDS-PAGE:***

**Gel preparation: SDS – loading gel**

**12% gel – 15mL for 2 gels**

5mL of ddH<sub>2</sub>O  
 6mL of 30% acrylamide  
 3.8mL of 1.5M Tris pH 8.8  
 75µL of 20% SDS  
 100µL of 15% APS  
 6µL of TEMED

*Pour ± 7mL of gel in each cassette. Add ethanol on top of the gel, until gel is ready (1mL left in the falcon tube serves as control). Wash it thoroughly with dH<sub>2</sub>O before loading the stacking gel.*

**SDS – stacking gel**

**5% gel – 6mL for 2 gels**

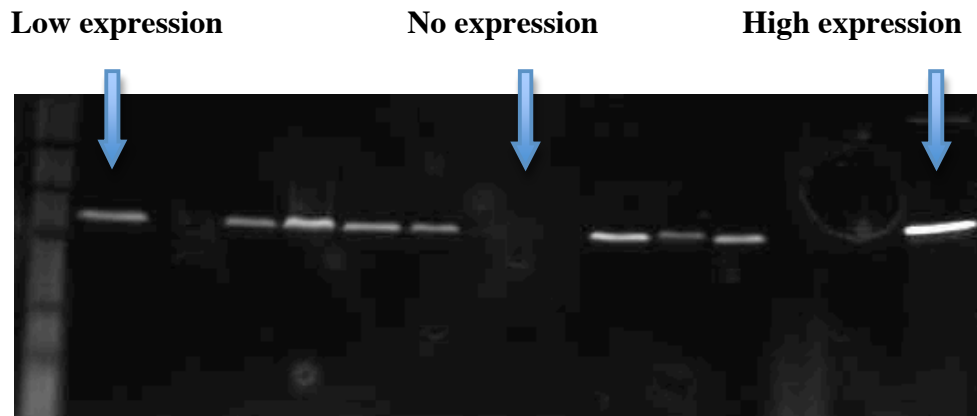
3.4mL of ddH<sub>2</sub>O  
 1mL of 30% acrylamide  
 1.5mL of 0.5M Tris pH 6.8  
 30µL of 20% SDS  
 40µL of 15% APS  
 6µL of TEMED

*Pour ± 3mL of gel in each cassette. Carefully place the comb into the cassette (use goggles, as some of the gel solution can splash out of the cassette). Use the remaining 1mL as control. When ready, remove the comb carefully (don't put too much pressure on it as it can break the gel easily). Wash thoroughly with dH<sub>2</sub>O. Place it into the tank, and add 1X SDS buffer immediately to prevent dryness of the gel.*

**Samples preparation:**

- Transfer 15 µl of each sample in a new tube
- Add 1 µl of B4F (0.6 mM) and incubate for 10' at r.t.
- Add 7.5 µl of LB (3X, without DTT)
- Mix up and down with the pipette
- Load 20 µl on the gel

**Gel picture:**





# APPENDIX F

## Streptavidin Refolding

### Culture

Culture in flasks (500 mL), centrifugation and freezing of the pellet

### Stock solutions

*Resuspension Buffer:*

- Tris/HCl (1 M, pH 7.4) = 250  $\mu$ L
- PMSF = 2.2 mg in 125  $\mu$ L of Ethanol
- H<sub>2</sub>O = up to 12.5 mL

*Inclusion Wash Buffer:*

- Triton X-100 = 5 mL (Cf: 0.5%)
- Tris/HCl (1 M, pH 7.4) = 20 mL (Cf: 20 mM)
- NaCl (5 M) = 20 mL (Cf: 100 mM)
- H<sub>2</sub>O = up to 1000 mL

*PBS IX:*

- NaCl = 8 g (Cf: 137 mM)
- KCl = 0.20 g (Cf: 2.7 mM)
- Na<sub>2</sub>HPO<sub>4</sub> (x 12H<sub>2</sub>O) = 3.58 g (Cf: 10 mM)
- KH<sub>2</sub>PO<sub>4</sub> = 0.24 g (Cf: 1.76 mM)
- mQ-H<sub>2</sub>O = up to 1 L
- pH = 7.4 (with NaOH/HCl)

*Annotation: the following steps should be stopped at any stage of the wash, by storing the protein in the fridge or freezer.*

- ⇒ Thaw the bacterial pellet at room temperature
- ⇒ Resuspend the pellet in 12.5 mL of *resuspension buffer*
- ⇒ Add a spatula of *DNaseI* and incubate under vigorous stirring
- ⇒ Centrifuge at 4400 rpm, 30', 4 °C: keep the supernatant just for negative control
  
- ⇒ Resuspend pellet in *Tris/HCl (20 mM, pH 7.4) = 3.25 mL*
- ⇒ Add *Tris/HCl (20 mM, pH 7.4) = 3.25 mL*
- ⇒ Add *Lysozyme (10 mg/mL) = 225  $\mu$ L*; shake for 5' at r.t.
- ⇒ Add a spatula of *DNaseI*, shake for 10' at r.t.
- ⇒ Finally add *Inclusion Wash Buffer = 12.5 mL*; mix by inverting the tube several times.
- ⇒ Centrifuge at 4400 rpm, 30', 4 °C (keep always the supernatant for control)

### First Wash:

- Resuspend the pellet in 3.25 mL of *inclusion wash buffer*: crush with spatula and shaking.
- Add 12.5 mL of *inclusion wash buffer*: mix by inverting tube
- Centrifuge at 4400 rpm, 30', 4 °C (keep supernatant for control)

### Second Wash:

- Resuspend the pellet in 3.25 mL of *inclusion wash buffer*: crush and shaking.
  - Add 12.5 mL of *inclusion wash buffer*: mix by inverting tube
- Centrifuge at 4400 rpm, 30', 4 °C (keep supernatant for control)

**Third Wash:**

- Resuspend the pellet in 3.25 mL of *inclusion wash buffer*: crush with spatula and shaking.
- Add 12.5 mL of *inclusion wash buffer*: mix by inverting tube
- Centrifuge at 4400 rpm, 30', 4 °C (keep supernatant for control)

**Fourth Wash:**

- Resuspend the pellet in 3.25 mL of *inclusion wash buffer*: crush with spatula and shaking.
- Add 12.5 mL of *inclusion wash buffer*: mix by inverting tube
- Centrifuge at 4400 rpm, 30', 4 °C (keep supernatant for control)

**Dissolving in Guanidinium/HCl:**

- Resuspend the pellet in 2 mL of Guanidinium/HCl (6 M, pH 1.5)
- Centrifuge at 4400 rpm, 30', 4 °C : keep supernatant with protein

*Refolding should be performed in the coldroom at 4 °C*

*For 2 mL of Guanidinium/HCl, you need 100 mL of PBS*

- Add supernatant into vortexing PBS with a micropipette as slowly as possible.

**Dialysis in Imino-biotin buffer (pH 9.8):**

- Pour the PBS solution into the dialysis bag
- Place the bag in a tank containing Imino-biotin buffer

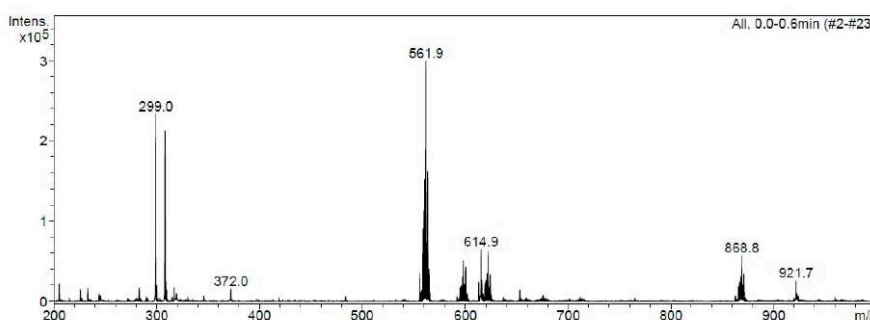
**Imino-biotin affinity column****Dialysis in Tris/HCl (pH 7.4, 10 mM)****Dialysis in dH<sub>2</sub>O****Dialysis in mQ-H<sub>2</sub>O****Lyophilisation**

# APPENDIX G

## Mass Spectrum for the Adduct

$[(\eta^6\text{-}p\text{-cymene})\text{Ru}(\text{Biot-L})\text{Cl}]\text{CF}_3\text{SO}_3(1)/\text{Glutathione (GSH)}$

(performed by Mr Malcolm Jeremy Zimbron)



Adduct complex **1**/GSH was prepared adding an excess of GSH (83  $\mu\text{M}$ ) to the Ru (II) complex (12  $\mu\text{M}$ ) in  $\text{H}_2\text{O}$ . The mass was recorded after only 5 min at 25  $^\circ\text{C}$ . Complex alone (561.9; 597.9; 621.9), GSH (308.0), glutathione dimer (614.9) and adduct (868.8) were identified in the mass spectrum.

# APPENDIX H

## Electrophoretic Mobility Shift Assays (EMSA) in 6% Acrylamide Gel

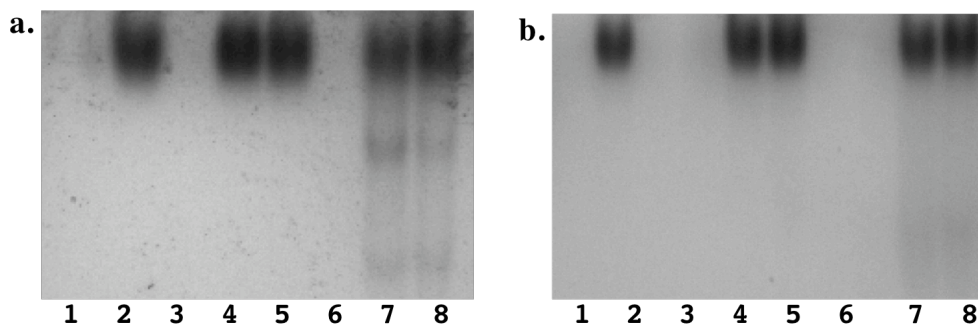
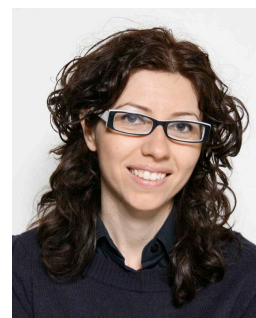


**Fig. D Interaction between telomeric G4A and drug-streptavidin assemblies: a) 1 C WT-Sav and b) 2 C WT-Sav.** The 6% acrylamide gel was run after incubation with of drug-protein assembly with 500 ng of telomeric G4A-DNA. Samples were loaded onto the gel in the following order: lane 1, G4A; lanes 2, Sav (20 μM); lane 3, a) Ru complex 1 (71.4 μM), b) Ru complex 2 (71.4 μM); lane 4, 1 or 2 C WT-Sav; lane 5, G4A and Sav; lane 6, Ru complex and G4A; lane 7, 1 or 2 C WT-Sav with G4A (in 20 mM MOPS); lane 8, 1 or 2 C WT-Sav with G4A (in 75 mM MOPS)

# ALESSIA SARDO



## Curriculum Vitae

### PERSONAL INFORMATION

---

<b>Nationality:</b>	Italian
<b>Date of Birth:</b>	August 19th, 1979
<b>Gender:</b>	Female
<b>Personal Address:</b>	Mülhauserstrasse, 99 – 4056 Basel - SWITZERLAND
<b>Personal Phone:</b>	+41 (0)61.535.70.69
<b>Mobile:</b>	+41 (0)78.785.62.22
<b>Email:</b>	<a href="mailto:Alessia.Sardo@unibas.ch">Alessia.Sardo@unibas.ch</a>
<b>Laboratory Address:</b>	UNIBAS – Universität Basel - Anorganische Chemie Institut Spitalstrasse, 51 – CH 4056 Basel +41 (0)61.267.10.43 <a href="http://www.chemie.unibas.ch/~ward/index.html">www.chemie.unibas.ch/~ward/index.html</a>

### LABORATORY TECHNIQUES

---

<b>Molecular Biology:</b>	PCR techniques & DNA cloning Rational protein re-design by site-directed mutagenesis Directed evolution by saturation
<b>Protein biochemistry:</b>	Protein expression and optimization in <i>E. coli</i> Protein purification: iminobiotin affinity chromatography Electrophoresis & EMSA (Electrophoresis Shift Mobility Assay)
<b>Protein assays:</b>	Protein activity assays
<b>Cell biology:</b>	FACScan™ Flow cytometry
<b>Crystallogensis:</b>	Sitting & hanging drop – <i>PHOENIX</i> robot Microbatch under oil crystallization X-ray diffraction: in house (Biozentrum) & <i>Paul Scherrer Institut</i> (Villigen, Switzerland)
<b>Pharmaceutical chemistry:</b>	Stereospecific synthesis of a lipopeptidic immunoadjuvant
<b>Computer skills:</b>	Microsoft Office tools (Word, Excel, PowerPoint), SciFinder, MDLISIS Draw, ChemOffice, Sigma Plot, Grafit, Internet, Apple tools.
<b>Driving license:</b>	Since 1999

**24 June 2010**

<b>Title of qualification:</b>	PhD in Natural Sciences (Philosophisch-Naturwissenschaftliche) under the supervision of Prof. Thomas R. Ward
<b>Subject:</b>	Project IBAAC: "Genetic Optimization of Biotin-Binding Proteins: Artificial Metalloenzymes and Beyond", supported by Marie Curie fellowship and Fonds National Suisse
<b>Organization providing education and training:</b>	<p>Université de Neuchâtel (<i>Sept 2006 – Jul 2008</i>)            Laboratory of Artificial Metalloenzymes            Avenue du 1er-Mars, 26 – CH 2000 Neuchâtel  <a href="http://www.unine.ch">www.unine.ch</a></p> <p>UNIBAS – Universität Basel (<i>Aug 2008 – Jun 2010</i>)            Anorganische Chemie Institut            Spitalstrasse, 51 – CH 4056 Basel  <a href="http://www.chemie.unibas.ch/~ward/index.html">www.chemie.unibas.ch/~ward/index.html</a></p>

**April – July 2006**

<b>Title of qualification:</b>	Post-graduate training in the cell biology laboratory under the supervision of Dr. Attilio Di Pietro
<b>Subject:</b>	Design and development of transmembrane inhibitors of BCRP
<b>Organization providing training:</b>	<p>Laboratoire des Protéines de Résistance aux Agents Chimiothérapeutiques            Institut de Biologie et Chimie des Protéines (IBCP) – Centre National de la Recherche Scientifique (CNRS) – Claude Bernard University Lyon 1 – UMR 5086 – Passage du Vercors, 7 – 69367 Lyon cedex 7, France  <a href="http://www.ibcp.fr">www.ibcp.fr</a></p>

**Sept 2005 – Mar 2006**

<b>Title of qualification:</b>	Post-graduate training "Leonardo Da Vinci – Unipharma Graduates" - Europass Mobility Project under the supervision of Dr. Attilio Di Pietro
<b>Subject:</b>	The breast cancer resistant protein BCRP/ABCG2 - responsible for multidrug resistance in cancer cells: purification of the recombinant transporter and modification of ligand interaction by R482T hot-spot mutation
<b>Organization providing training:</b>	<p>Laboratoire des Protéines de Résistance aux Agents Chimiothérapeutiques            Institut de Biologie et Chimie des Protéines (IBCP) – Centre National de la Recherche Scientifique (CNRS) – Claude Bernard University Lyon 1 – UMR 5086 – Passage du Vercors, 7 – 69367 Lyon cedex 7, France  <a href="http://www.ibcp.fr">www.ibcp.fr</a></p>

**Jun 2005**

**Title of qualification:** Pharmacist Qualification

**Organization providing education and training:** Università di Catania  
Facoltà di Farmacia  
Catania, Italy  
<http://www3.unict.it/fdf2/>

**Dec 2004 – Mar 2005**

**Title of qualification:** Post-graduate training in pharmacy

**Job description:** Magistral preparations in a galenic laboratory

**Organization providing training:** Pharmacy “Croceverde”  
Dr. F. Sgalambro  
Via D’Annunzio, 43 - 95128  
Catania, Italy

**Oct 1998 – Nov 2004**

**Title of qualification awarded:** Master degree in Pharmaceutical Chemistry and Technologies (Grade: 110/110 with honors)

**Principal subjects:** Stereospecific synthesis of a lipopeptidic immunoadjuvant for potential antitumor vaccines

**Organization providing education and training:** Università di Catania  
Facoltà di Farmacia  
Catania, Italy  
<http://www3.unict.it/fdf2/>

---

## TEACHING EXPERIENCE

**Date:** 2007-2010

**Title of qualification:** Teaching Assistant

**Subject:** Supervision of the analytical chemistry laboratory for 1<sup>st</sup> year undergraduate pharmacy and biology students

**Organization providing education and training:** Université de Neuchâtel (*Sept 2006 – Jul 2008*)  
Laboratory of Artificial Metalloenzymes  
Avenue du 1er-Mars, 26 – CH 2000 Neuchâtel  
[www.unine.ch](http://www.unine.ch)

UNIBAS – Universität Basel (*Aug 2008 – Jun 2010*)  
Anorganische Chemie Institut  
Spitalstrasse, 51 – CH 4056 Basel  
[www.chemie.unibas.ch/~ward/index.html](http://www.chemie.unibas.ch/~ward/index.html)

<b>Italian:</b>	Mother tongue		
<b>French:</b>	Reading skills: excellent	Writing skills: good	Verbal skills: excellent
<b>German:</b>	Reading skills: basic	Writing skills: basic	Verbal skills: basic
<b>English:</b>	Reading skills: good	Writing skills: good	Verbal skills: good

PUBLICATIONS

«Purification of Breast Cancer Resistance Protein ABCG2 and role of arginine-482», Pozza A., Perez-Victoria JM., Sardo A., Ahmed-Belkacem H., Di Pietro A., (2006) *Cell Mol Life Sci.*, 63, 1912-1922.

«X-ray structure and designed evolution of an artificial transfer hydrogenase», Creus M., Pordea A., Rossel T., Sardo A., Letondor C., Ivanova A., Letrong I., Stenkamp R. E., Ward T. R., (2008) *Angew. Chem, Int. Ed.*, 47, 1400-1404.

«Artificial metalloenzymes for asymmetric allylic alkylation on the basis of the biotin-avidin technology», Pierron J., Malan C., Creus M., Gradinaru J., Hafner I., Ivanova A., Sardo A., Ward T. R., (2008) *Angew. Chem, Int. Ed.*, 47, 701-705.

«Chemo-genetic optimization of DNA recognition by metallodrugs using a presenter protein strategy», Zimbron J. M., Sardo A., Heinisch T., Wohlschlager T., Gradinaru J., Massa C., Schirmer T., Creus M., Ward T. R. (in press).

«Burkavidin: a novel secreted biotin-binding protein from the human pathogen *Burkholderia pseudomallei*», Sardo A., Wohlschlager T., Lo C., Zoller H., Ward T. R., Creus M. (submitted).

«Protein based hybrid catalysts – design and evolution», Köhler V., Wilson Y. M., Lo C., Sardo A., Ward T. R. (submitted).

COMMUNICATIONS

Oral presentation at the “1<sup>st</sup> Year Graduate Student Symposium 2007”, Berne (CH), Sept. 2007.

Poster presentation at the “ VIII European Symposium”, Protein Society, June 14-18, 2009, Kongresshaus, Zurich (CH).

Several oral presentations during laboratory seminars.

AWARDS

<b>Distinction prize:</b>	<b>Sept 2005</b>
	Selection among the 50 Italian trainees to undertake a 24 week period of research internship at selected European Research Centers within the European Union vocational training project “ <b>Leonardo da Vinci</b> ” <b>UNIPHARMA-GRADUATES</b>
<b>Distinction prize:</b>	<b>Nov 2004</b>
	Nomination to FEDERFARMA PRIZE



**Prof. Dr. Thomas R. WARD**

UNIBAS – Universität Basel – Anorganische Chemie Institut  
Spitalstrasse, 51 – CH 4056 Basel  
[www.chemie.unibas.ch/~ward/index.html](http://www.chemie.unibas.ch/~ward/index.html)

Phone: +41 (0)61.267.10.04  
Fax: +41 (0)61.267.10.05  
Email: [thomas.ward@unibas.ch](mailto:thomas.ward@unibas.ch)

**Dr. Marc CREUS**

Phone: +41 (0)61.267.10.63  
Fax: +41 (0)61.267.10.05  
Email: [marc.creus@unibas.ch](mailto:marc.creus@unibas.ch)

**Dr. Attilio Di Pietro**

IBCP – CNRS – Claude Bernard  
University Lyon 1 – UMR 5086  
– Passage du Vercors, 7 – FR  
69367 Lyon cedex 7  
[www.ibcp.fr](http://www.ibcp.fr)

Phone: +33(0)4.72.72.26.29  
Fax: +33(0)4.72.72.26.04  
Email: [a.dipietro@ibcp.fr](mailto:a.dipietro@ibcp.fr)